Microhydrological niches in soils: how mucilage and EPS alter soil hydraulic properties and water dynamics

DISSERTATION

zur Erlangung des akademischen Grades eines

Doktors der Naturwissenschaften

(Dr. rer. nat.)

an der Fakultät für Biologie, Chemie und Geowissenschaften

der Universität Bayreuth

vorgelegt von

Pascal Benard

aus *Mühlacker*

Bayreuth, Mai 2019

Die vorliegende Arbeit wurde im Zeitraum von März 2016 bis Mai 2019 in Göttingen in der Abteilung für Bodenhydrologie und in Bayreuth am Lehrstuhl für Bodenphysik unter Betreuung von Herrn Prof. Dr. Andrea Carminati angefertigt**.**

Vollständiger Abdruck der von der Fakultät für Biologie, Chemie und Geowissenschaften der Universität Bayreuth genehmigten Dissertation zur Erlangung des akademischen Grades eines Doktors der Naturwissenschaften (*Dr. rer. nat.*).

Dissertation eingereicht am: 09.05.2019

Zulassung durch die Promotionskommission: 22.05.2019

Wissenschaftliches Kolloquium: 03.12.2019

Amtierender Dekan: Prof. Dr. Matthias Breuning

Prüfungsausschuss

Prof. Dr. Andrea Carminati   (Gutachter)

Prof. Dr. Jörg Bachmann   (Gutachter)

Prof. Dr. Martin Obst   (Vorsitz)

Prof. Dr. Tillmann Lüders

(Weiterer Gutachter: Prof. Dr. Hans-Jörg Vogel)

Acknowledgements

This work was possible through the support of many people to whom I want to express my gratitude.

I would like to thank my supervisor Andrea Carminati for his constant support, countless scientific discussions and inspiration throughout the last 5 years. He supported me not only during the PhD but also before, during the preparation of the proposal which this thesis is based on. I would also like to thank Mohsen Zare for his extensive support and for sharing his knowledge and office with me.

This work was improved and expanded by many cooperation partners and their expertise. I would like to thank Maire Holz, Eva Kröner, Mathilde Brax, Robin Kaltenbach, Vincent Felde, Estelle Couradeau, Anders Kaestner, Iwan Jerjen, Federica Marone, Mutez Ahmed, Clemens Hedwig, Judith Schepers and Ursula Bundschuh.

I would like to express my gratitude to Jörg Bachmann for his support and diverting our attention towards soil water repellency.

I would like to thank all my great colleagues from the group of Soil Hydrology (Göttingen) and Soil Physics (Bayreuth) for a pleasant time and a delightful working environment.

Finally, I would like to thank my family and in particular Mareike Henneberg for supporting me throughout this period.

Summary

The soil offers numerous challenges to life residing in its porous environment. One of these challenges are fluctuations in soil water content which are accompanied by shifts in soil hydraulic properties. In order to avoid undesirable alterations and optimise growth conditions, plants and bacteria engineer their local environment by release of mucilage and EPS (extracellular polymeric substances).

So far, modifications of soil properties were mainly attributed to the intrinsic properties of these highly polymeric blends. In this work, we focused on deriving a mechanistic understanding of how mucilage and EPS interact with the soil pore space and how these interactions impact soil hydraulic properties and water dynamics in the rhizosphere and other biological hotspots in soils.

Mucilage and EPS are capable of absorbing large volumes of water, increase the viscosity of the soil solution and decrease its surface tension. Upon drying, mucilage turns water repellent. Here, we proposed a conceptual model linking the intrinsic physical properties of mucilage to their impact on soil hydrology. The increase in viscosity is related to the high content of polymers which can form an interconnected network. As the soil dries, mucilage and EPS become increasingly concentrated, the viscosity of the soil solution locally increases and its surface tension decreases. When a critical viscosity is reached and parts of the polymer network are adsorbed to drying surfaces, the retreat of the liquid front is delayed and its break-up due to capillary forces is prevented.

This concept is confirmed by microscopy imaging and high resolution X-ray CT, which revealed that mucilage and EPS form filaments and two-dimensional structures in this process. Upon drying in porous media, mucilage at low concentrations (mass of dry gel per mass of dry soil) resulted in the formation of filaments. With increase in initial mucilage concentration, two-dimensional surfaces formed when the water content was relatively high and the liquid phase connected.

Complementary measurements of soil hydraulic properties of mucilage amended soils showed how the formation of these continuous two-dimensional structures impacts soil physical properties, such as soil hydraulic conductivity, soil water retention and vapour diffusion. The maintained liquid connectivity in drying soils, which is caused by the high viscosity, low surface tension and interaction of the polymer network with the soil

porous matrix, explains why the hydraulic conductivity of a mucilage amended sandy loam was higher at low soil water content when compared to its control, as shown in evaporation experiments. Additionally, the delayed retreat of the liquid phase at a critical mucilage concentration creates an additional matric (capillary) potential and enhances soil water retention. To separate and quantify this matric (capillary) effect from the intrinsic property of the polymer network to absorb water remains an open task. Furthermore, upon severe soil drying, the network of two-dimensional structures reduces vapour diffusion and thus delays soil drying. This effect was illustrated using time series neutron radiography to visualise the drying of mucilage amended sandy loam and a water saturated control.

Besides affecting soil hydraulic properties and evaporation rates during soil drying, mucilage impacts the rewetting kinetics. Mucilage amended soils showed water repellency. Precisely, a sharp decrease in wettability was observed near mucilage contents at which one-dimensional structures were replaced by two-dimensional continuous surfaces. Simulation of water drop infiltration experiments in mucilage amended soils showed that the creation of continuous clusters of non-wettable pores induced a substantial decrease in soil wettability, indicated by a transition of water drop penetration time from milliseconds to minutes.

Although most experiments presented here were based on simplified systems, such as mucilage amended porous media, we propose that the release of highly polymeric blends into the soil pore space represents a universal strategy of soil organisms. Plants and bacteria engineer the physical properties of their local environment in very similar and astoundingly effective ways. The mechanisms discovered in this thesis lead to hydraulic decoupling of biological hotspots (e.g. the rhizosphere or biocrust) and buffer the erratic fluctuations experienced by soil organisms in these microhydrological niches.

Zusammenfassung

Die poröse Struktur des Bodens stellt das Leben vor zahlreiche Herausforderungen. Eine dieser Herausforderungen sind Schwankungen des Bodenwassergehaltes welche von Veränderungen der hydraulischen Bodeneigenschaften begleitet werden. Um unliebsame Veränderungen zu vermeiden und Wachstumsbedingungen zu optimieren, modifizieren Pflanzen und Bakterien ihre lokale Umgebung durch die Freisetzung von Mucilage und EPS (Extrazelluläre Polymere Substanzen).

Daraus resultierende Veränderungen der Bodeneigenschaften wurden bislang haupt-sächlich den intrinsischen Eigenschaften dieser polymeren Substanzen zugeschrieben. In dieser Arbeit galt es ein Verständnis für die Mechanismen der Interaktion von Mucilage und EPS mit dem Porenraum zu erlangen und den Einfluss dieser Wechsel-wirkungen auf die hydraulischen Bodeneigenschaften und die Wasserdynamik in der Rhizosphäre und anderen biologischen Hotspots des Bodens zu ergründen.

Mucilage und EPS sind in der Lage große Mengen Wasser aufzunehmen, die Viskosität der Bodenlösung zu erhöhen und deren Oberflächenspannung zu verringern. Mucilage wird wasserabweisend, wenn sie trocknet. In dieser Arbeit präsentieren wir ein konzeptionelles Modell, welches die intrinsischen physikalischen Eigenschaften von Mucilage mit ihrem Einfluss auf die Bodenhydrologie verbindet. Die Erhöhung der Viskosität ist durch den hohen Gehalt an Polymeren begründet, welche ein verzweigtes Netzwerk formen können. Wenn der Boden trocknet, werden Mucilage und EPS konzentriert, die lokale Viskosität der Bodenlösung nimmt zu und die Oberflächen-spannung nimmt ab. Bei Erreichen einer kritischen Konzentration und wenn Teile des Netzwerks an trocknenden Oberfläen adsorbieren wird die zurückweichende Bodenlösung verlangsamt während ein Zerreißen der flüssigen Phase durch Kapillar-kräfte verhindert wird.

Mikroskopische Aufnahmen und hochauflösende Röntgen Computertomographie haben gezeigt, dass Mucilage und EPS in diesem Prozess Filamente und zwei-dimensionale Strukturen bilden. Diese Beobachtungen sind ein Beleg für die beschriebene Konzeption. Die Zugabe geringer Konzentrationen von Mucilage (Masse trockenen Gels pro Masse trockenen Bodens) zu einem porösen Medium führt bei Trocknung zur Formation von Filamenten. Bei höheren Konzentrationen entstehen zweidimensionale

Oberflächen bei relativ hohem Wassergehalt, während die Kontinuität der flüssigen Phase erhalten bleibt.

Komplementäre Messungen bodenhydraulischer Eigenschaften von mit Mucilage versetzten Böden haben gezeigt, dass die Bildung dieser durchgängigen zweidimensionalen Strukturen die physikalischen Bodeneigenschaften wie hydraulische Leitfähigkeit, Wasserhaltekapazität und Gasdiffusion beeinflusst. Der Erhalt der Kontinuität der flüssigen Phase im trocknenden Boden wird durch die erhöhte Viskosität, reduzierte Oberflächenspannung und die Interaktion des Polymernetzwerks mit der porösen Matrix hervorgerufen. Dieser Effekt erklärt die Ergebnisse aus Verdunstungsexperimenten, welche eine erhöhte hydraulische Leitfähigkeit von mit Mucilage versetztem sandigem Lehm bei geringem Wassergehalt im Vergleich zu einer unversetzten Kontrolle zeigten. Zusätzlich zu diesem Effekt führt der verzögerte Rückzug der flüssigen Phase ab einer kritischen Mucilage Konzentration zur Entstehung eines zusätzlichen Matrixpotentials (kapillar) und erhöhter Wasserhaltekapazität des Bodens. Die Quantifizierung dieses Effekts und seine Abgrenzung gegenüber der intrinsischen Eigenschaft des Polymernetzwerkes, Wasser zu absorbieren, steht aus. Bei starker Austrocknung eines Bodens kann das Netzwerk aus zweidimensionalen Strukturen die Gasdiffusion reduzieren und somit das weitere Austrocknen verlangsamen. Mit Hilfe von Zeitreihen-Neutronenradiographie konnte dieser Effekt in einem trocknenden sandigen Lehm und einer wassergesättigten Kontrolle verdeutlicht werden.

Neben einer Beeinflussung der hydraulischen Eigenschaften und der Verdunstungsrate beim Austrocknen eines Bodens, beeinflusst Mucilage die Rückfeuchtung des Bodens. Mit Mucilage versetzter Boden wurde wasserabweisend, wenn mit steigendem Mucilagegehalt eindimensionale Filamente durch zweidimensionale Oberflächen ersetzt wurden. Die Simulation von Wassertopfeninfiltrationsexperimenten mit Mucilage versetzter Böden hat gezeigt, dass die Entstehung von zusammenhängenden nicht benetzbaren Poren eine substantielle Reduzierung der Bodenbenetzbarkeit zur Folge hat. Dieser Übergang von eindimensionalen zu zweidimensionalen Strukturen spiegelte sich in einer Zunahme der Infiltrationszeit von Millisekunden auf Minuten wider.

Obwohl ein Großteil der hier gezeigten Experimente in vereinfachten Systemen wie mit Mucilage versetzten porösen Medien durchgeführt wurden postulieren wir auf Grundlage der Ergebnisse dieser Arbeit, dass die Abgabe von hochpolymeren Substanzen in die poröse Umgebung des Bodens eine universelle Strategie von

Bodenorganismen darstellt. Pflanzen und Bakterien modifizieren die physikalischen Eigenschaften ihrer lokalen Umgebung auf sehr ähnliche und erstaunlich effektive Art und Weise. Die in dieser Arbeit untersuchten Mechanismen führen zur hydraulischen Entkopplung von biologischen Hotspots (z.B. der Rhizosphäre oder Biokruste) und puffern die von Bodenorganismen erfahrenen wiederkehrenden Fluktuationen in diesen mikrohydrologischen Nischen.

Contents

List of Figures

List of Tables

List of Abbreviations

c_v	Saturated water vapor concentration
D	Vapor diffusivity
EPS	Extracellular polymeric substances
e(t)	Evaporation rate
H	Relative humidity
h	Pressure difference across the gas-liquid interface
L_{tot}	Total length of flow path
Oh	Ohnesorge number
PGA	Polygalacturonic acid
Q	Volumetric flow rate
R	Contact-line radius
SDM	Sessile drop method
SRXTM	Synchrotron-based X-ray tomographic microscopy
WDPT	Water drop penetration time
α	Contact angle
μ	Viscosity
ρ	Density
σ	Surface tension

Differing abbreviations in chapter 4

γ	Surface tension
η	Viscosity

Extended Summary

1.1. Introduction

Hosting a tremendous biodiversity (Philippot et al., 2013), the soil offers opportunities as well as immense challenges to organisms residing in its porous environment. The ever recurring cycle of drying and rewetting results not only in the depletion and return of an essential resource, but in fluctuations of soil water content and soil hydraulic conditions which can be rapid and severe. In order to avoid induced negative impacts on growth conditions, both plants and bacteria engineer their local environment by release of highly polymeric blends into the soil pore space. Induced alterations are most prominent in locations of high biological activity, like the rhizosphere defined as the part of the soil actively modified by plant root growth and exudation (Gregory, 2006; Hinsinger et al., 2009). Although the extent of the rhizosphere is on the order of a few millimetres (Gregory, 2006), its relevance is reflected by the vast amount of water transported through this thin layer, which amounts for approximately 40% of all terrestrial precipitation (Bengough, 2012).

Plants are capable to release substantial amounts of assimilated carbon into the soil by rhizodeposition (Nguyen, 2003). Among other substances, mucilage secreted at the root tip (e.g. Fig. 1.1) is mainly composed of various proportions of sugars and organic acids (Oades, 1978; Read and Gregory, 1997; Naveed et al., 2017). The polymers within the mucilage blend are capable to absorb and hold large quantities of water (McCully and Boyer, 1997; Read et al., 1999). For this reason, mucilage can be classified as hydrogel (Brinker and Scherer, 1990). Among

Fig. 1.1: Hydrated mucilage at the tip of a nodal root of maize (*Zea mays*)

polysaccharides, surface active agents inducing a reduction in interfacial tension at the gas-liquid interface were identified within the mucilage blend (Read and Gregory, 1997).

Though the composition and physical properties of mucilage among different plant species is highly variable (Naveed et al., 2017), they share their basic features. Root and

seed mucilage increase the viscosity of the soil solution (Read and Gregory, 1997; Read et al., 1999; Naveed et al., 2017), decrease the surface tension at the gas-liquid interface (Read and Gregory, 1997; Naveed et al., 2018) and can absorb water (McCully and Boyer, 1997; Read et al., 1999; Segura-Campos et al., 2014). The physical properties of mucilage from different root types of maize (*Zea mays*) were summarized by Carminati et al. (2017) (Fig. 1.2).
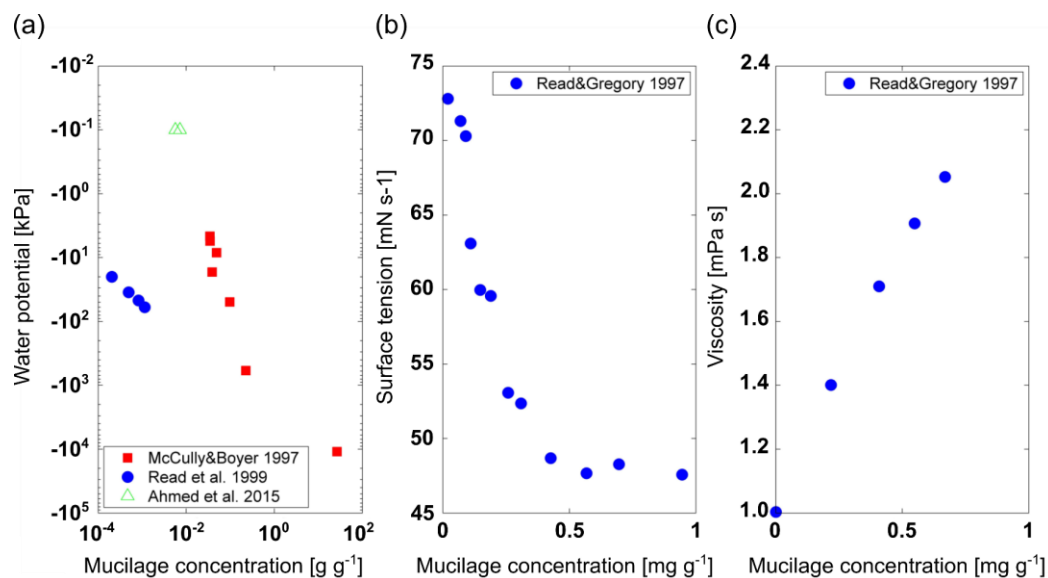
Fig. 1.2: Physical properties of maize (*Zea mays*) root mucilage (Figure adapted from Carminati et al. (2017)). **(a)** Water potential of mucilage at different concentrations (g dry mucilage per g of water). Data were taken from McCully and Boyer (1997), Ahmed et al. (2015) (both mucilages from nodal roots of maize (*Zea mays*)) and Read et al. (1999) (mucilage from seminal roots of maize (*Zea mays*) seedlings). **(b)** Surface tension of different concentrations of maize mucilage (*Zea mays*) (Read and Gregory 1997). **(c)** Viscosity of different concentrations of maize (*Zea mays*) mucilage (Read and Gregory 1997)

Although presented studies mainly focused on seed and root mucilage, the following paragraphs highlight some striking similarities between mucilage and bacterial EPS (extracellular polymeric substances) followed by a description of their comparable impacts on soil water dynamics and soil hydraulic properties.

Most bacteria are capable to form complex biofilms by release of a diverse blend of EPS into their surrounding media (Flemming and Wingender, 2010; Persat et al., 2015). These highly polymeric blends, like mucilage, can form an interconnected network that promotes favourable conditions (Flemming and Wingender, 2001). An outstanding example of EPS-based structures are biocrusts (Rossi et al., 2012, 2018; Chamizo et al., 2016), arguably the most extended biofilm on earth (Elbert et al., 2012; Rodriguez-Caballero et al., 2018). EPS contain high amounts of polysaccharides, as well as

proteins, DNA and lipids, and, like mucilage increase the viscosity of the soil solution (Körstgens et al., 2001; Stoodley et al., 2002; Wloka et al., 2004; Shaw et al., 2004; Lieleg et al., 2011). Lipopeptides (Raaijmakers et al., 2010) and a range of other compounds were identified (Flemming and Wingender, 2010) causing a reduction in surface tension at the gas-liquid interface. The diversity in biofilms and the EPS they are made of was felicitously described by Ian Sutherland: "The enormous number of microbial species capable of forming biofilms or interacting with others to do so, together with the very great range of polysaccharides produced, gives rise to an infinite number of permutations." (Sutherland, 2001).

Regardless of their diversity in chemical composition, mucilage and EPS share their basic traits (Table 1.1). Both contain high amounts of polymeric substances capable to form a network (Roberson et al., 1993; McCully and Boyer, 1997; Shaw et al., 2003; Flemming and Wingender, 2010) that absorbs water (Roberson and Firestone, 1992; McCully and Boyer, 1997; Read et al., 1999; Flemming and Wingender, 2001; Segura-Campos et al., 2014; Flemming et al., 2016). They increase the viscosity of the liquid phase (Flemming and Wingender, 2001, 2010; Stoodley et al., 2002; Naveed et al., 2017) while surface active constituents lower the interfacial tension at the gas-liquid interface (Read et al., 2003; Raaijmakers et al., 2010).

Table 1.1: Physical properties of EPS and mucilage and their effects in soil

		Bacterial EPS	Root mucilage	Seed mucilage
Intrinsic properties	**Increased viscosity / Viscoelasticity**	Körstgens et al. (2001); Stoodley et al. (2002); Wloka et al. (2004); Shaw et al. (2004); Lieleg et al. (2011)	Read and Gregory (1997); Naveed et al. (2017)	Naveed et al. (2017)
	Decreased surface tension	Raaijmakers et al. (2010) and references included	Read and Gregory (1997); Read et al. (2003)	Naveed et al. (2018)
	Adsorption of water	Roberson and Firestone (1992); Flemming et al. (2016)	McCully and Boyer (1997); Read et al. (1999)	(Segura-Campos et al., 2014)
	Reduced wettability	-	Ahmed et al. (2016); Zickenrott et al. (2016)	(Benard et al., 2018; Chapter 3)
Effect on soil hydraulics	**Increased soil water retention**	Roberson and Firestone (1992); Chenu (1993); Rosenzweig et al. (2012); Volk et al. (2016)	(Benard et al., 2019; Chapter 2)	Kroener et al. (2018), (Benard et al., 2019; Chapter 2)
	Slowed down evaporation from soil	Chenu (1993); Flemming (2011); Deng et al. (2015); Zheng et al. (2018), Adessi et al. (2018)	-	(Benard et al., 2019; Chapter 2)
	Increased relative hydraulic conductivity*	Volk et al. (2016); Zheng et al. (2018)	-	(Benard et al., 2019; Chapter 2)
	Induced soil water repellency	-	Ahmed et al. (2016); Carminati et al. (2010); Moradi et al. (2012)	(Benard et al., 2018; Chapter 3) (Benard et al., 2018; Chapter 4)

*The relative hydraulic conductivity is defined as the hydraulic conductivity divided by the saturated hydraulic conductivity. This means changes in hydraulic conductivity during drying of soils are eased.

We conclude that mucilage and bacterial EPS alter the physical properties of the soil solution in comparable ways. In light of their highly diverse composition, the magnitude of their impact can be assumed as diverse.

The effect of plant roots on the physical and hydraulic properties of the rhizosphere was observed many times (Young, 1995; Hallett et al., 2003; Carminati et al., 2010; Zarebanadkouki et al., 2016; Naveed et al., 2017). Fluctuations in soil water content during drying-wetting cycles in the rhizosphere of lupins (*Lupinus albus*) were attributed to the presence of root exuded mucilage (Carminati et al., 2010). Low wettability in the rhizosphere of lupins (*Lupinus albus*) was confirmed by a subsequent study (Moradi et al., 2012). Reduced wettability was also reported within the rhizosphere of maize and for dry maize root mucilage (*Zea mays*) (Ahmed et al., 2016). Zickenrott et al. (2016) reported reduced soil wettability induced by dry mucilage collected from seedlings of *Lupinus albus*, *Vicia faba*, *Triticum aestivum* and *Zea mays*. An increase in soil water retention during drying was observed in the rhizosphere of chickpea (*Cicer arietinum*), lupin (*Lupinus albus*), and maize (*Zea mays*) (Moradi et al., 2011). Similar increase in soil water retention of various chia seed mucilage (*Slavia hispanica*) amended soils was reported by Kroener et al. (2018). The effect of mucilage appeared amplified in fine soils which was attributed to the enhanced interaction of solid surfaces and mucilage due to the higher specific surface leading to the creation of a more stable network in drying soil. For soil amended with chia seed mucilage (*Slavia hispanica*) a decrease in saturated hydraulic conductivity was attributed to an increase in viscosity of the soil solution (Kroener et al., 2014).

Reported impacts of bacterial EPS on soil physical and hydraulic properties appear astoundingly similar. An increase in soil water retention was observed for soils inoculated with biofilm forming *Pseudomonas* species isolated from soil (Roberson and Firestone, 1992; Volk et al., 2016), rhizobacteria (*Bacillus subtilis*) (Zheng et al., 2018; Fig. 1.3) and EPS amended soil (Chenu, 1993; Rosenzweig et al., 2012).

Fig. 1.3: EPS structures created by Bacillus subtilis in sand (Zheng et al., 2018)

Upon extraction of EPS from biocrust, a reduced soil water retention was

observed (Adessi et al., 2018). Volk et al. (2016) reported a decrease in saturated hydraulic conductivity of inoculated soil when compared to a control. The unsaturated hydraulic conductivity decreased less with decrease in soil water potential upon drying. Beside these modifications, soils treated with EPS (Chenu, 1993; Zheng et al., 2018), inoculated with rhizobacteria (Zheng et al., 2018) and soil micromodels inoculated with *Sinorhizobium meliloti* (Deng et al., 2015) were shown to dry slower compared to control media. Biofilms of *S. meliloti* showed no resistance to drying outside a porous geometry (Deng et al., 2015). Ophir and Gutnick (1994) conducted desiccation studies comparing the survival rates of mucoid and non-mucoid strains of different bacteria (*E. coli*, *E. stewartia* and *A. calcoaceticus*) in the porous environment of Millipore filters. They reported significantly higher survival rates for mucoid strains capable to produce EPS.

Several studies highlighted the importance and lack of understanding of pore-scale interactions involved in the alteration of soil hydraulic properties and soil water dynamics (e.g. Deng et al., 2015; Volk et al., 2016; Kroener et al., 2018). When soil dries, water retreats towards the inter-particle space. Albalasmeh and Ghezzehei (2014) showed the formation of bridges between particles in this process using PGA (polygalacturonic acid) as a model substance for mucilage and EPS. Their observations partly explain how mucilage binds soil particles within the rhizosphere as shown for maize (*Zea mays*) by Watt et al. (1993). Nevertheless, observations like the absence of a resistance of biofilms to drying outside a porous medium (Deng et al., 2015) or the amplified effect of mucilage on soil water retention in fine textured soils (Kroener et al., 2018) indicate the need to shed light on the pore-scale mechanisms involved.

1.2. Objectives and Outline

The main objective of this study was to link the effect of mucilage and EPS on the physical properties of the soil solution and their interaction with the soil pore space to their impacts on soil hydraulic properties and soil water dynamics.

In Chapter 2 we derived a mechanistic description of the spatial configuration of the liquid phase in drying soils affected by mucilage and EPS. To validate our concept, we analysed the distribution of maize root mucilage (*Zea mays*) in the pore space of glass beads by synchrotron-based X-ray tomographic microscopy (SRXTM). As an example

of EPS-based structures, we also imaged soil biocrust collected from Moab, Utah (USA). Light microscopy was used in Chapter 2, 3 and 4 to image the spatial distribution of seed mucilage (*Salvia hispanica*) in different soils and glass beads. In Chapter 2, an evaporation method (Hyprop) was used to evaluate the effect of mucilage on soil water retention, hydraulic conductivity and evaporation dynamics. Additionally, the spatial distribution of water during soil drying was monitored using time-series neutron radiography.

The impact of the spatial distribution of dry mucilage structures on initial rhizosphere wettability and rewetting dynamics was evaluated in Chapter 3 and 4. Chapter 3 deals with the impact of soil texture, surface roughness and mucilage content on initial wettability. Therefore, the wettability of three soils with a range of particle sizes and glass beads was quantified. The initial contact angle was measured for dry mucilage (*Slavia hispanica*) contents ranging from no observable contact angle due to rapid infiltration across the repellent threshold to values > 90°. The effect of surface roughness was evaluated by quantifying the size of dry mucilage structures in sand and glass beads of comparable grain size at the same mucilage content. In Chapter 4, we focused on the rewetting dynamics of sand and glass beads of comparable particle size. The impact of mucilage distribution and surface roughness was evaluated by means of WDPT (water drop penetration time). Measured WDPT was simulated with a pore network model to assess the impact of heterogeneous pore-scale wettability on rhizosphere rewetting dynamics.

With regard to the specific chapters, the objectives of this work were to:

- provide a conceptual model of the spatial configuration of the liquid phase affected by mucilage and EPS in drying soil (Chapter 2)
- link induced alterations on the pore scale to macroscopic impacts of mucilage and EPS on soil hydraulic properties and soil water dynamics (Chapter 2)
- evaluate the impact of soil texture and surface roughness on mucilage distribution and rhizosphere wettability (Chapter 3)
- assess the impact of heterogeneous wettability on the pore scale and surface roughness on rhizosphere rewetting dynamics experimentally (Chapter 3)
- evaluate the impact of heterogeneous pore-scale wettability numerically by simulation of water drop infiltration experiments (Chapter 4)

1.3. Material and Methods

Mucilage

Most experiments described here (see Chapter 2, 3 and 4) were conducted using mucilage extracted from chia seeds (*Salvia hispanica*) as an analogue of root exuded mucilage. Its chemical composition (Lin et al., 1994) and physical properties are comparable to root mucilage of lupin and maize (Carminati and Vetterlein, 2013). To study the distribution of mucilage structures in 3D space, mucilage was collected from the nodal roots of 10 weeks old field grown maize (*Zea mays*) near Bayreuth, Germany.

Sample preparation

To study, illustrate and quantify the distribution and spatial extent of dry mucilage in the soil pore space (Chapter 2, 3 and 4) and its impact on soil wettability (Chapter 3) and rewetting dynamics (Chapter 4), thin layers of mucilage particle mixtures were prepared to mimic the rhizosphere. Soil and glass beads were mixed with hydrated chia seed mucilage. Mixtures were spread on object slides and air dried.

Additionally, undisturbed dry soil-mucilage mixtures were prepared. Dry mixtures of same batches were crumbled and their wettability was assessed employing the sessile drop method (SMD) described by Bachmann et al. (2000) (Chapter 3). Undisturbed samples were stained with an ink-water solution in order to facilitate optical discrimination of mucilage structures and particles.

In order to study the three-dimensional extent of dry mucilage structures, maize root mucilage was mixed with glass beads (0.1-0.2 mm) and sand (0.125-0.2mm) to achieve a mucilage content of 4 and 8 mg g^{-1} respectively (Chapter 2). Wet mixtures were packed into PVC cylinders with an inner diameter of 1.5 mm and a depth of 4.5 mm, and air dried.

Light microscopy imaging

In Chapter 2, images of dry mucilage structures were acquired with reflected light microscope equipped with a digital camera. Studies on the distribution and extent of mucilage structures within the pore space of different porous media reported in Chapter 3 were captured with a digital camera attached to a transmission light microscope. To

determine the effect of surface roughness on the spatial extent of dry mucilage structures, radii of mucilage structures at mid distance between particles were measured. Structures were measured in glass beads (0.1-0.2 mm) with a mucilage content of 0.86 and 2.15 mg g^{-1} and stained mixtures of fine sand (0.125-0.2 mm) with a mucilage content of 2.8 and 6.5 mg g^{-1}. Mucilage contents for this analysis were chosen to represent a content below and above the repellent transition threshold across which a substantial decrease of wettability was observed from the SDM measurements.

Synchrotron-based X-ray tomographic microscopy (SRXTM)

SRXTM of cylinders with air-dry maize mucilage amended glass beads were scanned, reconstructed and segmented in order to study their spatial extent (Chapter 2).

SRXTM of air-dry biocrust from Moab, Utah was performed at the Lawrence Berkley National Laboratory in order to compare the three-dimensional extent of mucilage structures in glass beads and naturally occurring structures of high EPS content.

Soil water retention, hydraulic conductivity and evaporation measurements

The soil water retention, unsaturated hydraulic conductivity and evaporative fluxes were derived using the Hyprop setup in an evaporation experiment (Chapter 2). Recorded data of water fluxes and matric potentials were used to parameterize the hydraulic properties of the samples and simulate water flow during the evaporation experiment in order to derive its hydraulic properties.

The evaporative fluxes from hydrated mucilage and deionized water apart from the porous environment of a soil were derived from changes in the weight of mucilage and water filled containers respectively over time. The initial concentration of mucilage was 5.6 mg g^{-1}.

Evaporation from mucilage amended soil – neutron radiography

To capture the effect of mucilage on the water redistribution during soil drying, the water content of mucilage amended loamy sand was monitored using time-series neutron radiography (Chapter 2). Containers of 10 x 1 x 1 cm were filled with sandy loam amended with chia seed mucilage (*Salvia hispanica*) at a content of 4.5 mg g^{-1} as well

as a control filled with sandy loam. Samples were pre-saturated prior to the experiment by capillary rise. To monitor the redistribution of water during soil drying, the water content distribution in sandy loam amended with mucilage and a control was monitored with a time series of neutron radiographies over the course of 4 days.

Quantification of initial wettability – Contact angle measurements

In Chapter 3, the initial wettability of undisturbed and disturbed dry glass bead- and sand-mucilage layers was quantified employing a modified version of the sessile drop method (SDM; Bachmann et al., 2000). Contact angles were determined by placing droplets of deionized water onto the sample surface and capturing the contact angle at the three-phase interface.

Water drop penetration time (WDPT) measurements

To quantify the rewetting behaviour and evaluate the effect of surface roughness, water drops were placed on dry mucilage amended sand, and glass bead mixtures (Chapter 4). Each drop volume was approximated from its optically detected geometry. WDPT was captured across the repellent transition ranging from no observable drop geometry (infiltration within <300 ms) to several minutes above the threshold mucilage content.

1.4. Conceptual model of mucilage and EPS in drying soil (Study 1)

One objective of this study was to provide a mechanistic understanding of the spatial configuration of the liquid phase on the pore scale as affected by mucilage and EPS. The derived concept was to be linked to induced impacts on macroscopic soil hydraulic properties and soil-water dynamics.

Mucilage and EPS increase the viscosity of the soil solution and decrease its surface tension at the gas-liquid interface (Table 1.1). When these highly polymeric blends, as part of the soil solution retreat towards the inter-particle space in drying soil, viscosity increases while surface tension decreases (Fig. 1.2, e.g. Read and Gregory (1997)). Stretching of the gas-liquid interface is eased by a decrease in surface tension according to the Young-Laplace equation (1.2):

$$h = \sigma \left(\frac{1}{r_1} + \frac{1}{r_2} \right) \qquad (1.2)$$

With $h = P_w - P_a$ [Pa] denoting the difference in pressure between the liquid (P_w) and the gas phase (P_a), σ [mN m^{-1}] denoting the surface tension of the gas-liquid interface, and r_1 and r_2 [m] are the radii of the curvature of the gas-liquid interface (negative when the radius points towards the liquid phase). When viscous forces dominate over surface tension and inertia, the break-up of the liquid phase is avoided (Carminati et al., 2017). This relation was described by Ohnesorge (1936) for pendular bridges between particles (1.3):

$$Oh = \frac{\mu}{\sqrt{\rho \sigma r}} \qquad (1.3)$$

with μ [Pa s^{-1}] denoting viscosity, ρ [g m^{-3}] density of the liquid and r [m] the characteristic length corresponding to the radius of the liquid connection. When polymers are concentrated in drying soil, a critical viscosity is reached at which the break-up of liquid connections between particles is prevented. This point is determined by the physical properties of the soil solution, the interaction of mucilage and EPS with the solid matrix and how both parameters change when mucilage and EPS are concentrated during drying.

Fig. 1.4 illustrates the impact of mucilage and EPS content (dry weight of exudate per weight of soil) on the final shape of resulting structures. At low initial content, thin filamentous structures are formed when the critical viscosity is reached at low water content. At intermediate content, break-up is prevented when the viscosity at the gas-liquid interface reaches a critical value while liquid bridges are larger hence at higher water content. The retreat of the polymer network is delayed by high viscosity and when parts of it become attached to solid surfaces behind the drying front. This results in cylindrical bridges between neighbouring particles. At high mucilage and EPS content,

retreat of the polymer network is delayed at even higher water content when the liquid phase is still connected.
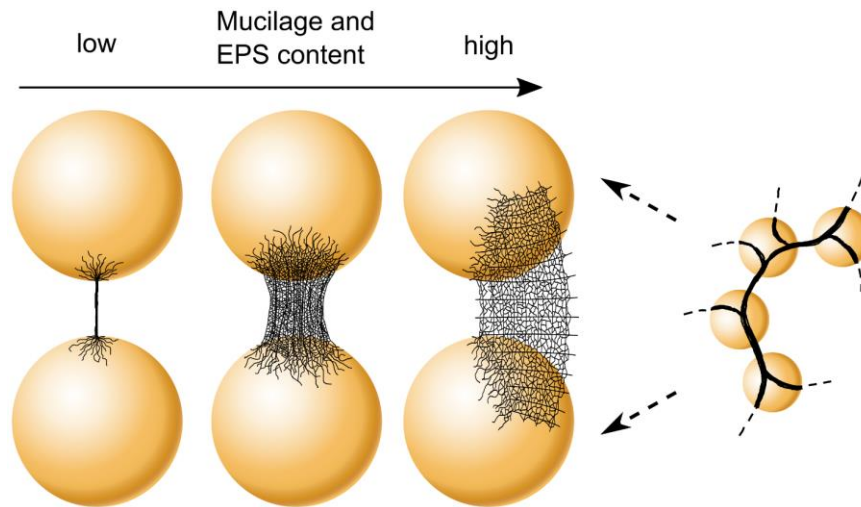
Fig. 1.4: Spatial configuration of EPS and mucilage after drying in porous media. Increased viscosity and decreased surface tension of the liquid phase induced by highly polymeric and surface-active substances released by bacteria and plants lead to the formation of characteristic structures in the pore space of drying soil. At low contents, isolated threads between particles form in large pores at low water content. Hollow cylinders form in small pores and at intermediate contents. Interconnected two-dimensional structures spanning across multiple pores form at high contents.

We hypothesize that this process results in two-dimensional structures that span across multiple soil pores and their formation is closely linked to observed impacts on macroscopic soil properties. Complementary imaging methods were used to support this conceptual model and its implications for macroscopic soil hydraulic properties and soil water dynamics.

Conceptual model of rhizosphere water repellency

When mucilage is concentrated in the pore space upon soil drying, it recedes towards the inter-particle space. In this process, the viscosity of the liquid phase increases while its surface tension decreases (see Chapter 2). For a low mucilage content (weight of dry mucilage per weight of soil), mucilage separates from the liquid phase creating non-wettable structures that can be bypassed by water (Fig. 1.5 left side). Pores become non-wettable when a critical mucilage content is reached, and water can no longer bypass dry mucilage deposits (Fig. 1.5 right side). When a critical fraction of pores is affected in such way, macroscopic soil water repellency is observed.
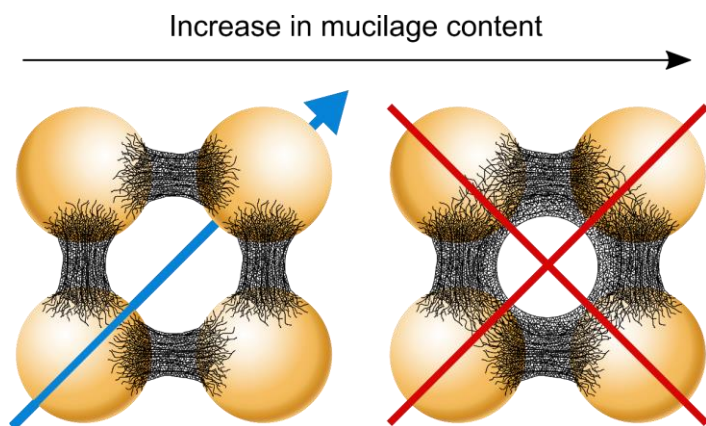
Fig. 1.5: Conceptual model of mucilage induced soil water repellency. At low mucilage content, dry mucilage structures can be bypassed by infiltrating water (left side), while at high mucilage content, structures extend into the open pore space (right side). At this point, a pore turns water repellent. Macroscopic soil water repellency is observed when a critical fraction of pores is affected in this way.

Model of water drop infiltration

To evaluate the impact of heterogeneous pore-scale wettability on water infiltration in the rhizosphere, we developed a simple pore-network model (Chapter 4). Like in a percolation system, pores of different size (normally distributed) are randomly distributed on a cubic lattice. Under the assumption that small pores are affected first, at low mucilage content respectively, mucilage is distributed preferentially in small pores. The contact angle of each pore depends on its surface area and mucilage content according to Fig. 1.6. Due to the combined effect of preferential distribution and the relation of surface area to mucilage content, large pores turn non-wettable only at high mucilage contents.
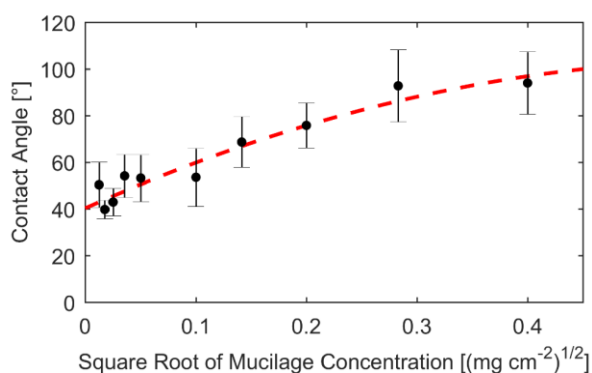
Fig. 1.6: Contact angle measured on glass slides covered with different concentrations of mucilage per surface area (dots). Standard deviation indicated by error bars. Fit of measured contact angles against square root of mucilage concentration per surface area (dashed line).

Flow is assumed to be capillary driven with pores only being filled from the wet surface or from adjacent saturated pores through a cylindrical pipe by integrating the Young-Laplace equation into the Hagen-Poiseuille equation; The first denoting the driving force or capillary pressure in a cylindrical tube and the latter the resistance to flow due to the

no-slip condition at the boundary. Given the volumetric flow rate $Q = V/t$ [mm³ ms⁻¹] one obtains the time t [ms] to fill a pore of volume V [mm³] through a cylindrical pipe (1.1):

$$t = \frac{\mu\,8}{\pi\,r^4}\frac{r}{2\,\sigma\,cos(\alpha)}\frac{L_{tot}}{1}\frac{V}{1} \tag{1.1}$$

with capillary radius r [mm], surface tension σ [mN mm⁻¹], contact angle α [deg.], viscosity of water μ [mN ms mm⁻²] and total length of the flow path L_{tot} [mm].

The shortest time to fill the next pore is calculated at each iteration and the water content of each pore currently being filled is updated according to this time step. At the same time, evaporation from the surface of the drop is approximated according to the method of Hu and Larson (2002). Maximum time step is fixed to 1 s to allow for a constant update of evaporative loss. Simulation ends once the drop volume is depleted. An exemplary simulation of drop infiltration in a wettable fine sand is illustrated in Fig. 1.7.
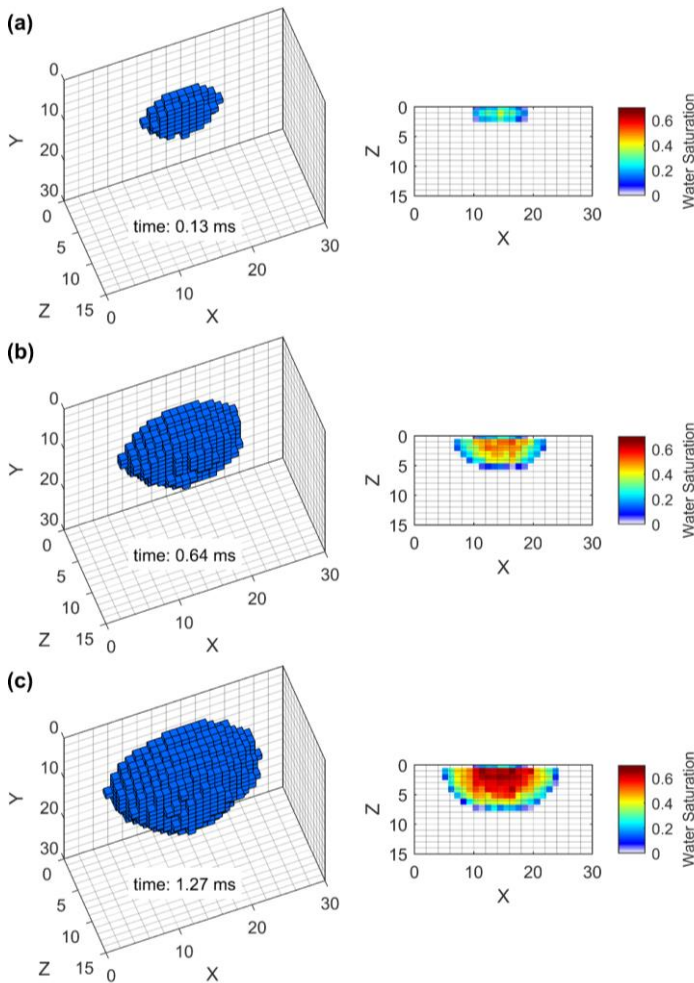
Fig. 1.7: Exemplary water drop infiltration in a wettable fine sand. Left parts of **(a)**, **(b)**, **(c)** illustrate the distribution of saturated pores at different times during infiltration. Right parts illustrate the average water saturation of the domain in y-direction. Time increases from **(a)** to **(c)**, with **(c)** illustrating the final distribution of a 1 μL drop-let in the soil pore space after 1.27 ms.

1.5. Results & Discussion

Microhydrological niches in soils: how mucilage and EPS alter the biophysical properties of the rhizosphere and other biological hotspots (Study 1)

Fig. 1.8 summarizes the results of different imaging studies on the spatial distribution of dry mucilage and EPS structures in soil. These results provide evidence supporting the conceptual model previously presented. At low mucilage (*Slavia hispanica*) content, mucilage structures are shaped like thin threads stretching across large pores (e.g. Fig. 1.8a). At intermediate mucilage (*Slavia hispanica*) content, mucilage forms hollow cylinders between particles (Fig. 1.8b; the interior of such a structure is shown in Fig. 1.14b). Two-dimensional layers predicted for high mucilage content are shown in Fig. 1.8c-e. Mucilage (*Zea mays*) formed a continuous surface across multiple pores. Similar structures were observed in biocrusts as well (Fig. 1.8c). The apparent similarity (thickness and spatial extent) between two-dimensional mucilage and EPS structures is striking.

Mucilage and EPS alter the physical properties of the soil solution and by that the spatial configuration of the liquid phase in drying soil. This results in the formation of characteristic structures upon drying in porous media as shown in Fig. 1.8. The process leading to their formation on the pore scale can be linked to alterations of macroscopic soil hydraulic properties and water dynamics.

Fig. 1.9 shows the water retention curve of mucilage amended soil and a control soil saturated with water. Water retention of the treated soil was increased at all matric potentials. Soil hydraulic conductivity on the other hand was initially lower than in the control soil but its drop with decrease in water potential was less pronounced. At about -10^4 cm, lines cross and the hydraulic conductivity of the treated soil was higher when compared to the control (Fig. 1.9b).
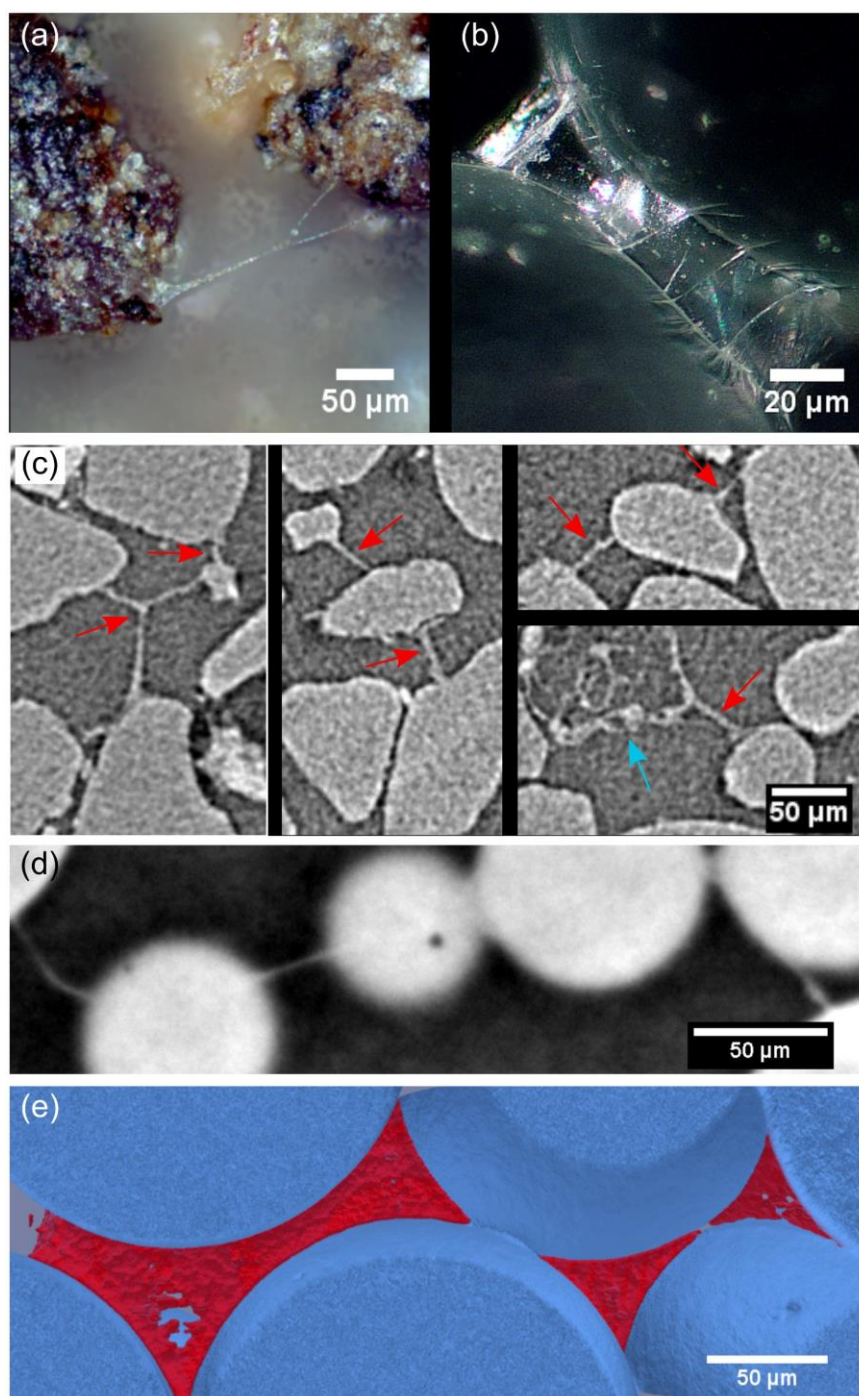
Fig. 1.8: Examples of dry mucilage and EPS structures in porous media. (a) Light microscope image of threads of mucilage (*Slavia hispanica*; mucilage content 4.5 mg g⁻¹ [mg dry mucilage per g of particles]) formed across a large pore during drying; **(b)** Light microscope image of a cylindrical bridge formed between neighbouring glass beads (1.7-2 mm in diameter) at intermediate mucilage content (0.7 mg g⁻¹); **(c)** Two-dimensional EPS structures joining quartz grains in intact biocrusts imaged with synchrotron-based X-ray tomographic microscopy (Couradeau et al., 2018). High EPS content resulted in the formation of characteristic structures (red arrows) comparable to those formed by maize mucilage. The blue arrow marks a cyanobacterial bundle with the EPS sheath surrounding the trichomes of *Microcoleus vaginatus*. **(d)** Cross-section through a synchrotron-based X-ray tomographic microscopy volume of dry maize mucilage (*Zea mays*) structures in glass beads (mucilage content 8 mg g⁻¹; glass bead diameter 0.1 – 0.2 mm); **(e)** 3D segmentation of dry mucilage structures (red) from (d) which formed interconnected surfaces of approximately 1 µm thickness within the pore space of glass beads (blue).

15

(a)

(b)

So far, alterations of soil hydraulic properties and water dynamics, like increased soil water retention induced by mucilage and EPS were mostly ascribed to the hygroscopic properties of their polymer network. The fact that neither mucilage (see Fig. 1.11 and McCully and Boyer 1997) nor EPS (Deng et al., 2015) show a substantial resistance to drying outside a porous geometry and water retention in fine soils is amplified (Kroener et al., 2018) indicates that the hygroscopic properties alone cannot explain observed alterations of macroscopic soil properties.

When mucilage and EPS dry within a porous medium, collapse of the polymer network by decrease in capillary pressure is partly prevented when viscosity dominates over inertia and surface tension ($Oh > 1$) and the continuity of the liquid phase is preserved (Fig. 1.10b). Additionally, the entanglement of polymers with solid surfaces and their accumulation at the gas-liquid interface limits the velocity of the retreating water. These mechanisms have a combined effect on soil hydraulic conductivity and soil water retention (Fig. 1.10). Soil water retention is increased due to the intrinsic affinity of mucilage and EPS to absorb water *and* possibly further enhanced by the fixation of the hydrated polymer network to the dense stiff polymer network at the gas-liquid

interface which itself is partly fixed to solid surfaces. In this way, the interaction of the polymer network with soil particles can lead to the creation of a force opposing the decrease in capillary pressure in drying soil, an additional matric potential. Although this theory appears conclusive, quantification of contributing forces, namely water absorption and additional matric potential created in a porous environment is missing.

Fig. 1.11 summarizes the results of the evaporation experiments conducted with mucilage amended soil using the Hyprop setup. Chia seed mucilage apart from the porous geometry of a soil showed no distinct resistance to drying when compared to water (Fig. 1.11a). On the other hand, mucilage strongly reduced the evaporative flux from soil (Fig. 1.11ab). Monitored water content distribution from time-series neutron radiography showed similarly slow drying of mucilage treated soil (Fig. 1.12b). The upper layer of the treated soil quickly dried while the lower volume remained at a higher water content when compared to the control soil till the end of the experiment.

Such decrease in drying rate was observed for EPS affected soil as well (Zheng et al., 2018). The authors related it to a decrease in saturated hydraulic conductivity and surface tension induced by EPS causing a discrepancy between evaporative flux from the soil surface and replenishment by capillary transport from the bulk soil. This leads to a break-up of the liquid phase which marks the transition from Stage I (evaporation from the soil surface) to Stage II of soil drying (Zheng et al., 2018). At this point, drying is mainly controlled by vapour diffusion through the pore space (Lehmann et al., 2008).

We showed that drying of mucilage and EPS within soil leads to the formation of 2D surfaces spanning across the pore space. The quick drying of the upper layer of mucilage treated soil (Fig. 1.12b) can be explained according to the interpretation of Zheng et al. (2018) by a discrepancy in evaporated water from the soil surface and limited supply by capillary transport. The share of lowered hydraulic conductivity and reduced surface tension leading to a break-up of the liquid phase remains unknown but the quick transition to vapor diffusion dominated soil drying is evident. In addition to the fast transition from Stage I to Stage II in soil drying, which leads to a reduction in drying rates, 2D mucilage surfaces (e.g. Fig. 1.8d-e) formed during the transition could reduce vapor diffusion through the dry soil layer. A similar effect can be expected in EPS affected soils as biocrusts, since a quick transition to vapor diffusion dominated drying is likely to occur in sandy soils of arid regions and the EPS structures observed from dry biocrust appear very similar to those of mucilage (Fig. 1.8c-e).

Increased soil water retention, hydraulic conductivity in dry soil and decelerated soil drying provide several advantages to organisms like plants and bacteria inhabiting the soil pore space. Described alterations allow to extend periods of biological activity and grant additional time for metabolic adaptions to endure less favourable hydraulic conditions.
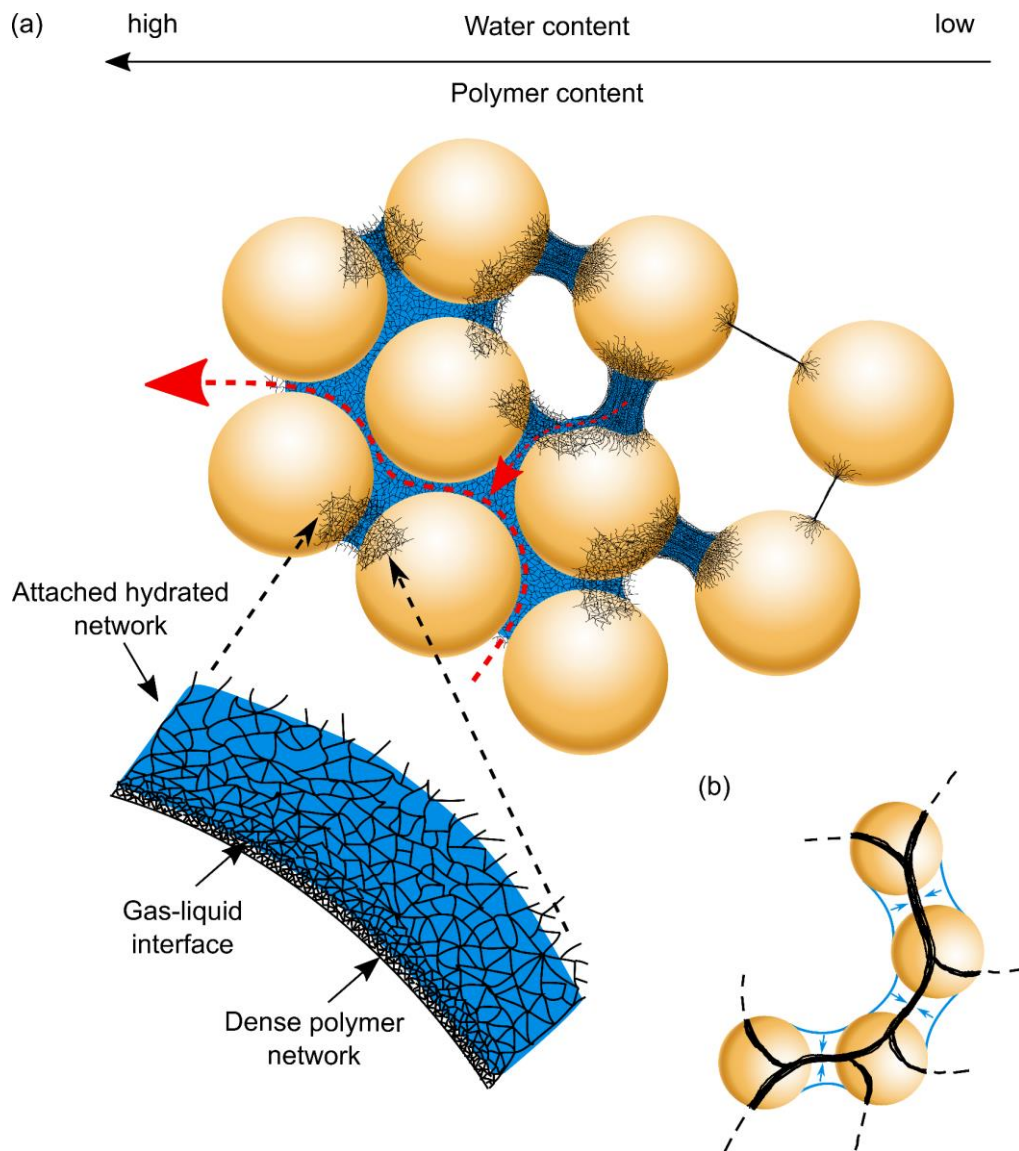
Fig. 1.10: Configuration of the liquid phase in soils containing EPS or mucilage. (a) In this illustration, the concentration of EPS or mucilage increases from the right to the left side. During drying, the gas-liquid interface retreats and polymers accumulate at this interface. At low polymer contents, the gas-liquid interface retreats but the liquid phase is not broken, which results in the formation of thin threads. At higher polymer contents, the gas-liquid interface stiffens due to the entanglement of polymers among themselves and with soil particles. As drying progresses, the gas-liquid interface can no longer be stretched and starts to act as an additional matrix. Together with the hygroscopic nature of the polymers, this leads to an amplified soil water retention. Beside this effect, evolving structures preserve the continuity of the liquid phase (the flow of water is illustrated by the dashed red arrows. **(b)** The liquid phase remains connected during drying, with the liquid converging into two-dimensional surfaces as imaged in Fig. 1.8c-e. This induces a shift towards higher hydraulic conductivity in dry soils (e.g. Fig. 1.9b).

18
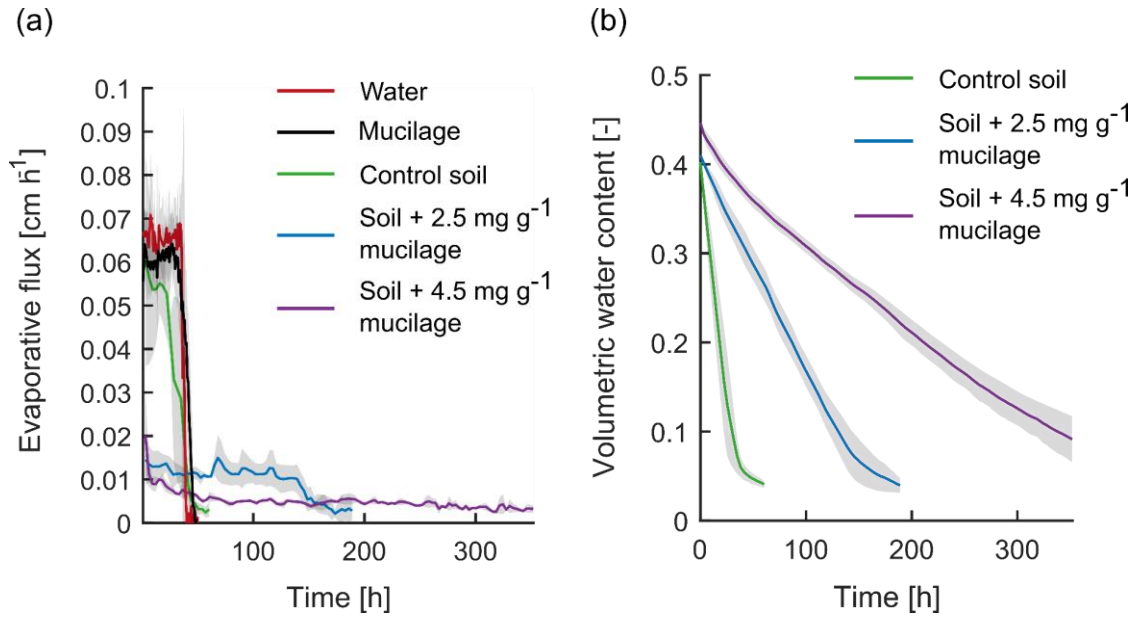
Fig. 1.11: Evaporative flux and decrease in water content for water and mucilage separated and mixed with soil. Mucilage within the pore space of sandy soil results in a marked decrease in evaporative flux and a delay in soil drying. **(a)** Evaporative flux from free water (red), mucilage (black), control soil saturated with water (green), and soil treated with mucilage (mucilage content 2.5 mg g^{-1} (blue); mucilage content 4.5 mg g^{-1} (purple); *Salvia hispanica*); **(b)** Decrease in water content from an evaporation experiment in soil amended with mucilage (control soil (green), mucilage content 2.5 mg g^{-1} (blue); mucilage content 4.5 mg g^{-1} (purple); *Salvia hispanica*); solid lines indicate the mean of three measurements and grey areas indicate the 95% confidence interval of three replicates.

Fig. 1.12: Delay in evaporation induced by the formation of dense polymer layers in the soil pore space. (a) Dense layers of desiccated polymeric structures limit the evaporative flux of water vapor through the soil and delay its drying; **(b)** Neutron radiographs of two soil columns saturated with water (top) and amended with mucilage (mucilage content 4.5 mg g^{-1}; *Salvia hispanica*; bottom) over the course of 4 days. The uppermost layer (red arrow) of the mucilage treated soil dried comparably quick while the underlying pore space remained wet.

19

Pore-scale distribution of mucilage affecting water repellency in the rhizosphere (Study 2)

The aim of this study was to evaluate the impact of pore-scale mucilage distribution, soil texture and surface roughness on initial rhizosphere wettability. Fig. 1.13 summarizes the results of contact angle measurements of mucilage amended textures. Initial contact angles showed a threshold-like increase while the range of mucilage contents across observed thresholds increased with decreasing particle size. Disturbed samples showed no such behaviour but a gradual increase in apparent contact angle with increase in mucilage content.

Results of the microscopy study of mucilage structures are summarized in Table 1.2. The average radius of dry mucilage structures increased while their number decreased across the repellent transition for both smooth glass beads and fine sand of comparable grain size. The extent of structures above the repellent transition in glass beads reached about 80 µm in radius at 2 mg g^{-1} while similar extent was achieved for fine sand for mucilage content three times higher (6 mg g^{-1}). The higher standard deviation in radii at high mucilage content in sand (76 µm) compared to glass beads (48 µm) can be interpreted as a higher diversity in the shape of mucilage structures.

Table 1.2: Mean dry mucilage bridge radii in glass beads and fine sand for mucilage contents in the mixture below and above the 300-ms infiltration threshold (in mg g^{-1}). Differences in the distribution of bridge radii between different mucilage contents within the same particle size were significant ($p < 0.05$). Mean bridge radii increased and number of observed discrete structures (n) decreased with increasing mucilage content.

Parameter	Dry mucilage bridge radius			
	Glass beads (0.1–0.2mm)		Fine sand (0.125–0.2mm)	
	0.86 mg g^{-1}	2.15 mg g^{-1}	2.8 mg g^{-1}	6.5 mg g^{-1}
Mean bridge radius, µm	30.09	79.59	20.9	80.42
Standard deviation	27.86	48.25	31.09	76.16
Standard error	1.90	3.90	2.28	6.02
n	215	153	186	160
p value	<0.05		<0.05	

Higher mucilage content was needed to cross the repellent transition with decrease in particle size (Fig. 1.13). This is explained by the two-dimensional geometry of dry mucilage structures in the pore space (e.g. Fig. 1.8). Fig. 1.14ab shows broken bridges of dry mucilage, formed between glass beads of 1.7-2 mm in diameter. The connection is shaped like a hollow cylinder. Assuming the pore volume in fine and coarse soil is equal while the number of pores increases with decreasing particle size, more two-

dimensional mucilage structures can be expected to form in finer textures. Due to their geometry, the volume to surface area ratio is bigger when less, big structures are formed in coarse soil. This explains why wettability is more effectively reduced by hydrophobic mucilage structures in coarse textures.
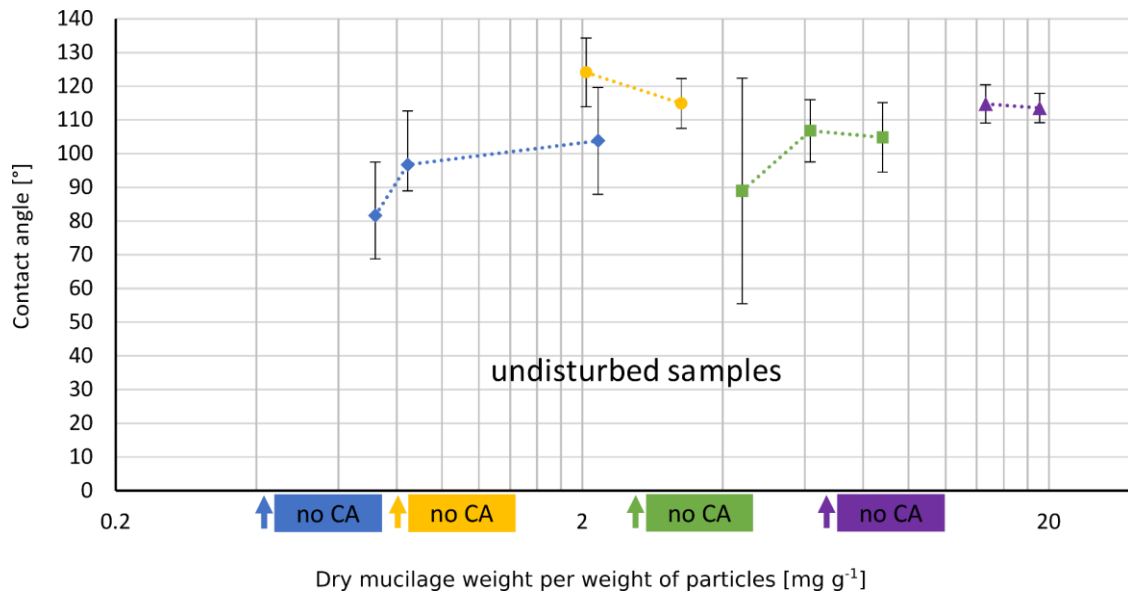
Fig. 1.13: Mean contact angle of (a) undisturbed dry mucilage–soil mixtures at various dry mucilage contents in sand and glass beads of different particle diameters. Contact angles of undisturbed samples followed a threshold-like behaviour with a sudden occurrence of apparent contact angles **(a)**. Different particle sizes are indicated by different colours. Standard deviations are indicated by grey error bars.

A similar explanation applies to the comparison of smooth glass beads and fine sand. In fine sand, surface roughness results in a higher fractionation of the liquid phase during drying. This results in mucilage being trapped in cavities and along surface irregularities across the inter-particle space which finally results in a larger number of mucilage structures (e.g. Fig. 1.14cd). These structures being less effective in blocking a given pore volume. This explains the observed decrease in macroscopic wettability with in-crease in particle size and vice versa.
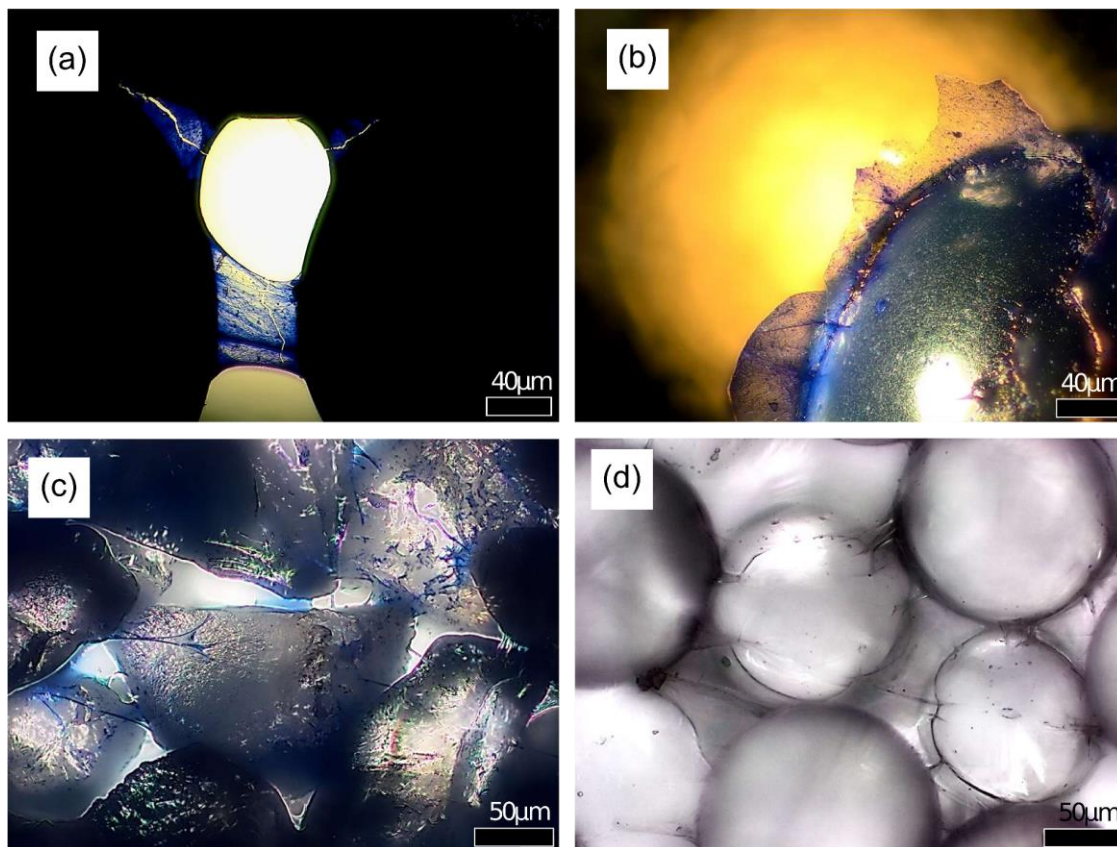
Fig. 1.14: Transmission light microscopy images of dry undisturbed samples of mucilage (*Salvia hispanica*) particle mixtures. (a,b): Images of dry, stained mucilage bridges between glass beads (1.7-2 mm in diameter) at a mucilage content of 0.35 mg g^{-1} stained with a 33% ink–water solution. Images illustrate the two-dimensional extent of mucilage structures, here similar to hollow cylinders (see also Fig. 1.4 and Fig. 1.8). **(c,d)**: dry mucilage (*Salvia hispanica*) structures at comparable content in fine sand (2.8 mg g^{-1}, c) and glass beads (2.15 mg g^{-1}, **d**). Comparison illustrates the effect of surface roughness on the extent of dry mucilage structures and the fraction of pore volume affected by these structures.

Impact of pore-scale wettability on rhizosphere rewetting (Study 3)

The aim of Study 3 was to assess the impact of heterogeneous pore-scale wettability and specific soil surface area on rhizosphere rewetting dynamics. Assessment was done experimentally by means of WDPT (water drop penetration time) tests. The impact of heterogeneous pore-scale wettability was evaluated numerically by simulation of water drop infiltration experiments.

Results of WDPT measurements and simulations are displayed in Fig. 1.15. Fitted measurement and simulation in glass beads and sand showed an increase in WDPT with increase in mucilage content. The threshold mucilage content was identified from simulations between 2.5 and 2.8 mg g^{-1} for glass beads and at about 4.9 mg g^{-1} in sand. In both cases, decrease in penetration time was followed by a substantial decline in

macroscopic wettability. A high variability in penetration time was observed from measurements and simulations across the repellent transition.

The simple pore network model employed to evaluate the impact of heterogeneous pore-scale wettability was capable to capture the threshold-like nature of water infiltration in mucilage affected porous media. Despite the simplicity of the employed model, it highlights the relevance of heterogeneous wettability on the pore scale for water flow through the rhizosphere. With regard to the concept presented in Study 1, the connectivity of dry mucilage structures appears to be not only of fundamental importance for the physical properties of biological hotspots when soil dries but also for the rewetting rate. Water repellency during rewetting of the rhizosphere was observed for different combinations of plant species and soils (Carminati et al., 2010; Moradi et al., 2012; Ahmed et al., 2016). For mucilage contents above the repellent transition, substantially affected (water repellent) pores created a continuous cluster preventing water to percolate through the system. In relation to previous observations like reduced drying rates by limited vapor diffusion through dry mucilage affected soil (Study 1), this study provides further evidence for the potential impact of mucilage induced increase in connectivity of the soil pore space from a different perspective. Bearing in mind observations of rhizosphere water repellency and continuous clusters of water repellent pores inducing a similar effect, the presence of highly connected mucilage structures as shown in Fig. 1.8 appears most likely within the complex environment of the rhizosphere.
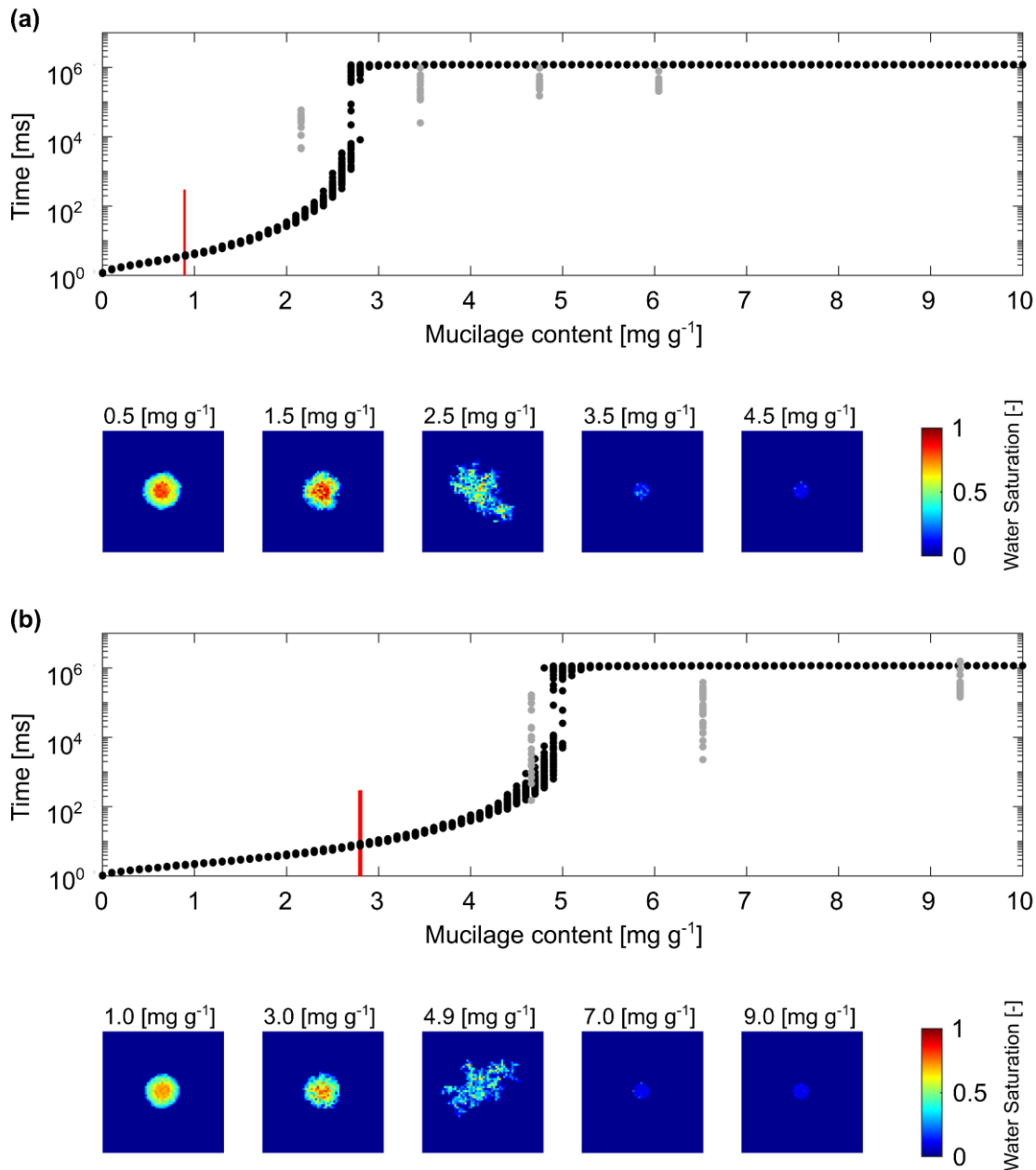
Fig. 1.15: Water drop penetration time (WDPT) derived from optically detected drop volume decrease (grey dots) and simulated WDPT (black dots) alongside top views of average final water saturation of exemplary simulations across the repellent transition. **(a)** WDPT measured and simulated in glass beads (0.1-0.2 mm diameter); Detection limit of 300 ms indicated by a red bar at 0.9 mg g^{-1}. **(b)** WDPT measured and simulated in sand (0.125-0.2 mm diameter); Detection limit of 300 ms indicated by a red bar at 2.8 mg g^{-1}.

1.6. Summary, conclusions and outlook

The aim of this work was to gain a mechanistic understanding of how mucilage and EPS interact with the soil matrix and how these interactions impact local soil physical properties during drying and rewetting. The induced increase in viscosity, decrease in surface tension and the entanglement of the polymeric solution with the soil matrix in-

duces the formation of a viscous, interconnected network. When the soil dries, the liquid phase retreats towards the inter-particle space and mucilage and EPS become increasingly concentrated. Consequently, the viscosity of the soil solution increases and acts against the decreasing surface tension in shaping the three-dimensional liquid phase. Simultaneously, the polymers which are dragged along the soil solid surfaces, are progressively stretched and accumulate at the air-liquid interface. This process eventually delays the retreat of the liquid phase, prevents the break-up of the liquid phase and induces shifts in soil hydraulic properties and soil water dynamics. The main mechanisms are summarised in these points:

1. Break-up of the liquid phase is prevented when a critical viscosity is reached that dominates over surface tension in shaping the soil solution. This preserves the liquid connectivity during soil drying and increases the soil hydraulic conductivity.

2. An additional matric potential is created when the retreat of the liquid phase is impeded by the polymer solution and its entanglement with the solid particles. Once the retreat is limited, the hydrated part of the polymer network attached to its dense stiff part at the gas-liquid interface is no longer free to move. Along with the hygroscopic nature of the polymer solution, this process leads to an increased soil water retention by creation of an additional matric (capillary) potential.

3. The formation of clusters of 2D surfaces across the pore space limits the diffusion of water vapour through dry soils and delays the drying of underlying wet soil. Beside other mechanisms (e.g. the mitigation of a decrease in hydraulic conductivity of dry soil), these barriers represent another form of hydraulic decoupling.

4. The heterogeneous distribution of dry mucilage on the pore scale induces the threshold-like emergence of macroscopic soil water repellency. Wettability of amended soil abruptly decreases when clusters of 2D surfaces start to form. In combination with the low hydraulic conductivity of highly concentrated mucilage in form of 2D structures, this partly explains the low wettability of dry rhizosphere described in the literature (e.g. Carminati et al. 2010).

The physical alteration of the soil solution by mucilage and EPS and the interaction of these highly polymeric blends with the soil pore space have manifold implications for the edaphic way of life. When soil dries and water is drained from its pores, the liquid connectivity diminishes. Consequently, the availability of water and solutes (e.g. nutrients) fades as well. Induced physical alterations of the soil solution prevent the break-up of the liquid phase and buffer fluctuations of hydraulic conductivity. In this way, mucilage and EPS support biological activity in a challenging environment like drying soil. Mucilage in the rhizosphere could help plants to sustain high transpiration in drying soils by mitigating a sharp drop in hydraulic conductivity close to the roots. Bacteria could ensure the diffusion of nutrients and chemical signals from their surroundings. The effect of this mechanism is enhanced by the hygroscopic nature of the polymer network attracting water to regions of high liquid connectivity. In severely dry soils, mucilage and EPS act as a diffusion barrier for water vapor, decelerating water loss from the underlying wet pore space. Like the increased connectivity of the soil solution or enhanced water retention, this process hydraulically decouples biological hotspots from the rest of the bulk soil. Dry mucilage structures delay the rewetting of the rhizosphere. In this way, mucilage can prevent the leaching of nutrients and microorganisms from the rhizosphere and the exposure of bacteria to harmful gradients in osmotic pressure.

In order to identify and describe the pore-scale physical mechanisms involved in changes of soil hydraulic properties and water dynamics induced by mucilage and EPS, many of the presented experiments were conducted using simplified set-ups – chia and maize mucilage in sand and loess. Imaging, analysis and quantification of EPS and mucilage in undisturbed environments will be needed in order to understand the ultimate impact of our findings. This could help to select for more stress resistant crops and associated microbial communities.

1.7. Contribution to included publications

Study 1: Microhydrological niches in soils: how mucilage and EPS alter the biophysical properties of the rhizosphere and other biological hotspots

Articles in press in Vadose Zone Journal, 2019, doi: http://dx.doi.org/10.2136 %20/vzj2018.12.0211

Author contributions: P.B. wrote the manuscript under supervision of A.C.. P.B., A.C. and M.Z. developed the conceptual model. E.C. conducted the synchrotron-based X-ray tomographic microscopy of biocrust at ALS (LBNL) and V. F. analysed the data. P.B., A.C., I.J. and F.M. conducted the synchrotron-based X-ray tomographic microscopy of maize mucilage in glass beads and sand at SLS (PSI). P.B. and M.Z. analysed and segmented particles and mucilage structures from reconstructed volumes. M.Z. conducted the measurements of water retention and hydraulic conductivity using the Hyprop setup. P.B. and M.Z. conducted the experiments to determine the evaporative flux and decrease in volumetric water content from seed mucilage and seed mucilage amended silty soil. M.Z. and A.K. conducted the neutron radiography of the evaporation experiment from mucilage amended silty soil and control soil. M.B. and R.K. conducted ESEM imaging of seed mucilage structures in glass beads which were not included in the manuscript. P.B. conducted the light microscopy imaging of seed mucilage structures in soils and glass beads. All authors reviewed and commented on the manuscript.

Study 2: Pore-scale distribution of mucilage affecting water repellency in the rhizosphere

Published in Vadose Zone Journal, 2018, doi: http://dx.doi.org/10.2136/vzj2017. 01.0013

Author contributions: P.B. prepared the samples of soil-mucilage mixtures under supervision of M.Z.. P.B. quantified the wettability of dry soil-mucilage mixtures and stained, imaged and quantified mucilage structures using light microscopy. P.B. and A.C. developed the conceptual model. P.B. wrote the manuscript under supervision of A.C.. M.H. did the statistical analysis. C.H. performed preliminary experiments to locate thresholds of mucilage contents in different textures. All authors reviewed and commented on the manuscript.

Study 3: Impact of pore-scale wettability on rhizosphere rewetting

Published in Frontiers in Environmental Science, 2018, doi: http://dx.doi.org/10.3389/fenvs.2018.00016

Author contributions: P.B., M.Z., and A.C. conceived the experimental set-up. P.B. conducted the experiments and processed the data. P.B. and A.C. developed the conceptual model. P.B. developed the numerical code and wrote the manuscript in consultation with M.Z. and A.C..

1.8. References

Adessi, A., R. Cruz de Carvalho, R. De Philippis, C. Branquinho, and J. Marques da Silva. 2018. Microbial extracellular polymeric substances improve water retention in dryland biological soil crusts. Soil Biology and Biochemistry 116: 67–69. doi: 10.1016/j.soilbio.2017.10.002

Ahmed, M.A., E. Kroener, P. Benard, M. Zarebanadkouki, A. Kaestner, et al. 2016. Drying of mucilage causes water repellency in the rhizosphere of maize: measurements and modelling. Plant and Soil 407(1–2): 161–171. doi: 10.1007/s11104-015-2749-1

Albalasmeh, A.A., and T.A. Ghezzehei. 2014. Interplay between soil drying and root exudation in rhizosheath development. Plant and Soil 374(1–2): 739–751. doi: 10.1007/s11104-013-1910-y

Bachmann, J., A. Ellies, and K.H. Hartge. 2000. Development and application of a new sessile drop contact angle method to assess soil water repellency. Journal of Hydrology 231: 66–75. doi:10.1016/S0022-1694(00)00184-0

Benard, P., Zarebanadkouki, M., Brax, M., Kaltenbach, R., Jerjen, I., Marone, F., Couradeau, E., Felde, V. J. M. N. L., Kaestner, A., Carminati, A. 2019. Microhydrological niches in soils: how mucilage and EPS alter the biophysical properties of the rhizosphere and other biological hotspots. Vadose Zone Journal doi: 10.2136/vzj2018.12.0211

Benard, P., Zarebanadkouki, M., and Carminati, A. 2018. Impact of Pore-Scale Wettability on Rhizosphere Rewetting. Frontiers in Environmental Science 6. doi: 10.3389/fenvs.2018.00016

Benard, P., Zarebanadkouki, M., Hedwig, C., Holz, M., Ahmed, M.A., Carminati, A. 2018. Pore-Scale Distribution of Mucilage Affecting Water Repellency in the Rhizosphere. Vadose Zone Journal 17(1): 0. doi: 10.2136/vzj2017.01.0013

Bengough, A.G. 2012. Water Dynamics of the Root Zone: Rhizosphere Biophysics and Its Control on Soil Hydrology. Vadose Zone Journal 11(2): 0. doi: 10.2136 /vzj2011.0111

Brinker, C.J., and G.W. Scherer. 1990. Sol-gel science: the physics and chemistry of sol-gel processing. Academic Press, Boston.

Carminati, A., P. Benard, M.A. Ahmed, and M. Zarebanadkouki. 2017. Liquid bridges at the root-soil interface. Plant and Soil. doi: 10.1007/s11104-017-3227-8

Carminati, A., A.B. Moradi, D. Vetterlein, P. Vontobel, E. Lehmann, et al. 2010. Dynamics of soil water content in the rhizosphere. Plant and Soil 332(1–2): 163– 176. doi: 10.1007/s11104-010-0283-8

Carminati, A., and D. Vetterlein. 2013. Plasticity of rhizosphere hydraulic properties as a key for efficient utilization of scarce resources. Annals of Botany 112(2): 277– 290. doi: 10.1093/aob/mcs262

Chamizo, S., J. Belnap, D.J. Eldridge, Y. Cantón, and O. Malam Issa. 2016. The Role of Biocrusts in Arid Land Hydrology. In: Weber, B., Büdel, B., and Belnap, J., editors, Biological Soil Crusts: An Organizing Principle in Drylands. Springer International Publishing, Cham. p. 321–346

Chenu, C. 1993. Clay-or sand-polysaccharide associations as models for the interface between micro-organisms and soil: water related properties and microstructure. Geoderma 56(1–4): 143–156. doi: 10.1016/0016-7061(93)90106-U

Couradeau, E., V.J.M.N.L. Felde, D. Parkinson, D. Uteau, A. Rochet, et al. 2018. In Situ X-Ray Tomography Imaging of Soil Water and Cyanobacteria From Biological Soil Crusts Undergoing Desiccation. Frontiers in Environmental Science 6. doi: 10.3389/fenvs.2018.00065

Deng, J., E.P. Orner, J.F. Chau, E.M. Anderson, A.L. Kadilak, et al. 2015. Synergistic effects of soil microstructure and bacterial EPS on drying rate in emulated soil micromodels. Soil Biology and Biochemistry 83: 116–124. doi: 10.1016 /j.soilbio.2014.12.006

Elbert, W., B. Weber, S. Burrows, J. Steinkamp, B. Büdel, et al. 2012. Contribution of cryptogamic covers to the global cycles of carbon and nitrogen. Nature Geoscience 5(7): 459–462. doi: 10.1038/ngeo1486

Flemming, H.-C., and J. Wingender. 2001. Relevance of microbial extracellular polymeric substances (EPSs)-Part I: Structural and ecological aspects. Water science and technology 43(6): 1–8. doi: 10.2166/wst.2001.0326

Flemming, H.-C., and J. Wingender. 2010. The biofilm matrix. Nature Reviews Microbiology 8(9): 623–633. doi: 10.1038/nrmicro2415

Flemming, H.-C., J. Wingender, U. Szewzyk, P. Steinberg, S.A. Rice, et al. 2016. Biofilms: an emergent form of bacterial life. Nature Reviews Microbiology 14(9): 563–575. doi: 10.1038/nrmicro.2016.94

Gregory, P.J. 2006. Roots, rhizosphere and soil: the route to a better understanding of soil science? European Journal of Soil Science 57(1): 2–12. doi: 10.1111/j.1365-2389.2005.00778.x

Hallett, P.D., D.C. Gordon, and A.G. Bengough. 2003. Plant influence on rhizosphere hydraulic properties: direct measurements using a miniaturized infiltrometer. New Phytologist 157(3): 597–603. doi: 10.1046/j.1469-8137.2003.00690.x

Hinsinger, P., A.G. Bengough, D. Vetterlein, and I.M. Young. 2009. Rhizosphere: biophysics, biogeochemistry and ecological relevance. Plant and Soil 321(1–2): 117–152. doi: 10.1007/s11104-008-9885-9

Hu, H., and R.G. Larson. 2002. Evaporation of a Sessile Droplet on a Substrate. The Journal of Physical Chemistry B 106(6): 1334–1344. doi: 10.1021/jp0118322

Körstgens, V., H.C. Flemming, J. Wingender, and W. Borchard. 2001. Influence of calcium ions on the mechanical properties of a model biofilm of mucoid Pseudomonas aeruginosa. Water Sci. Technol. 43(6): 49–57. doi: 10.2166/wst.2001.0338

Kroener, E., M. Holz, M. Zarebanadkouki, M. Ahmed, and A. Carminati. 2018. Effects of Mucilage on Rhizosphere Hydraulic Functions Depend on Soil Particle Size. Vadose Zone Journal 17(1): 0. doi: 10.2136/vzj2017.03.0056

Kroener, E., M. Zarebanadkouki, A. Kaestner, and A. Carminati. 2014. Nonequilibrium water dynamics in the rhizosphere: How mucilage affects water flow in soils. Water Resources Research 50(8): 6479–6495. doi: 10.1002/2013WR014756

Lehmann, P., S. Assouline, and D. Or. 2008. Characteristic lengths affecting evaporative drying of porous media. Physical Review E 77(5). doi: 10.1103/PhysRevE.77.056309

Lieleg, O., M. Caldara, R. Baumgärtel, and K. Ribbeck. 2011. Mechanical robustness of Pseudomonas aeruginosa biofilms. Soft Matter 7(7): 3307. doi: 10.1039/c0sm01467b

Lin, K.-Y., J.R. Daniel, and R.L. Whistler. 1994. Structure of chia seed polysaccharide exudate. Carbohydrate Polymers 23(1): 13–18. doi: 10.1016/0144-8617(94)90085-X

McCully, M.E., and J.S. Boyer. 1997. The expansion of maize root-cap mucilage during hydration. 3. Changes in water potential and water content. Physiologia Plantarum 99(1): 169–177. doi: 10.1111/j.1399-3054.1997.tb03445.x

Moradi, A.B., A. Carminati, A. Lamparter, S.K. Woche, J. Bachmann, et al. 2012. Is the Rhizosphere Temporarily Water Repellent? Vadose Zone Journal 11(3): 0. doi: 10.2136/vzj2011.0120

Moradi, A.B., A. Carminati, D. Vetterlein, P. Vontobel, E. Lehmann, et al. 2011. Three-dimensional visualization and quantification of water content in the rhizosphere. New Phytologist 192(3): 653–663. doi: 10.1111/j.1469-8137.2011.03826.x

Naveed, M., L.K. Brown, A.C. Raffan, T.S. George, A.G. Bengough, et al. 2017. Plant exudates may stabilize or weaken soil depending on species, origin and time: Effect of plant exudates on rhizosphere formation. European Journal of Soil Science (68): 806–816. doi: 10.1111/ejss.12487

Naveed, M., L.K. Brown, A.C. Raffan, T.S. George, A.G. Bengough, et al. 2018. Rhizosphere-Scale Quantification of Hydraulic and Mechanical Properties of Soil Impacted by Root and Seed Exudates. Vadose Zone Journal 17(1): 0. doi: 10.2136/vzj2017.04.0083

Nguyen, C. 2003. Rhizodeposition of organic C by plants: mechanisms and controls. Agronomie 23(5–6): 375–396. doi: 10.1051/agro:2003011

Oades, J.M. 1978. Mucilages at the root surface. European Journal of Soil Science 29(1): 1–16. doi: 10.1111/j.1365-2389.1978.tb02025.x

Ohnesorge, W.V. 1936. Die Bildung von Tropfen an Düsen und die Auflösung flüssiger Strahlen. ZAMM-Journal of Applied Mathematics and Mechanics/Zeitschrift für Angewandte Mathematik und Mechanik 16(6): 355–358. doi: 10.1002/zamm.19360160611

Ophir, T., and D.L. Gutnick. 1994. A role for exopolysaccharides in the protection of microorganisms from desiccation. Applied and Environmental Microbiology 60(2): 740–745.

Persat, A., C.D. Nadell, M.K. Kim, F. Ingremeau, A. Siryaporn, et al. 2015. The Mechanical World of Bacteria. Cell 161(5): 988–997. doi: 10.1016/j.cell.2015.05.005

Philippot, L., J.M. Raaijmakers, P. Lemanceau, and W.H. van der Putten. 2013. Going back to the roots: the microbial ecology of the rhizosphere. Nature Reviews Microbiology 11(11): 789–799. doi: 10.1038/nrmicro3109

Raaijmakers, J.M., I. De Bruijn, O. Nybroe, and M. Ongena. 2010. Natural functions of lipopeptides from *Bacillus* and *Pseudomonas*: more than surfactants and antibiotics. FEMS Microbiology Reviews 34(6): 1037–1062. doi: 10.1111/j.1574-6976.2010.00221.x

Read, D.B., A.G. Bengough, P.J. Gregory, J.W. Crawford, D. Robinson, et al. 2003. Plant roots release phospholipid surfactants that modify the physical and chemical properties of soil. New phytologist 157(2): 315–326. doi: 10.1046/j.1469-8137.2003.00665.x

Read, D.B., and P.J. Gregory. 1997. Surface tension and viscosity of axenic maize and lupin root mucilages. New Phytologist 137(4): 623–628. doi: 10.1046/j.1469-8137.1997.00859.x

Read, D.B., P.J. Gregory, and A.E. Bell. 1999. Physical properties of axenic maize root mucilage. Plant and Soil 211(1): 87–91. doi: 10.1023/A:1004403812307

Roberson, E.B., C. Chenu, and M.K. Firestone. 1993. Microstructural changes in bacterial exopolysaccharides during desiccation. Soil Biology and Biochemistry 25(9): 1299–1301. doi: 10.1016/0038-0717(93)90230-9

Roberson, E.B., and M.K. Firestone. 1992. Relationship between desiccation and exopolysaccharide production in a soil Pseudomonas sp. Applied and Environmental Microbiology 58(4): 1284–1291.

Rodriguez-Caballero, E., J. Belnap, B. Büdel, P.J. Crutzen, M.O. Andreae, et al. 2018. Dryland photoautotrophic soil surface communities endangered by global change. Nature Geoscience 11(3): 185–189. doi: 10.1038/s41561-018-0072-1

Rosenzweig, R., U. Shavit, and A. Furman. 2012. Water retention curves of biofilm-affected soils using xanthan as an analogue. Soil Science Society of America Journal 76(1): 61–69. doi: 10.2136/sssaj2011.0155

Rossi, F., G. Mugnai, and R. De Philippis. 2018. Complex role of the polymeric matrix in biological soil crusts. Plant and Soil 429(1–2): 19–34. doi: 10.1007/s11104-017-3441-4

Rossi, F., R.M. Potrafka, F.G. Pichel, and R. De Philippis. 2012. The role of the exopolysaccharides in enhancing hydraulic conductivity of biological soil crusts. Soil Biology and Biochemistry 46: 33–40. doi: 10.1016/j.soilbio.2011.10.016

Segura-Campos, M.R., N. Ciau-Solís, G. Rosado-Rubio, L. Chel-Guerrero, and D. Betancur-Ancona. 2014. Chemical and Functional Properties of Chia Seed (*Salvia hispanica* L.) Gum. International Journal of Food Science 2014: 1–5. doi: 10.1155/2014/241053

Shaw, E., D.R. Hill, N. Brittain, D.J. Wright, U. Tauber, et al. 2003. Unusual Water Flux in the Extracellular Polysaccharide of the Cyanobacterium Nostoc commune. Applied and Environmental Microbiology 69(9): 5679–5684. doi: 10.1128/AEM.69.9.5679-5684.2003

Shaw, T., M. Winston, C.J. Rupp, I. Klapper, and P. Stoodley. 2004. Commonality of Elastic Relaxation Times in Biofilms. Physical Review Letters 93(9). doi: 10.1103/PhysRevLett.93.098102

Stoodley, P., R. Cargo, C.J. Rupp, S. Wilson, and I. Klapper. 2002. Biofilm material properties as related to shear-induced deformation and detachment phenomena. Journal of Industrial Microbiology and Biotechnology 29(6): 361–367. doi: 10.1038/sj.jim.7000282

Sutherland, I.W. 2001. Biofilm exopolysaccharides: a strong and sticky framework. Microbiology 147(1): 3–9. doi: 10.1099/00221287-147-1-3

Volk, E., S.C. Iden, A. Furman, W. Durner, and R. Rosenzweig. 2016. Biofilm effect on soil hydraulic properties: Experimental investigation using soil-grown real biofilm: HYDRAULIC PROPERTIES OF BIOFILM AMENDED SOIL. Water Resources Research 52(8): 5813–5828. doi: 10.1002/2016WR018866

Watt, M., M.E. McCully, and C.E. Jeffree. 1993. Plant and bacterial mucilages of the maize rhizosphere: comparison of their soil binding properties and histochemistry in a model system. Plant and Soil 151(2): 151–165. doi: 10.1007/BF00016280

Wloka, M., H. Rehage, H.-C. Flemming, and J. Wingender. 2004. Rheological properties of viscoelastic biofilm extracellular polymeric substances and comparison to the behavior of calcium alginate gels. Colloid and Polymer Science 282(10): 1067–1076. doi: 10.1007/s00396-003-1033-8

Young, I.M. 1995. Variation in moisture contents between bulk soil and the rhizosheath of wheat (Triticum aestivum L. cv. Wembley). New Phytologist 130(1): 135–139. doi: 10.1111/j.1469-8137.1995.tb01823.x

Zarebanadkouki, M., M.A. Ahmed, and A. Carminati. 2016. Hydraulic conductivity of the root-soil interface of lupin in sandy soil after drying and rewetting. Plant and Soil 398(1–2): 267–280. doi: 10.1007/s11104-015-2668-1

Zheng, W., S. Zeng, H. Bais, J.M. LaManna, D.S. Hussey, et al. 2018. Plant Growth-Promoting Rhizobacteria (PGPR) Reduce Evaporation and Increase Soil Water Retention. Water Resources Research. doi: 10.1029/2018WR022656

Zickenrott, I.-M., S.K. Woche, J. Bachmann, M.A. Ahmed, and D. Vetterlein. 2016. An efficient method for the collection of root mucilage from different plant species-A case study on the effect of mucilage on soil water repellency. J. Plant Nutr. Soil Sci. 179(2): 294–302. doi: 10.1002/jpln.201500511

2. MICROHYDROLOGICAL NICHES IN SOILS: HOW MUCILAGE AND EPS ALTER THE BIO-PHYSICAL PROPERTIES OF THE RHIZOSPHERE AND OTHER BIOLOGICAL HOTSPOTS [†]

Benard P.[1,2*], Zarebanadkouki M.[1], Brax M.[3], Kaltenbach R.[3], Jerjen I.[4], Marone F.[4], Couradeau E.[5,6], Felde V.[7], Kaestner A.[8], Carminati A.[1]

[1] University of Bayreuth, Faculty for Biology, Chemistry, and Earth Sciences, Chair of Soil Physics, Universitätsstraße 30, 95447 Bayreuth, BY, Germany

[2] University of Göttingen, Faculty of Agricultural Sciences, Group of Soil Hydrology, Büsgenweg 2, 37077 Göttingen, NI, Germany

[3] University Koblenz-Landau, Institute for Environmental Sciences, Group of Environmental and Soil Chemistry, Fortstraße 7, 76829 Landau, RLP, Germany

[4] Paul Scherrer Institute, Swiss Light Source, Forschungsstrasse 111, 5232 Villigen, Switzerland

[5] Lawrence Berkeley National Laboratory, Environmental Genomics and Systems Biology, 1 Cyclotron Road, 94720 Berkeley, CA, United States

[6] Arizona State University, School of Life Sciences, 427 E Tyler Mall, 85281 Tempe, AZ, United States

[7] University of Kassel, Department of Soil Science, Mönchebergstraße 19, 34125 Witzenhausen, HE, Germany

[8] Paul Scherrer Institute, Laboratory for Neutron Scattering and Imaging, Forschungsstrasse 111, 5232 Villigen, Switzerland

[*] Corresponding Author

Abstract

Plant roots and bacteria are capable of buffering erratic fluctuations of water content in their local soil environment by releasing a diverse, highly polymeric blend of substances (e.g. extracellular polymeric substances EPS and mucilage). Despite this concept is well accepted, the physical mechanisms by which EPS and mucilage interact with the soil matrix and determine the soil water dynamics remain unclear. High-resolution X-ray CT revealed that upon drying in porous media mucilage (from maize roots) and EPS (from intact biocrusts) form filaments and two-dimensional interconnected structures spanning across multiple pores. Unlike water, these mucilage and EPS structures connecting soil particles did not break up upon drying, which is explained by the high viscosity and low surface tension of EPS and mucilage. Measurements of water retention and evaporation with soils mixed with seed mucilage show how these one- and two-dimensional pore-scale structures impact macroscopic hydraulic properties: i.e. they enhance water retention, preserve the continuity of the liquid phase in drying soils and decreases vapor diffusivity and local drying rates. In conclusion, we propose that the release of viscous polymeric substances and the consequent creation of a network bridging the soil pore space represent a universal strategy of plants and bacteria to engineer their own soil microhydrological niches where stable conditions for life are preserved.

2.1. Introduction: Effects of mucilage and EPS on soil hydraulic properties

Hosting a tremendous biodiversity (Philippot et al., 2013), the soil offers opportunities and numerous challenges to plants and microorganisms therein. Prominent among these challenges are fluctuations in soil water content, which affect growth conditions of plants and soil microorganisms. Since soils are periodically affected by precipitation and evaporation, shifts in hydraulic conditions are mostly inevitable. For example, during severe soil drying, the soil hydraulic conductivity drops and limits the capacity of roots to extract water at the rate required to sustain transpiration. Plants can respond to soil drying by closing stomata, growing deeper roots, chancing the root permeability or altering the properties of the soil in their vicinity, the *rhizosphere*. Mucilage secreted by the roots keeps the rhizosphere wet when the soil dries and avoids its quick rewetting after rain or irrigation events (Carminati et al., 2010).

Similar to the effect of mucilage, EPS produced by microorganism buffers fluctuations in soil moisture a hotspot of high biological activity, like the rhizosphere (Kuzyakov and Blagodatskaya, 2015), microbial colonies (Or et al., 2007; Zheng et al., 2018) and biocrusts (Chamizo et al., 2016; Couradeau et al., 2018; Rossi et al., 2018). Biocrusts stand out as an example, arguably the most extended biofilm on the planet (Elbert et al., 2012; Rodriguez-Caballero et al., 2018).

The physico-chemical properties of mucilage and EPS highly differ among plant (Naveed et al., 2017) and bacterial (Flemming and Wingender, 2001) species. However, regardless of their diverse composition, mucilage and EPS have some basic traits in common and appear to impact soil hydraulic properties in comparable ways. In this paper we provide experimental evidence and mechanistic explanation of the similarities between mucilage and EPS in shaping the pore-scale spatial configuration of the liquid phase and the consequences on macroscopic hydraulic properties.

Mucilage and EPS have a high polymeric content that confer to mucilage and EPS the hydrogel behaviour (Brinker and Scherer, 1990), and as such, increasing the viscosity of the liquid phase (Flemming and Wingender, 2001, 2010; Stoodley et al., 2002; Naveed et al., 2017) and form an interconnected network (Roberson et al., 1993; McCully and Boyer, 1997; Flemming and Wingender, 2010). They act like a porous matrix capable to absorb and hold large quantities of water (Roberson and Firestone, 1992; McCully and Boyer, 1997; Read et al., 1999; Flemming and Wingender, 2001; Segura-Campos et al., 2014). Furthermore, among the exuded compounds, some are powerful surfactants, which decrease the surface tension at the gas-liquid interface (Read et al., 2003; Raaijmakers et al., 2010).

A number of modifications of soil hydraulic properties have been ascribed to mucilage and EPS. An increase in soil water retention was observed within the rhizosphere (Carminati et al., 2010; Moradi et al., 2011) and for seed mucilage (Kroener et al., 2018). Similarly, enhanced water retention was observed for soil inoculated with *Pseudomonas* species previously isolated from soil (Roberson and Firestone, 1992; Volk et al., 2016) and EPS (Chenu, 1993; Rosenzweig et al., 2012) while the non-destructive extraction of EPS from biocrust was found to reduce the water holding capacity of a soil (Adessi et al., 2018).

Due to their high viscosity, mucilage and EPS decrease the saturated soil hydraulic conductivity (Kroener et al., 2014; Volk et al., 2016). The effects on unsaturated conditions are less clear. The decline in hydraulic conductivity with soil water potential was less steep in soils inoculated with biofilm forming bacteria (*Pseudomonas putida*) (Volk et al., 2016). In fine textured soils, EPS was even shown to increase the unsaturated conductivity (Volk et al., 2016). Along with these modifications, EPS treated soils (Chenu, 1993; Zheng et al., 2018), soils inoculated with a strain of *Bacillus subtilis* (Zheng et al., 2018) and soil micromodels inoculated with a mucoid strain of *Sinorhizobium meliloti* (Deng et al., 2015) dried slower compared to unamended control soil. The reduction in drying rates was absent when respective biofilms of *S. meliloti* were studied outside a porous matrix (Deng et al., 2015). Desiccation studies on biofilm forming bacterial strains of *E. coli*, *E. stewartia* and *A. calcoaceticus* in the porous environment of Millipore filters showed a substantially increased survival rate when compared to their non-mucoid counterparts (Ophir and Gutnick, 1994).

Despite the consensus on the effects of mucilage and EPS on soil water dynamics (Table 2.1), the mechanisms of how they interact with the soil matrix and alter soil hydraulic properties are still unknown. The polymer networks of EPS and mucilage can absorb large quantities of water (Roberson and Firestone, 1992; McCully and Boyer, 1997; Read et al., 1999; Flemming and Wingender, 2001), but what forces are responsible to hold this water in soils remains unclear (Flemming, 2011). EPS and mucilage can hold water at negative potentials (Chenu, 1993; McCully and Boyer, 1997) but their effect on soil water retention is amplified in fine textured soils (Kroener et al., 2018), which suggests that additional forces emerge from the interaction between polymers and soil matrix. Similarly, mucilage separated from soil showed no resistance to drying (McCully and Boyer, 1997) and being in a porous system is a prerequisite to allow the polymer network to utilize its full hydraulic capacity (Deng et al., 2015; Kroener et al., 2018). In summary, there is no conclusive theory on the mechanisms by which EPS and mucilage interact with soil and affect their physical properties.

We hypothesize that: 1) EPS and mucilage increase viscosity and decrease surface tension of the soil solution and consequently cause the formation of interconnected strands and thin surfaces spanning through multiple pores; and 2) these pore-scale structures increase water retention, maintain the connectivity of the liquid phase and decrease gas diffusion on the macroscopic scale. We propose that these mechanisms

underlie a universal strategy of plants and bacteria to engineer their local soil physical environment by shaping favourable hydrological niches in soils. We support this statement using existing evidences on EPS and mucilage (Table 2.1) and a set of novel experiments with porous media (soils of varying textures and glass beads) mixed with maize (*Zea mays*) and seed mucilage (*Salvia hispanica*), and natural biocrusts.

Table 2.1: Physical properties of EPS and mucilage and their effects in soil

		Bacterial EPS	Root mucilage	Seed mucilage
Intrinsic properties	Increased viscosity / Viscoelasticity	Körstgens et al. (2001); Stoodley et al. (2002); Wloka et al. (2004); Shaw et al. (2004); Lieleg et al. (2011)	Read and Gregory (1997); Naveed et al. (2017)	Naveed et al. (2017)
	Decreased surface tension	Raaijmakers et al. (2010) and references included	Read and Gregory (1997); Read et al. (2003)	Naveed et al. (2018)
	Adsorption of water	Roberson and Firestone (1992); Flemming et al. (2016)	McCully and Boyer (1997); Read et al. (1999)	Segura-Campos et al. (2014)
Effect on soil hydraulics	Increased soil water retention	Roberson and Firestone (1992); Chenu (1993); Rosenzweig et al. (2012); Volk et al. (2016)	This study (Maize mucilage in glass beads; Fig. S2.7)	Kroener et al. (2018), This study
	Slowed down evaporation from soil	Chenu (1993); Flemming (2011); Deng et al. (2015); Zheng et al. (2018), Adessi et al. (2018)	-	This study
	Increased relative hydraulic conductivity*	Volk et al. (2016); Zheng et al. (2018)	-	This study

*The relative hydraulic conductivity is defined as the hydraulic conductivity divided by the saturated hydraulic conductivity. This means changes in hydraulic conductivity during drying of soils are eased.

2.2. Conceptual model: Spatial configuration of EPS and mucilage in the rhizosphere and other biological hotspots

As the soil dries, the concentration of polymeric substances in the rhizosphere and other biological hotspots increases. Consequently, the viscosity of the liquid phase increases, and the surface tension decreases, as shown for root mucilage (Read and Gregory, 1997). Changes in viscosity and surface tension affect the spatial configuration of the gas-liquid interface in the pore space. Low surface tension eases the stretching of the gas-liquid interface and decreases its curvature (for a given water potential) according to the Young-Laplace equation:

$$h = \sigma \left(\frac{1}{r_1} + \frac{1}{r_2} \right) \qquad (2.1)$$

Where $h = P_w - P_a$ [Pa] is the difference in pressure between the liquid (P_w) and the gas phase (P_a), σ [mN m^{-1}] is the surface tension of the gas-liquid interface, and r_1 and r_2 [m] are the radii of the curvature of the gas-liquid interface (negative when the radius points towards the liquid phase). Viscosity affects the shape of the liquid bridges between soil particles by avoiding the capillary break-up of the liquid phase (Carminati et al., 2017). The contribution of viscous and surface tension forces on the shape of liquid pendular bridges between particles is elegantly described by the Ohnesorge number, *Oh* (eq. 2.2) (Ohnesorge, 1936):

$$Oh = \frac{\mu}{\sqrt{\rho \sigma r}} \qquad (2.2)$$

where μ [Pa s^{-1}] is viscosity, ρ [g m^{-3}] density and r [m] a characteristic length corresponding to the radius of the liquid connection. For Newtonian fluids filaments do not breakup for *Oh* >1 (Castrejón-Pita et al., 2012). For mucilage and EPS, the Ohnesorge number increases as the soil progressively dries. When a critical concertation of polymers in the liquid solution is reached, viscosity dominates over inertia and surface tension (*Oh* >> 1) and the rupture of liquid bridges is prevented. Sattler et al. (2012) showed that even a small concentration of polymer in a liquid solution prevents the break-up of filaments undergoing drying.

Fig. 2.1 shows our conceptual model of the spatial configurations of mucilage and EPS at different contents (dry weight of exudate per weight of soil) after drying in porous media. For low mucilage and EPS contents and large pores, the final shape of arising structures are thin filaments. At intermediate content or at the contact between soil particles, the pendular bridges are cylindrical (Albalasmeh and Ghezzehei, 2014; Benard et al., 2018). They form during soil drying as the gas-liquid interface retreats and the polymers adhering to the soil particle surface are stretched. As the soil dries further, the viscosity increases until a critical point beyond which the polymers cannot be further stretched. At this point the polymers begin to behave as an additional matrix. The bridges

can be drained by air invasion or cavitation. At higher polymer contents, the critical point when neither the network nor the bonds between polymers and particle surfaces can be disrupted is reached at higher volumetric water content when the liquid phase is still connected. In this way, the connectivity of the liquid phase is maintained. We hypothesize that this process results in the formation of two-dimensional interconnected networks that span throughout the porous medium.

Complementary imaging methods are used to support this conceptual model as well as its implications for macroscopic soil hydraulic properties.
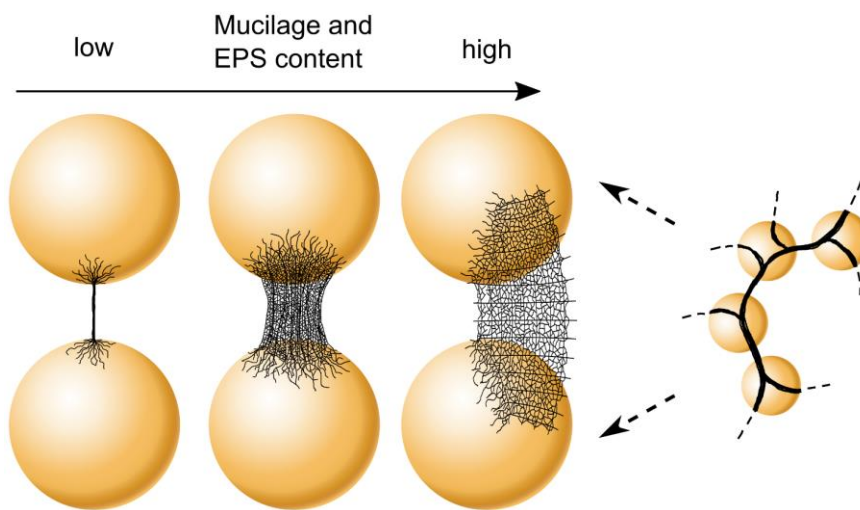
Fig. 2.1: Spatial configuration of dry mucilage and EPS structures in porous media. Increased viscosity and decreased surface tension of the liquid phase induced by highly polymeric and surface-active substances released by bacteria and plants lead to the formation of characteristic structures in the pore space of drying soil. At low mucilage and EPS contents, isolated threads between particles form in large pores at low water content. Hollow cylinders form in small pores at intermediate mucilage and EPS contents when water is still captured at the inter-particle space. Interconnected two-dimensional structures spanning across multiple pores form at high contents when the liquid phase is still connected (e.g. at considerably high water content).

2.3. Material and Methods

Light Microscopy

To illustrate the shape of mucilage structures formed during soil drying, mucilage was mixed with different particles, let dry and imaged with light microscopy. Samples were prepared according to (Benard et al., 2018). Chia seed mucilage (*Salvia hispanica*) was mixed with a sandy loam at a mucilage content of 4.5 mg g^{-1} (mg dry mucilage per g soil) (Fig. 2.2a), with glass beads of 1.7-2 mm in diameter at a mucilage content of 0.7 mg g^{-1} (Fig. 2.2b) and fine sand (90% 63-125 µm, 9% 36-63 µm, 1% <36 µm) at a content of 4 mg g^{-1} (Fig. S2.10). The sandy loam was collected near Reinhausen

(Göttingen, Germany). C_{tot} was 2.0%, N_{tot} was 0.17% and pH was 4.9. The soil texture was distributed as follows: Clay: 8.6%, silt: 18.5%, sand: 73%. The mixtures of particles and mucilage were spread on object slides and left to evaporate at 20°C for 48 hours at ambient humidity. Images were acquired with reflected light microscope (Axio Imager 2; Carl Zeiss AG) equipped with a digital camera (Axiocam 305, software Zen 2 core; Carl Zeiss AG).

Synchrotron-based X-ray tomographic microscopy (SRXTM) of maize mucilage in glass beads and sand

Three-dimensional imaging of maize mucilage in porous media was conducted using SRXTM. Experiments were conducted at the TOMCAT beamline (Stampanoni et al., 2006) at the Swiss Light Source at the Paul Scherrer Institute in Switzerland. Hydrated mucilage was collected manually from the nodal roots of 10 weeks old field grown maize (*Zea mays*) near Bayreuth, Germany. Mucilage was sucked from nodal roots before they reached the soil on a humid day following a rain event. Mucilage was visible as a blob surrounding the roots. Mucilage concentration was determined by oven drying 50 g of hydrated mucilage. No steps of preprocessing like sterilization were undertaken to minimize alteration of the physical structure and composition of mucilage. Mucilage was frozen after collection, defrosted prior to the experiment and air dried for 8 hours by evaporation. The process was accelerated by a constant air stream above the sample under a fume hood. In this way the initial mucilage concentration in the liquid phase was increased from 8.15 mg g^{-1} to 15, respectively 30 mg g^{-1} [mg of dry mucilage per g of hydrated mucilage] and mixed with glass beads of 0.1-0.2 mm in diameter (SWARCO VESTGLAS GmbH, Recklinghausen, Germany), achieving a mucilage content of 4 and 8 mg per g of particles. An exemplary result from a segmented cross section at 4 mg g^{-1} is shown in Fig. S2.8. Additionally, fine sand (0.125-0.2 mm in diameter) was amended with mucilage from *Zea mays* in the same way at a content of 8 mg g^{-1} (exemplary cross sections are shown in Fig. S2.9). Note that Zickenrott et al. (2016) claimed that it is reasonable to expect a mucilage content between 0.05 and 50 mg g^{-1} depending on plant species and conditions. Contents of 4-8 mg g^{-1} are therefore at the upper edge of the plausible range of values. Considering that mucilage content is expected to decrease from the root surface to the bulk soil, the used content is likely to be representative of the soil very close to the root surface (i.e. at a distance smaller than ca. 100 µm).

Mixtures were packed in PVC cylinders with an inner diameter of 1.5 and depth of 4.5 mm. After air drying (at a relative humidity of about 50%), samples were scanned at 40 keV, with an exposure time of 140 ms per projection, pixel size of 0.325 µm and field of view of 2560 by 2160 pixels. The sample-detector distance was 24.5 mm. 1501 projections were acquired equiangularly spaced over 180°. The acquired projection images were flat- and darkfield corrected before phase retrieval according to Paganin et al. (2002). Sinograms were then reconstructed to axial tomographic slices using highly optimized routines based on the Fourier transform method (Marone et al., 2017). After reconstruction of 3D volumetric data, particles, air filled pores, and mucilage structures were segmented using a thresholding technique in Matlab 2017b (The MathWorks, Inc.). A series of opening and closing filters followed by a morphological reconstruction algorithm and application of a local threshold were performed to increase the contrast and subsequent segmentation of objects.

Synchrotron-based X-ray tomographic microscopy (SRXTM) of biocrust from Moab

As an example of two-dimensional EPS structures formed in a natural system, SRXTM of biocrust from Moab, Utah was performed at the Beamline 8.3.2 of the Advanced Light Source (ALS), at Lawrence Berkeley National Laboratory, California, USA. X-ray energy was 25.7 keV and 1025 projections were acquired for the scan at 0.25s acquisition time. The resulting voxel edge length was 1.3 µm. A more detailed description of the procedure can be found elsewhere (Couradeau et al., 2018).

Soil water retention, hydraulic conductivity and evaporation measurements

To study the impact of pore-scale spatial configuration of mucilage and EPS on macroscopic soil hydraulic properties, we conducted an evaporation experiment that provides the water retention curve, the unsaturated hydraulic conductivity and evaporative fluxes (Schindler et al., 2010). This method is implemented in Hyprop (METER Group, Inc. USA). A cylinder with inner diameter of 8 cm and height of 5 cm was filled with wet sandy loam (see description of light microscopy for details; bulk density of 1.57 g cm^{-3}) and pre-saturated by capillary rise. Note that the porosity of

mucilage amended soil was slightly higher due to its swelling behaviour which explains the offset in initial water content (Fig. 2.4a). Evaporation rate and soil matric potentials were recorded during soil drying at a temperature of 25°C. The measurements were repeated two times for a soil mixed with mucilage extracted from chia seeds (*Salvia hispanica*) at a content of 2.5 mg g^{-1} and a control soil pre-saturated with deionized water. As a model of root exuded mucilage, we used chia seed mucilage, which can be extracted in sufficient amounts and its physical properties and impacts on soil hydraulic properties are comparable to those of root exuded mucilage (e.g. *Zea mays*; Naveed et al., 2017). The procedure of mucilage extraction is described elsewhere (Kroener et al., 2018). To parameterize the hydraulic properties of the mucilage amended soil and the control soil, data of fluxes and matric potentials were used to simulate water flow during soil drying. Flow of water was simulated by solving the Richards equation using a fully implicit Euler time discretization and a centred finite difference space discretization scheme in Matlab (Celia and Binning, 1992). Soil water retention and hydraulic conductivity curves were parametrized according to the PDI model (Peters et al., 2015) and were inversely adjusted to best reproduce the recorded matric potentials and average soil water content.

The evaporation rate of deionized water and mucilage (apart from soil) was monitored at 25°C using the scales of the Hyprop setup. Mucilage extracted from chia seeds extracted as described in the previous paragraph and deionized water were used. Three replicates of water, respectively mucilage filled cylindrical containers with an inner diameter of 4 cm and a depth of 1 cm were prepared and evaporative fluxes were derived from changes in weight over time. The initial concentration of extracted mucilage was 0.56 g of dry matter per 100 g of liquid solution.

Evaporation from mucilage amended soil – Neutron radiography

Neutron radiography allows for quantitative imaging of water in soils (Lehmann and Wagner, 2010). Here, it was used to investigate the effect of mucilage on soil moisture distribution during water evaporation from soils. The measurements were performed at the ICON beamline at the Paul Scherrer Institute (PSI), Villigen, Switzerland. Containers of size 10×1×1 cm were filled with a sandy loam (see description of light microscopy for details) amended with chia seed mucilage (*Salvia hispanica*) at mucilage

content of 4.5 mg g^{-1}. As a control, we used the same soil without mucilage addition. To achieve the same porosity, the containers were filled with wet soil (mixed with hydrated mucilage, respectively water) in order to achieve a bulk density of 1.57 g cm^{-3}. Subsequently, the soil was saturated by capillary rise for 48 h. Porosity of mucilage amended soil was slightly higher which explains the offset in initial water content (Fig. 2.6b). A time-series of neutron radiographs was acquired to monitor water redistribution over a drying period of 4 days. Details on neutron radiography technique and image processing can be found elsewhere (Carminati et al., 2010).

2.4. Results and Discussion

Imaging of EPS and mucilage in soils

Evidence supporting the conceptual model (Fig. 2.1) for seed mucilage forming filaments and hollow cylinders is shown in Fig. 2.2ab. Similar structures are created by *Bacillus subtilis* in sand (Zheng et al., 2018).

The two-dimensional thin layers predicted for high polymer concentrations are shown for dry maize mucilage (*Zea mays*) in glass beads (Fig. 2.2d-e) scanned with synchrotron X-ray tomography. A thin layer of dry mucilage forms a continuous surface spanning across multiple pores at a mucilage content of 8 mg g^{-1}. Note that structures of similar extent were also observed at a mucilage content of 4 mg g^{-1} and an exemplary result of a segmented cross section is shown in Fig. S2.8.

Similar filaments and surfaces are visible also in biocrusts. Fig. 2.2c shows examples of the two-dimensional thin surfaces visible in the pore space of soil biocrust collected in Moab, Utah (Couradeau et al., 2018) observed with synchrotron based X-ray tomography. The similarity between the observed structures of plant and bacterial origin is striking. Their thickness as well as their vertical extent are comparable (e.g. Fig. 2.2). Note that these structures might not be solely composed of EPS. However, the high biological activity and EPS amount found in soil biocrust support the hypothesis the observed structures are mostly composed of EPS.
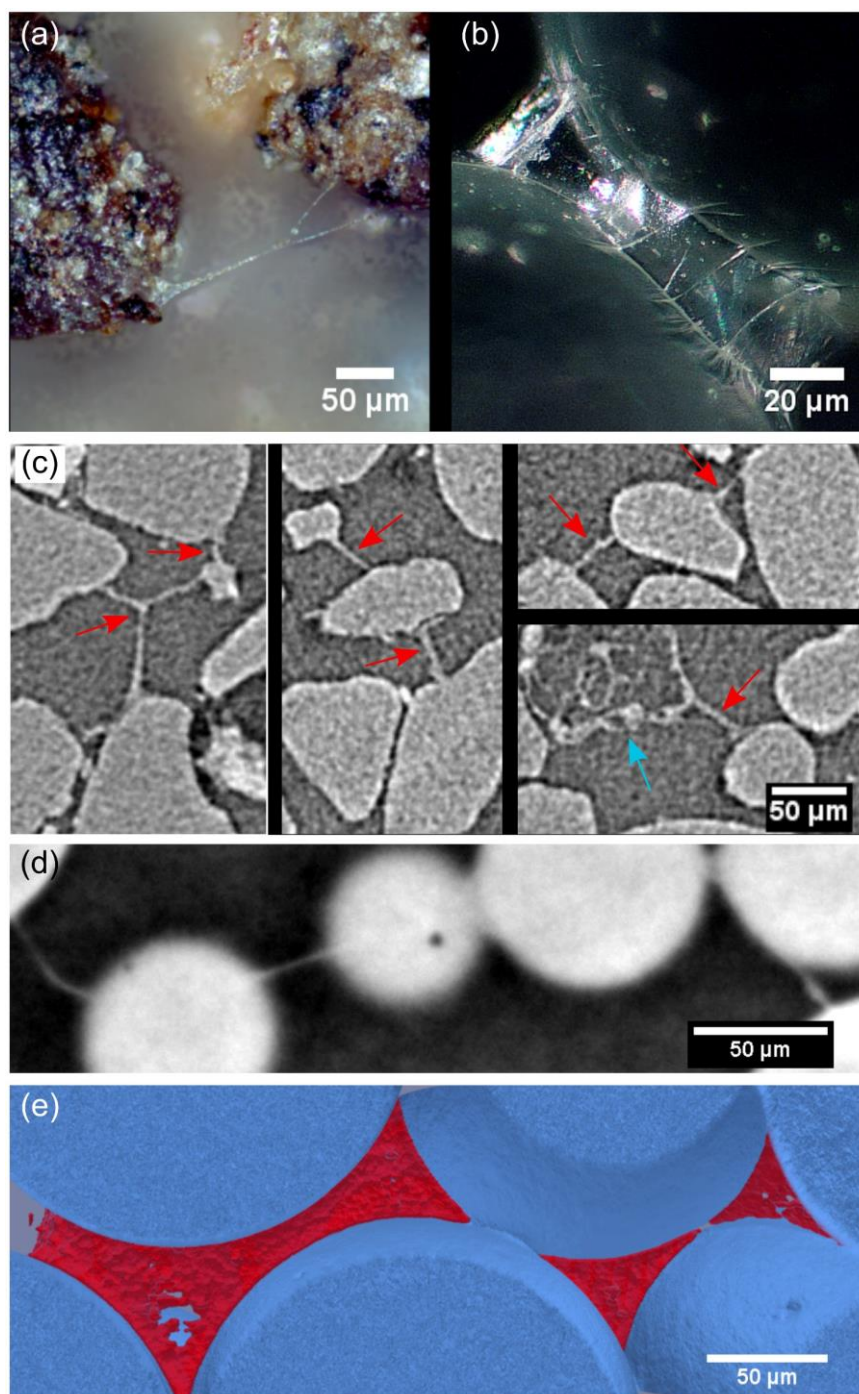
Fig. 2.2: Examples of polymeric structures formed by mucilage and EPS in porous media. (a) Light microscope image of threads of mucilage (*Slavia hispanica*; mucilage content 4.5 mg g^{-1} [mg dry mucilage per g of particles]) formed across a large pore during drying; **(b)** Light microscope image of cylinder formed between neighbouring glass beads (1.7-2 mm in diameter) at intermediate mucilage content (0.7 mg g^{-1}); **(c)** Two-dimensional EPS-based structures joining quartz grains in intact biocrusts imaged with synchrotron-based X-ray tomographic microscopy (Couradeau et al., 2018). High EPS content resulted in the formation of characteristic structures (red arrows) comparable to those formed by maize mucilage. The blue arrow marks a cyanobacterial bundle with the EPS sheath surrounding the trichomes of *Microcoleus vaginatus*. **(d)** Cross-section through a synchrotron-based X-ray tomographic microscopy volume of dry maize mucilage (*Zea mays*) structures in glass beads (bright circles) (mucilage content 8 mg g^{-1}; glass bead diameter 0.1 – 0.2 mm); **(e)** 3D segmentation of dry mucilage structures (red) from **(d)** which formed interconnected surfaces of approximately 1 µm thickness within the pore space of glass beads (blue). Additional images of mucilage in porous media can be found in the supplemental material section (Fig. Fig. S2.8 - Fig. S2.10).

Water retention and hydraulic conductivity

Drying of mucilage and EPS in porous media leads to the formation of a matrix that affects the retention and connectivity of water (e.g. Fig. Fig. 2.3 and Fig. 2.4). The enhanced water retention in soils is partly explained by the hygroscopic properties of mucilage, but the interaction of mucilage with porous media can further increase this effect.

When mucilage and EPS dry outside a porous medium, the decreasing capillary pressure leads to the collapse of their polymer network (Brinker and Scherer, 1990). The situation is different when mucilage and EPS dry within a porous medium. Their high viscosity and entanglement with the soil solid particles prevent their complete collapse leading to the formation of aforementioned filaments and thin layers that act as a new matrix (Fig. Fig. 2.2 - Fig. 2.3). Water is retained within the matrix, either inside isolated hollow cylinders (Fig. 2.2b) or between interconnected gas-liquid interfaces where a dense and stiff layer of polymers prevents air invasion (Fig. 2.2c-e). The emerging matrix creates an additional matric potential that can further enhance the retention of water in soils. To what extent the emerging matrix augments the water retention of soils is still not known. Kroener et al. (2018) reported greater water retention of mucilage in fine compared to coarse textured soils. The pronounced water retention in fine-textured soils can be explained by the higher specific surface area of these soils and the amplified entanglement of polymers with the soil particles, which favours the formation of the polymer matrix across the pore space. This result supports our hypothesis that the emerging polymer matrix is capable of increasing water retention in soils.

Besides enhancing water retention (Fig. Fig. 2.3a, Fig. 2.4a), the high viscosity and low surface tension of mucilage maintain the connectivity of the liquid phase in drying soils (Fig. 2.3b), which has an important effect on the unsaturated soil hydraulic conductivity. The hydraulic conductivity of a sandy loam (see description of light microscopy for details) amended with seed mucilage (*Salvia hispanica*) did not decline as much as that of the control soil and at water potentials lower than -10^4 cm (equivalent to -1MPa), is even higher (Fig. 2.4b). The latter is explained by the maintained connectivity of the liquid phase during drying, which enables film flow at low water potentials. This result shows that the maintained connectivity of the liquid phase during drying counteracts the expected decrease in permeability caused by the shrinkage of the polymer matrix (Kroener et al., 2018).

Note that the relative importance of these counteracting processes (i.e. the enhanced retention and connectivity versus the increasing viscosity) on the unsaturated conductivity is soil texture dependent, as seen in previous studies (Volk et al., 2016; Zheng et al., 2018).
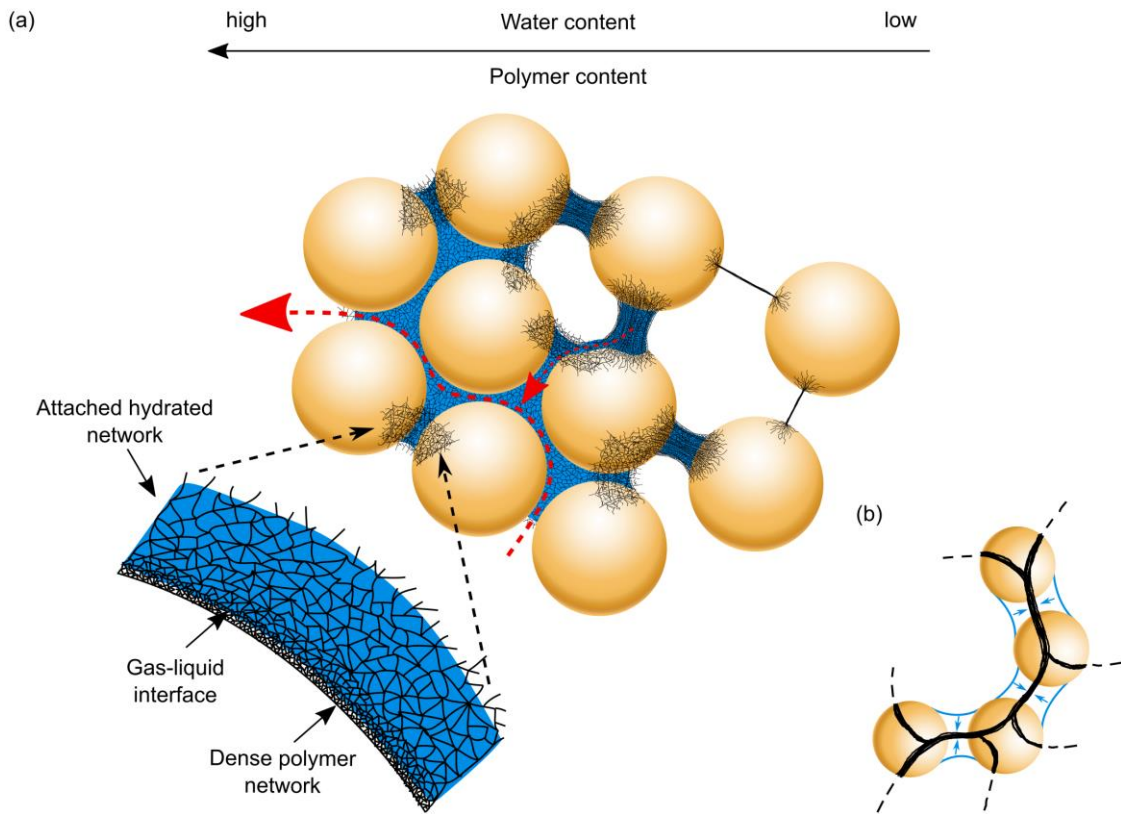
Fig. 2.3: Configuration of the liquid phase in soils containing EPS or mucilage. **(a)** In this illustration, the concentration of EPS or mucilage increases from the right to the left. During drying, the gas-liquid interface retreats and the polymers accumulate at this interface. At low polymer contents, the gas-liquid interface retreats but the liquid phase is not broken, which results in the formation of thin threads. At higher polymer contents, the gas-liquid interface becomes stiffer because of the entanglement of the polymers among themselves and with the soil particles. As drying progresses, the gas-liquid interface can no longer be stretched and starts to act as an additional matrix. Together with the hygroscopic nature of the polymers, this leads to an amplified soil water retention. Besides increasing the water retention, the polymer network preserves the continuity of the liquid phase (the flow of water is illustrated by the dashed red arrows. **(b)** The liquid phase remains connected during drying, with the liquid converging into the two-dimensional surfaces imaged in Fig. 2c-e. This induces a shift towards higher hydraulic conductivity in dry soils.

Fig. 2.4: Water retention and hydraulic conductivity of sandy loam and sandy loam amended with seed mucilage. (a) Water retention and **(b)** hydraulic conductivity curve of a sandy loam without (blue) and amended with seed mucilage (mucilage content 2.5 mg g^{-1}; Salvia hispanica; red); solid lines indicate the mean of three replicates and grey areas indicate the 95% confidence interval of three replicates.
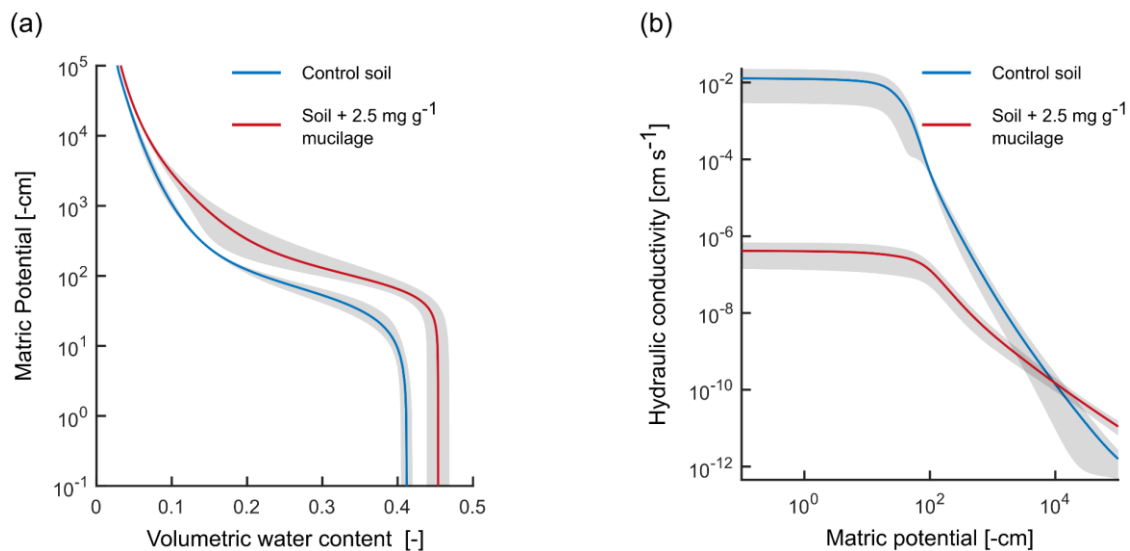
Evaporation from soils

Fig. 2.5 displays the evaporative fluxes in water, mucilage and in a sandy loam (see description of light microscopy for details) mixed with varying amount of mucilage from chia seeds (*Salvia hispanica*). Mucilage strongly reduced the evaporative fluxes in soil. However, the evaporation rates in water and mucilage (outside the soil) were similar. For soils embedded with EPS, a similar deceleration in soil drying was explained by the decrease in both saturated hydraulic conductivity and surface tension, which limit capillary rise, causing a discrepancy between evaporative flow and capillary flow and the consequent break-up of the liquid phase. This point marks the transition from Stage I (evaporation from the soil surface) to Stage II of soil drying (Zheng et al., 2018), when evaporation is reduced and controlled by vapor diffusion through the pore space (Lehmann et al., 2008).

We propose that the suppression of evaporation in soils amended with EPS and mucilage is further reduced by the thin layers shown in Fig. 2.2c-e. These structures are fostered by the decrease in saturated hydraulic conductivity, which does not allow capillary flow to match the evaporative rate, causing a fast drying of the soil surface (Fig. 2.6a). Once these structures are formed, they limit the diffusion of vapor through the soil. Fig. 2.6b shows a timeline of neutron radiographs of two soil columns, one amended with chia

48

seed mucilage at a content of 4.5 mg g^{-1} (bottom) and one control initially saturated with water (top). The uppermost layer of the mucilage amended sample quickly dried (black arrow) confirming our interpretation of the process.

Since evaporation from mucilage and EPS (Deng et al., 2015) (outside the geometry of a porous matrix) showed no substantial resistance to drying (e.g. Fig. 2.5a), the water adsorptive potential of the polymer network is of secondary importance in slowing down soil drying. Instead, the thin layers of desiccated mucilage and EPS forming in porous media are the main reason for the suppression of evaporation from drying soils. Note that beside reducing vapour diffusion, the dry polymeric layers are also expected to limit the diffusion of oxygen and other gases, with additional potential consequences for plant and soil processes.
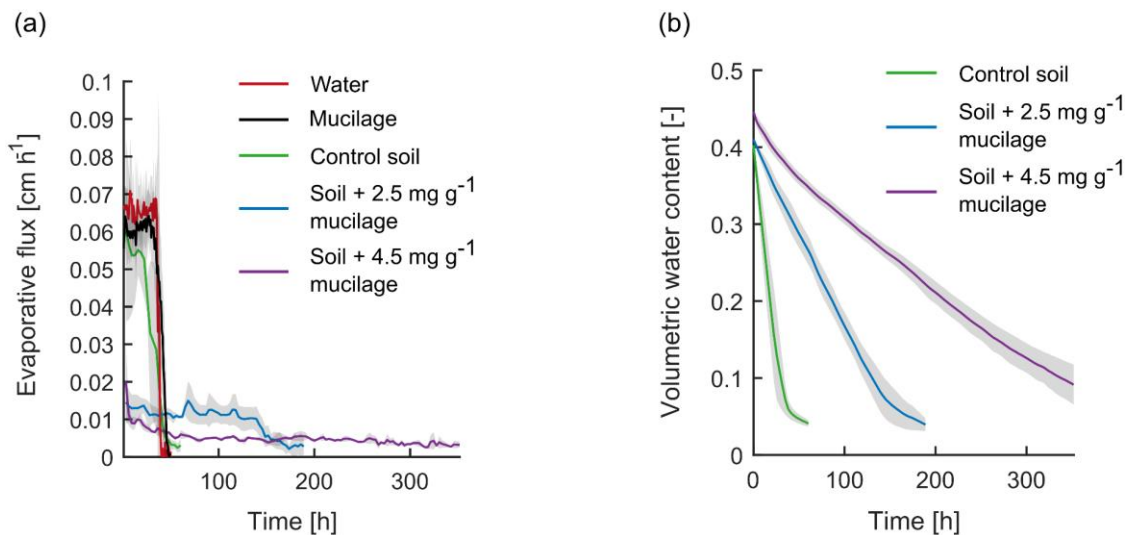
Fig. 2.5: Evaporative flux and decrease in water content for water and mucilage separate and mixed with soil. Mucilage within the pore space of sandy loam results in a marked decrease in evaporative flux and a delay in soil drying. **(a)** Evaporative flux from free water (red), mucilage (black), control soil saturated with water (green), and soil treated with mucilage (mucilage content 2.5 mg g^{-1} (blue); mucilage content 4.5 mg g^{-1} (purple); *Salvia hispanica*); **(b)** Decrease in water content from an evaporation experiment in soil amended with mucilage (control soil (green), mucilage content 2.5 mg g^{-1} (blue); mucilage content 4.5 mg g^{-1} (purple); *Salvia hispanica*); solid lines indicate the mean of three measurements and grey areas indicate the 95% confidence interval of three replicates.

Fig. 2.6: Delay in evaporation induced by the formation of dense polymer layers in the soil pore space. (a) Dense layers of desiccated polymers limit the evaporative flux of water vapor through the soil and delay its drying; **(b)** Neutron radiographs of two soil columns saturated with water (top) and amended with mucilage (mucilage content 4.5 mg g^{-1}; *Salvia hispanica*; bottom) over the course of 4 days. The uppermost layer (red arrow) of the mucilage treated soil dried comparably quick while the underlying pore space remained wet.

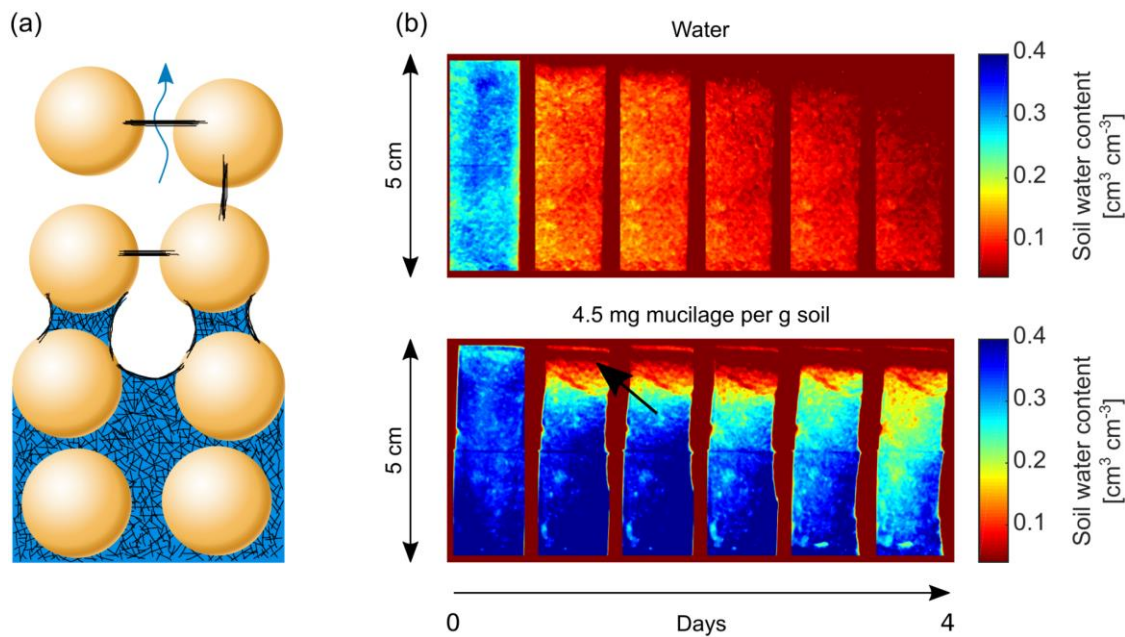The suppressed evaporation is of particular importance for the hydrology of biocrust. Due to their global extent and role in nutrient cycling, biocrusts are an important example of soil regions with high EPS content. The formation of thin surfaces spanning throughout the pore space of biocrusts reduces evaporative fluxes, maintains the soil moisture and preserves the continuity of the liquid phase. By slowing down the desiccation, the network of thin surfaces could be beneficial for the microbial community by granting it more time to perform the metabolic shift underlying the transition to inactive, dry period.

2.5. Conclusions

This study provides a key missing link between pore-scale mechanisms and macroscopic alterations of soil hydraulic properties and soil water dynamics induced by mucilage and EPS. The highly polymeric blend of substances composing mucilage and EPS forms a network, increases the viscosity of the soil solution and lowers its surface tension. As soils dry, the polymer network is stretched and its high viscosity and entanglement with soil particles result in the formation of interconnected one- and two-dimensional

structures. The formed matrix increases the water retention and liquid connectivity in porous media and decreases the diffusion of gases. The formation of thin layers spanning through the soil pore space decreases vapor diffusion.

The interactions between the highly polymeric blend of mucilage and EPS with the soil pore space have not been recognized so far. The impact on soil hydraulic properties was mostly ascribed to the intrinsic properties of these blends. Our experimental results provided first evidence that the spatial configuration of the liquid phase and the interactions of mucilage and EPS with the soil matrix need to be considered in order to grasp their impact on soil hydraulics and water dynamics.

The mechanisms described in this paper have been based on model systems (mucilage mixed with repacked soil particles of varying texture) and further research is needed to prove the relevance of mucilage structure formation in the rhizosphere of varying plant species and soil types and their putative function on water and solute uptake. The biocrust images prove that 2D structures reaching across multiple pores can be found in intact soil samples with high biological activity. We propose that the formation of a viscous polymer matrix takes place in biological hotspots in soils, such as the rhizosphere and microbial colonies and their consequences are manifold. The enhanced retention of continuity of the liquid phase maintains the flow of water and diffusion of solutes required by plants and microorganisms. For plants exposed to severe soil drying this would enable the root system to sustain transpiration and nutrient uptake. The suppressed evaporation can be particularly important for bacterial colonies (such as in biocrust), slowing down the local soil drying and reducing pace and likeliness of severe desiccation. In such biological hot spots, the creation of these microhydrological niches might be critical to support life in soil. We propose that the edaphic way of life might have selected common strategies across taxa to tackle the challenges of highly variable soil water dynamics.

In summary, this study explains basic biophysical mechanisms supporting the conditions for life in soils. Countless experiments and observations prove that bacteria and plants are capable to engineer soil hydraulic properties to their advantage. Magnitude and relevance are manifold, as well as the composition of the polymeric blends released, but the underlying mechanisms of how bacteria and plant roots create their microhydrological niches appear universal.

2.6. Acknowledgements

2.7. Author Information

The datasets generated, and material used in and/or analysed during the current study are available from the corresponding author on reasonable request.

2.8. References

Adessi, A., R. Cruz de Carvalho, R. De Philippis, C. Branquinho, and J. Marques da Silva. 2018. Microbial extracellular polymeric substances improve water retention in dryland biological soil crusts. Soil Biol. Biochem. 116: 67–69. doi: 10.1016/j.soilbio.2017.10.002

Albalasmeh, A.A., and T.A. Ghezzehei. 2014. Interplay between soil drying and root exudation in rhizosheath development. Plant Soil 374(1–2): 739–751. doi: 10.1007/s11104-013-1910-y

Benard, P., M. Zarebanadkouki, C. Hedwig, M. Holz, M.A. Ahmed, et al. 2018. Pore-Scale Distribution of Mucilage Affecting Water Repellency in the Rhizosphere. Vadose Zone J. 17(1): 0. doi: 10.2136/vzj2017.01.0013

Brinker, C.J., and G.W. Scherer. 1990. Sol-gel science: the physics and chemistry of sol-gel processing. Academic Press, Boston.

Carminati, A., P. Benard, M.A. Ahmed, and M. Zarebanadkouki. 2017. Liquid bridges at the root-soil interface. Plant Soil. doi: 10.1007/s11104-017-3227-8

Carminati, A., A.B. Moradi, D. Vetterlein, P. Vontobel, E. Lehmann, et al. 2010. Dynamics of soil water content in the rhizosphere. Plant Soil 332(1–2): 163–176. doi: 10.1007/s11104-010-0283-8

Castrejón-Pita, A.A., J.R. Castrejón-Pita, and I.M. Hutchings. 2012. Breakup of Liquid Filaments. Phys. Rev. Lett. 108(7). doi: 10.1103/PhysRevLett.108.074506

Celia, M.A., and P. Binning. 1992. A mass conservative numerical solution for two-phase flow in porous media with application to unsaturated flow. Water Resour. Res. 28(10): 2819–2828. doi: 10.1029/92WR01488

Chamizo, S., Y. Cantón, E. Rodríguez-Caballero, and F. Domingo. 2016. Biocrusts positively affect the soil water balance in semiarid ecosystems: The Role of Biocrusts in the Local Water Balance. Ecohydrology 9(7): 1208–1221. doi: 10.1002/eco.1719

Chenu, C. 1993. Clay-or sand-polysaccharide associations as models for the interface between micro-organisms and soil: water related properties and microstructure. Geoderma 56(1–4): 143–156. doi: 10.1016/0016-7061(93)90106-U

Couradeau, E., V.J.M.N.L. Felde, D. Parkinson, D. Uteau, A. Rochet, et al. 2018. In Situ X-Ray Tomography Imaging of Soil Water and Cyanobacteria From Biological Soil Crusts Undergoing Desiccation. Front. Environ. Sci. 6. doi: 10.3389/fenvs.2018.00065

Deng, J., E.P. Orner, J.F. Chau, E.M. Anderson, A.L. Kadilak, et al. 2015. Synergistic effects of soil microstructure and bacterial EPS on drying rate in emulated soil micromodels. Soil Biol. Biochem. 83: 116–124. doi: 10.1016/j.soilbio.2014.12.006

Elbert, W., B. Weber, S. Burrows, J. Steinkamp, B. Büdel, et al. 2012. Contribution of cryptogamic covers to the global cycles of carbon and nitrogen. Nat. Geosci. 5(7): 459–462. doi: 10.1038/ngeo1486

Flemming, H.-C. 2011. The perfect slime. Colloids Surf. B Biointerfaces 86(2): 251–259. doi: 10.1016/j.colsurfb.2011.04.025

Flemming, H.-C., and J. Wingender. 2001. Relevance of microbial extracellular polymeric substances (EPSs)-Part I: Structural and ecological aspects. Water Sci. Technol. 43(6): 1–8. doi: 10.2166/wst.2001.0326

Flemming, H.-C., and J. Wingender. 2010. The biofilm matrix. Nat. Rev. Microbiol. 8(9): 623–633. doi: 10.1038/nrmicro2415

Körstgens, V., H.C. Flemming, J. Wingender, and W. Borchard. 2001. Influence of calcium ions on the mechanical properties of a model biofilm of mucoid Pseudomonas aeruginosa. Water Sci. Technol. J. Int. Assoc. Water Pollut. Res. 43(6): 49–57. doi: 10.2166/wst.2001.0338

Kroener, E., M. Holz, M. Zarebanadkouki, M. Ahmed, and A. Carminati. 2018. Effects of Mucilage on Rhizosphere Hydraulic Functions Depend on Soil Particle Size. Vadose Zone J. 17(1): 0. doi: 10.2136/vzj2017.03.0056

Kroener, E., M. Zarebanadkouki, A. Kaestner, and A. Carminati. 2014. Nonequilibrium water dynamics in the rhizosphere: How mucilage affects water flow in soils. Water Resour. Res. 50(8): 6479–6495. doi: 10.1002/2013WR014756

Kuzyakov, Y., and E. Blagodatskaya. 2015. Microbial hotspots and hot moments in soil: Concept & review. Soil Biol. Biochem. 83: 184–199. doi: 10.1016/j.soilbio.2015.01.025

Lehmann, P., S. Assouline, and D. Or. 2008. Characteristic lengths affecting evaporative drying of porous media. Phys. Rev. E 77(5). doi: 10.1103/PhysRevE.77.056309

Lehmann, E.H., and W. Wagner. 2010. Neutron imaging at PSI: a promising tool in materials science and technology. Appl. Phys. A 99(3): 627–634. doi: 10.1007/s00339-010-5606-3

Lieleg, O., M. Caldara, R. Baumgärtel, and K. Ribbeck. 2011. Mechanical robustness of Pseudomonasaeruginosa biofilms. Soft Matter 7(7): 3307. doi: 10.1039/c0sm01467b

Marone, F., A. Studer, H. Billich, L. Sala, and M. Stampanoni. 2017. Towards on-the-fly data post-processing for real-time tomographic imaging at TOMCAT. Adv. Struct. Chem. Imaging 3(1). doi: 10.1186/s40679-016-0035-9

McCully, M.E., and J.S. Boyer. 1997. The expansion of maize root-cap mucilage during hydration. 3. Changes in water potential and water content. Physiol. Plant. 99(1): 169–177. doi: 10.1111/j.1399-3054.1997.tb03445.x

Moradi, A.B., A. Carminati, D. Vetterlein, P. Vontobel, E. Lehmann, et al. 2011. Three-dimensional visualization and quantification of water content in the rhizosphere. New Phytol. 192(3): 653–663. doi: 10.1111/j.1469-8137.2011.03826.x

Naveed, M., L.K. Brown, A.C. Raffan, T.S. George, A.G. Bengough, et al. 2017. Plant exudates may stabilize or weaken soil depending on species, origin and time: Effect of plant exudates on rhizosphere formation. Eur. J. Soil Sci. (68): 806–816. doi: 10.1111/ejss.12487

Ohnesorge, W.V. 1936. Die bildung von tropfen an düsen und die auflösung flüssiger strahlen. ZAMM-J. Appl. Math. Mech. Für Angew. Math. Mech. 16(6): 355–358. doi: 10.1002/zamm.19360160611

Ophir, T., and D.L. Gutnick. 1994. A role for exopolysaccharides in the protection of microorganisms from desiccation. Appl. Environ. Microbiol. 60(2): 740–745.

Or, D., S. Phutane, and A. Dechesne. 2007. Extracellular Polymeric Substances Affecting Pore-Scale Hydrologic Conditions for Bacterial Activity in Unsaturated Soils. Vadose Zone J. 6(2): 298. doi: 10.2136/vzj2006.0080

Paganin, D., S.C. Mayo, T.E. Gureyev, P.R. Miller, and S.W. Wilkins. 2002. Simultaneous phase and amplitude extraction from a single defocused image of a homogeneous object. J. Microsc. 206(1): 33–40. doi: 10.1046/j.1365-2818.2002.01010.x

Peters, A., S.C. Iden, and W. Durner. 2015. Revisiting the simplified evaporation method: Identification of hydraulic functions considering vapor, film and corner flow. J. Hydrol. 527: 531–542. doi: 10.1016/j.jhydrol.2015.05.020

Philippot, L., J.M. Raaijmakers, P. Lemanceau, and W.H. van der Putten. 2013. Going back to the roots: the microbial ecology of the rhizosphere. Nat. Rev. Microbiol. 11(11): 789–799. doi: 10.1038/nrmicro3109

Raaijmakers, J.M., I. De Bruijn, O. Nybroe, and M. Ongena. 2010. Natural functions of lipopeptides from *Bacillus* and *Pseudomonas*: more than surfactants and antibiotics. FEMS Microbiol. Rev. 34(6): 1037–1062. doi: 10.1111/j.1574-6976.2010.00221.x

Read, D.B., A.G. Bengough, P.J. Gregory, J.W. Crawford, D. Robinson, et al. 2003. Plant roots release phospholipid surfactants that modify the physical and chemical properties of soil. New Phytol. 157(2): 315–326. doi: 10.1046/j.1469-8137.2003.00665.x

Read, D.B., and P.J. Gregory. 1997. Surface tension and viscosity of axenic maize and lupin root mucilages. New Phytol. 137(4): 623–628. doi: 10.1046/j.1469-8137.1997.00859.x

Read, D.B., P.J. Gregory, and A.E. Bell. 1999. Physical properties of axenic maize root mucilage. Plant Soil 211(1): 87–91. doi: 10.1023/A:1004403812307

Roberson, E.B., C. Chenu, and M.K. Firestone. 1993. Microstructural changes in bacterial exopolysaccharides during desiccation. Soil Biol. Biochem. 25(9): 1299–1301. doi: 10.1016/0038-0717(93)90230-9

Roberson, E.B., and M.K. Firestone. 1992. Relationship between desiccation and exopolysaccharide production in a soil Pseudomonas sp. Appl. Environ. Microbiol. 58(4): 1284–1291.

Rodriguez-Caballero, E., J. Belnap, B. Büdel, P.J. Crutzen, M.O. Andreae, et al. 2018. Dryland photoautotrophic soil surface communities endangered by global change. Nat. Geosci. 11(3): 185–189. doi: 10.1038/s41561-018-0072-1

Rosenzweig, R., U. Shavit, and A. Furman. 2012. Water retention curves of biofilm-affected soils using xanthan as an analogue. Soil Sci. Soc. Am. J. 76(1): 61–69.

Rossi, F., G. Mugnai, and R. De Philippis. 2018. Complex role of the polymeric matrix in biological soil crusts. Plant Soil 429(1–2): 19–34. doi: 10.1007/s11104-017-3441-4

Sattler, R., S. Gier, J. Eggers, and C. Wagner. 2012. The final stages of capillary break-up of polymer solutions. Phys. Fluids 24(2): 023101. doi: 10.1063/1.3684750

Schindler, U., W. Durner, G. von Unold, and L. Müller. 2010. Evaporation Method for Measuring Unsaturated Hydraulic Properties of Soils: Extending the Measurement Range. Soil Sci. Soc. Am. J. 74(4): 1071. doi: 10.2136/sssaj2008.0358

Segura-Campos, M.R., N. Ciau-Solís, G. Rosado-Rubio, L. Chel-Guerrero, and D. Betancur-Ancona. 2014. Chemical and Functional Properties of Chia Seed (*Salvia hispanica* L.) Gum. Int. J. Food Sci. 2014: 1–5. doi: 10.1155/2014/241053

Shaw, T., M. Winston, C.J. Rupp, I. Klapper, and P. Stoodley. 2004. Commonality of Elastic Relaxation Times in Biofilms. Phys. Rev. Lett. 93(9). doi: 10.1103/PhysRevLett.93.098102

Stampanoni, M., A. Groso, A. Isenegger, G. Mikuljan, Q. Chen, et al. 2006. Trends in synchrotron-based tomographic imaging: the SLS experience. In: Bonse, U., editor. p. 63180M. doi: 10.1117/12.679497

Stoodley, P., R. Cargo, C.J. Rupp, S. Wilson, and I. Klapper. 2002. Biofilm material properties as related to shear-induced deformation and detachment phenomena. J. Ind. Microbiol. Biotechnol. 29(6): 361–367. doi: 10.1038/sj.jim.7000282

Volk, E., S.C. Iden, A. Furman, W. Durner, and R. Rosenzweig. 2016. Biofilm effect on soil hydraulic properties: Experimental investigation using soil-grown real biofilm: HYDRAULIC PROPERTIES OF BIOFILM AMENDED SOIL. Water Resour. Res. 52(8): 5813–5828. doi: 10.1002/2016WR018866

Wloka, M., H. Rehage, H.-C. Flemming, and J. Wingender. 2004. Rheological properties of viscoelastic biofilm extracellular polymeric substances and comparison to the behavior of calcium alginate gels. Colloid Polym. Sci. 282(10): 1067–1076. doi: 10.1007/s00396-003-1033-8

Zheng, W., S. Zeng, H. Bais, J.M. LaManna, D.S. Hussey, et al. 2018. Plant Growth-Promoting Rhizobacteria (PGPR) Reduce Evaporation and Increase Soil Water Retention. Water Resour. Res. doi: 10.1029/2018WR022656

Zickenrott, I.-M., S.K. Woche, J. Bachmann, M.A. Ahmed, and D. Vetterlein. 2016. An efficient method for the collection of root mucilage from different plant species- A case study on the effect of mucilage on soil water repellency. J. Plant Nutr. Soil Sci. 179(2): 294–302. doi: 10.1002/jpln.201500511

2.9. Supplemental Material

Water retention of maize mucilage amended glass beads – Neutron radiography

The effect of maize mucilage (*Zea mays*) on water retention was tested by mixing hydrated mucilage at concentrations of 15 and 30 mg g^{-1} [mg of dry mucilage per g of hydrated mucilage] with glass beads of 0.1-0.2 mm in diameter (SWARCO VESTGLAS GmbH, Recklinghausen, Germany) to achieve mucilage content of 4, respectively 8 mg g^{-1}. Mixtures were then packed beside water saturated glass beads in containers with inner dimensions of 0.8 ×0.5×0.3 cm (L×H×W). Mucilage amended glass beads were packed to one side of the container over a length of 0.25 cm in contact with their non-amended counterparts. By evaporation a range of water contents in different samples was achieved and then the containers were sealed with aluminium tape. After 2 days of equilibration at room temperature, the water content in the mucilage affected and unaffected part of the containers was measured using neutron radiography. Measurements were performed at the ICON beam line at the Paul Scherrer Institute, Villigen, Switzerland. The details on neutron radiography technique and image processing can be found elsewhere (Carminati et al., 2010). Results are shown in Fig. S2.7.

Imaging of EPS and mucilage in soils

All images shown were taken from samples prepared according to the procedure described in the Material & Methods section.

Fig. S2.8 shows an exemplary cross section and its segmented counterpart. Dry mucilage structures appeared comparable in their spatial extent as those obtained from samples at a mucilage content of 8 mg g^{-1}. Dry mucilage bridged several large pores and formed a continuous structure spanning throughout the pore space. Note that due to their small thickness, mucilage structures appear disconnected across the contact region between particles although they are most likely not. Discontinuity arises from the fact that the resolution of the acquired images is limited while the spatial distance decreases towards the contact region of particles.
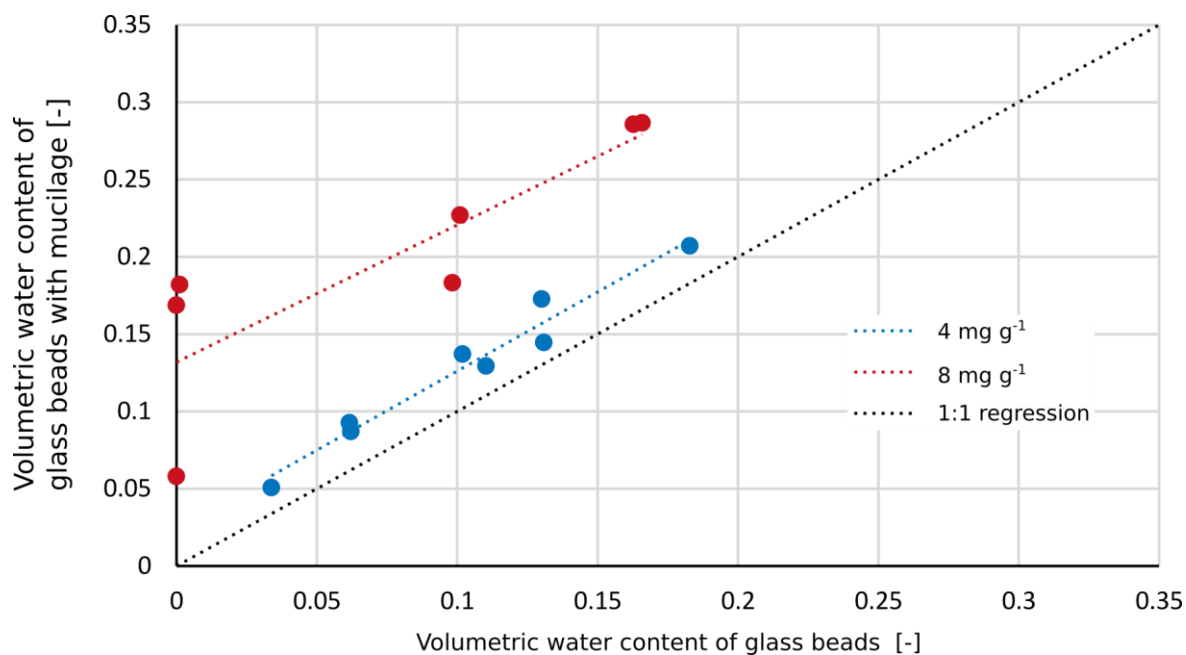
Fig. S2.7: Increase in water retention of mucilage amended glass beads. For mucilage content of 4 (blue dashed line) and 8 (red dashed line) mg g^{-1} [mg dry mucilage per g glass beads] glass beads hold approximately 25, respectively 125% more water at same negative water potential (deviation from 1:1 regression; black dashed line).

Fig. S2.9 shows an exemplary cross section through a dried sample of fine sand amended with mucilage at 8 mg g^{-1}. As shown for glass beads, structures were continuous surfaces reaching across multiple pores.

Fig. S2.10 shows a light microscopy image of dry mucilage structures in fine sand. Samples were prepared according to the description given in the main text. Mucilage shaped the soil pore space by adhering to small particles during drying.

Fig. S2.11 shows exemplary cross sections of the pore space of soil biocrust collected in Moab, Utah (Couradeau et al., 2018) observed with synchrotron based X-ray tomography. Shape of EPS-based structures connecting adjacent particles is similar to the ones observed in mucilage amended sand (Fig. S2.9) and glass beads (Fig. 2.2de and Fig. S2.8).
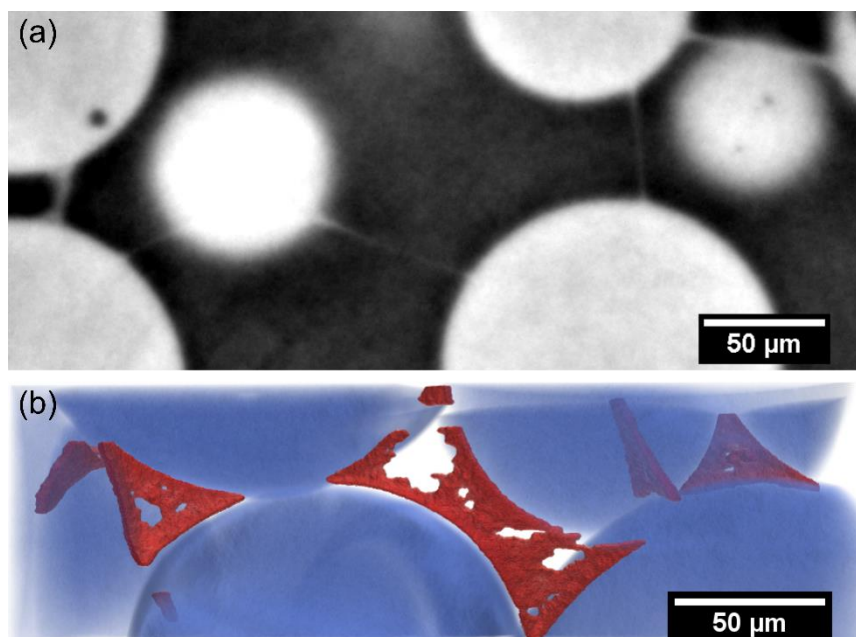
Fig. S2.8: Example of mucilage structures formed by mucilage in glass beads. **(a)** Cross-section through a synchrotron-based X-ray tomogram of dry maize mucilage (*Zea mays*) structures in glass beads (bright circles) (mucilage content 4 mg g^{-1}; glass bead diameter 0.1 – 0.2 mm); **(b)** 3D segmentation of dry mucilage structures (red) showing interconnected surfaces of approximately 1 µm thickness within the pore space of glass beads (blue).
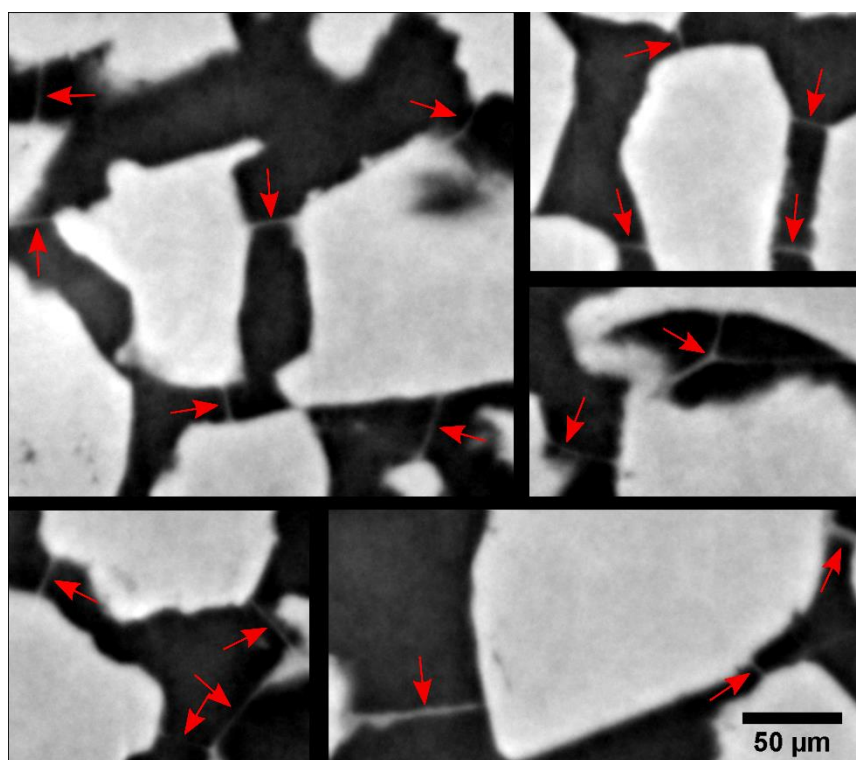
Fig. S2.9: Example of mucilage structures in fine sand. Two-dimensional dry mucilage (*Zea mays*, mucilage content 8 mg g^{-1}) structures (red arrows) in sand (particle diameter 0.125 – 0.2 mm) imaged with synchrotron-based X-ray tomographic microscopy.
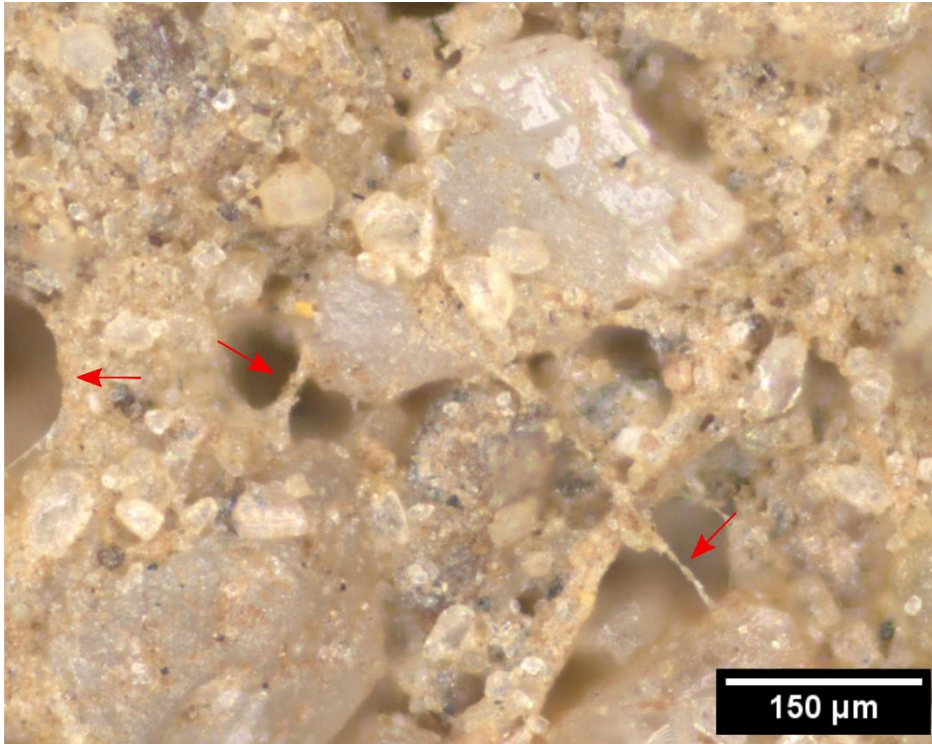
Fig. S2.10: Example of mucilage structures in fine sand. Light microscope image of dry mucilage (Slavia hispanica; mucilage content 4 mg g⁻¹) structures (red arrows) in fine sand.
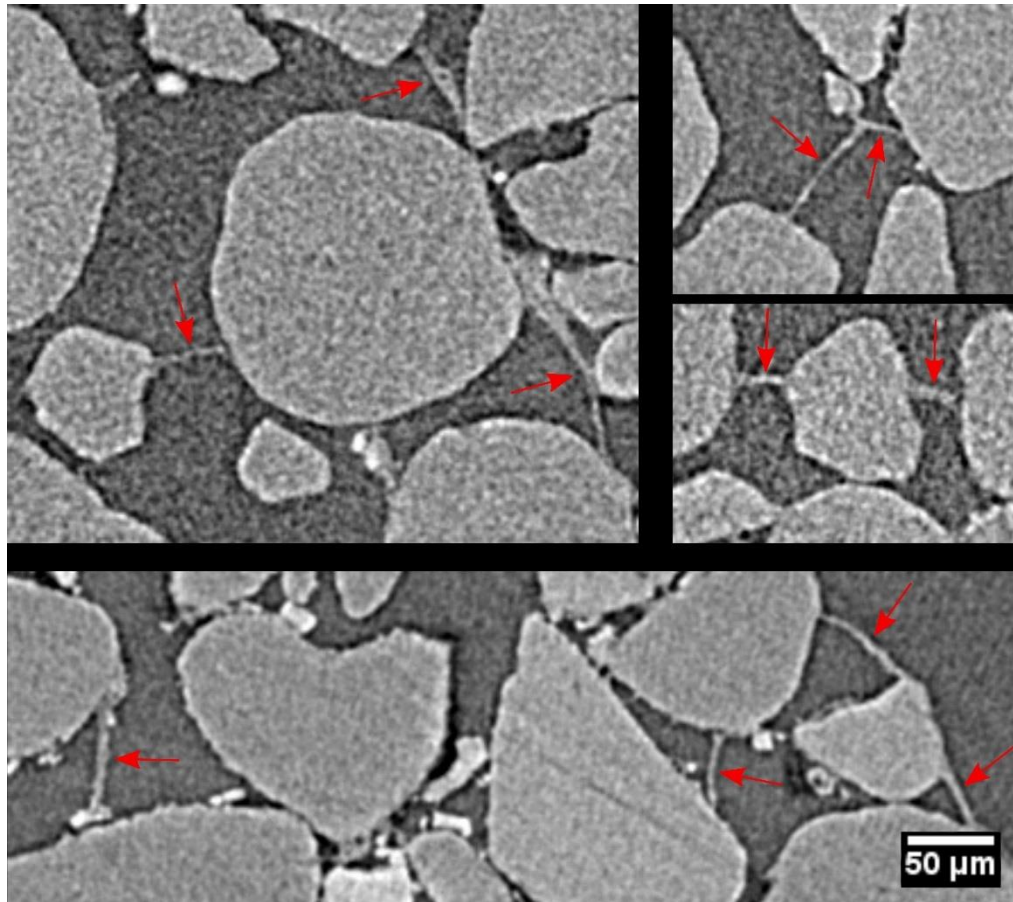
Fig. S2.11: Examples EPS-based structures in biocrust. Two-dimensional EPS-based structures joining quartz grains in intact biocrusts imaged with synchrotron-based X-ray tomographic microscopy (Couradeau et al., 2018). High EPS content resulted in the formation of characteristic structures (red arrows) comparable to those formed by maize mucilage.

3. PORE-SCALE DISTRIBUTION OF MUCILAGE AFFECTING WATER REPELLENCY IN THE RHIZOSPHERE[†]

Benard P.[1*], Zarebanadkouki M.[1], Hedwig C.[1], Holz M.[1], Ahmed M. A.[1,2], Carminati A.[1]

[1]   Division of Soil Hydrology, Georg-August-University of Göttingen, Germany, Büsgenweg 2, 37077 Göttingen

[2]   Department of Agricultural Engineering, University of Khartoum, Khartoum North, 13314, Shambat, Sudan

[*]   Corresponding Author

Core ideas

- During drying mucilage is preferentially deposited in small pores

- This microscopic heterogeneity critically affects macroscopic wettability

- Infiltration is impeded when a critical fraction of pores is blocked by dry mucilage

- Dry mucilage bridges are shaped like hollow cylinders connecting particles

Abstract

The physical properties of the rhizosphere are strongly influenced by root-exuded mucilage, and there is increasing evidence that mucilage affects the wettability of soils on drying. We introduce a conceptual model of mucilage deposition during soil drying and its impact on soil wettability. We hypothesized that as soil dries, water menisci recede and draw mucilage toward the contact region between particles. At low mucilage contents (milligrams per gram of soil), mucilage deposits have the shape of thin filaments that are bypassed by infiltrating water. At higher contents, mucilage deposits occupy a large fraction of the pore space and make the rhizosphere hydrophobic. This hypothesis was confirmed by microscope images and contact angle measurements. We measured the initial contact angle of quartz sand (0.5–0.63- and 0.125–0.2-mm diameter), silt (36–63-µm diameter), and glass beads (0.1–0.2-mm diameter) mixed with varying amounts of chia (*Salvia hispanica* L.) seed mucilage (dry content range 0.2–19 mg g^{-1}) using the sessile drop method. We observed a threshold-like occurrence of water repellency. At low mucilage contents, the water drop infiltrated within 300 ms. Above a critical mucilage content, the soil particle–mucilage mixture turned water repellent. The critical mucilage content decreased with increasing soil particle size. Above this critical content, mucilage deposits have the shape of hollow cylinders that occupy a large fraction of the pore space. Below the critical mucilage content, mucilage deposits have the shape of thin filaments. This study shows how the microscopic heterogeneity of mucilage distribution impacts the macroscopic wettability of mucilage-embedded soil particles.

3.1. Introduction

With an extent of millimeters to a few centimeters, the rhizosphere is the part of soil actively modified by root growth and exudation (Gregory, 2006; Hinsinger et al., 2009; York et al., 2016; Roose et al., 2016). Its impact on soil hydrology might be profound, as about 40% of all terrestrial precipitation flows through the rhizosphere–plant–atmosphere continuum (Bengough, 2012). In view of this immense flow of water, Dakora and Phillips (2002) and Sposito (2013) proposed rhizosphere research as key for the sustainable management of water resources.

One of the substances released by root tips is mucilage, a gel consisting mainly of polysaccharides and <1% lipids (Oades, 1978; Read et al., 2003). In combination with other sources of organic matter and root hairs, plant mucilage contributes to the formation of the rhizosheath, a region of interconnected soil particles bound to the root surface (Watt et al., 1993). The enhanced connection between roots and soil is supposed to have a major effect on microbial growth and plant nutrient uptake (Dakora and Phillips, 2002). Furthermore, mucilage is known to alter the hydraulic properties of the rhizosphere (Young, 1995; Hallett et al., 2003; Carminati et al., 2010; Moradi et al., 2012; Carminati, 2013; Zarebanadkouki et al., 2016). After a drying cycle, Carminati et al. (2010) found the rewetting of the rhizosphere of lupin (*Lupinus albus* L.) to be markedly slower than that of the adjacent bulk soil. Similar observations were made by Ahmed et al. (2016) for maize (*Zea mays* L.). In earlier experiments, Watt et al. (1993) observed mucilage to form connections between soil particles on drying and related the inability of a hydrophilic dye (coomassie blue) to penetrate dry mucilage to its hydrophobic dry state. Similarly, Moradi et al. (2012) explained the high contact angle of a dry rhizosphere by the hydrophobicity of mucilage. The results of Ahmed et al. (2016), which showed high contact angles of dry mucilage from the nodal roots of maize, support this hypothesis. However, Zickenrott et al. (2016) reported that there are significant differences in contact angles of root mucilages from different plant species, which makes the generalization of mucilage behavior in soils difficult. Zickenrott et al. (2016) showed that mucilage exuded from the seedlings of different species (*Lupinus albus*, *Vicia faba* L., and *Triticum aestivum* L.), and mucilage collected from the seminal roots of maize led to an increase in the measured contact angle of sand with an increase in the dry amount of mucilage. In those experiments, they did not find the mucilage–sand mixture to become hydrophobic (contact angle >90°), but it cannot be excluded

64

that at higher mucilage contents (defined as weight of dry mucilage per weight of dry soil) the mucilage–sand mixtures might become hydrophobic. Additionally, those researchers crushed the mucilage–sand packings and repacked them as two-dimensional layers, altering the microscopic distribution of mucilage in the pore space. This might have an impact on the wettability of the porous medium.

Albalasmeh and Ghezzehei (2014) showed and modeled the preferential deposition of organic matter in the interparticle space. They tested their concept using polygalacturonic acid (PGA) and xanthan to mimic the deposition of plant mucilage and bacterial biofilms in drying soil. Using environmental scanning electron microscope imaging, they observed the transport of PGA toward the interparticle space as the water content progressively decreased. At a critical water content, the biofilm bridges cemented the particles together. This concept explains nicely a former observation that mucilage binds particles only on drying (Watt et al., 1993).

In line with Albalasmeh and Ghezzehei (2014), we conceptualized that when the soil dries, mucilage moves toward the interparticle space. At a critical concentration of mucilage in the liquid phase (mass of dry mucilage per volume of liquid), mucilage is deposited and forms connections between particles. At low mucilage contents only fine pores are affected by the presence of mucilage because deposition occurs when large pores are already drained. With an increase in mucilage content, larger pores are also affected, and they might have a strong impact on the ability of water to infiltrate throughout the porous medium.

Our hypothesis is that the microscopic deposition of mucilage in the pore space affects soil wettability on a macroscopic scale. We expect that water repellency occurs when a sufficient fraction of the pore space is blocked. To test our hypothesis, we mixed different amounts of chia seed mucilage with particles of four grain size distributions and measured the contact angle of dry samples after 300 ms. We compared undisturbed samples in which mucilage was deposited in the pore space during drying with disturbed samples in which particles were repacked in two-dimensional layers with a rather random distribution of mucilage. The final state of mucilage deposition in dry soil was visualized by transmission light microscopy. Mucilage structures were analyzed in terms of their extent and compared for different mucilage contents in fine sand and glass beads of comparable grain size.

3.2. Conceptual Model

At high soil water contents, freshly exuded root mucilage (e.g., maize) behaves like a liquid except that its surface tension is lower than that of water and it is slightly more viscous (Read et al., 1999). As the soil dries, liquid and hydrogels (like root mucilage) move from surfaces with positive curvature (soil particles) to ones with negative curvature, e.g., contact areas between adjacent particles (Brinker and Scherer, 1990) (Fig. 3.1a). This causes the movement of water and mucilage toward this region. Upon further drying, the concentration (mass of dry mucilage per volume of liquid) and viscosity of mucilage increase. At a critical concentration, mucilage becomes so viscous that it can no longer flow as fast as water and it is deposited into bridges between soil particles (Albalasmeh and Ghezzehei, 2014; Carminati et al., 2017). The extent of these bridges increases with mucilage amount. We hypothesized that when a critical fraction of the pore space is occupied by these bridges, water infiltration is impeded (Fig. 3.1b).
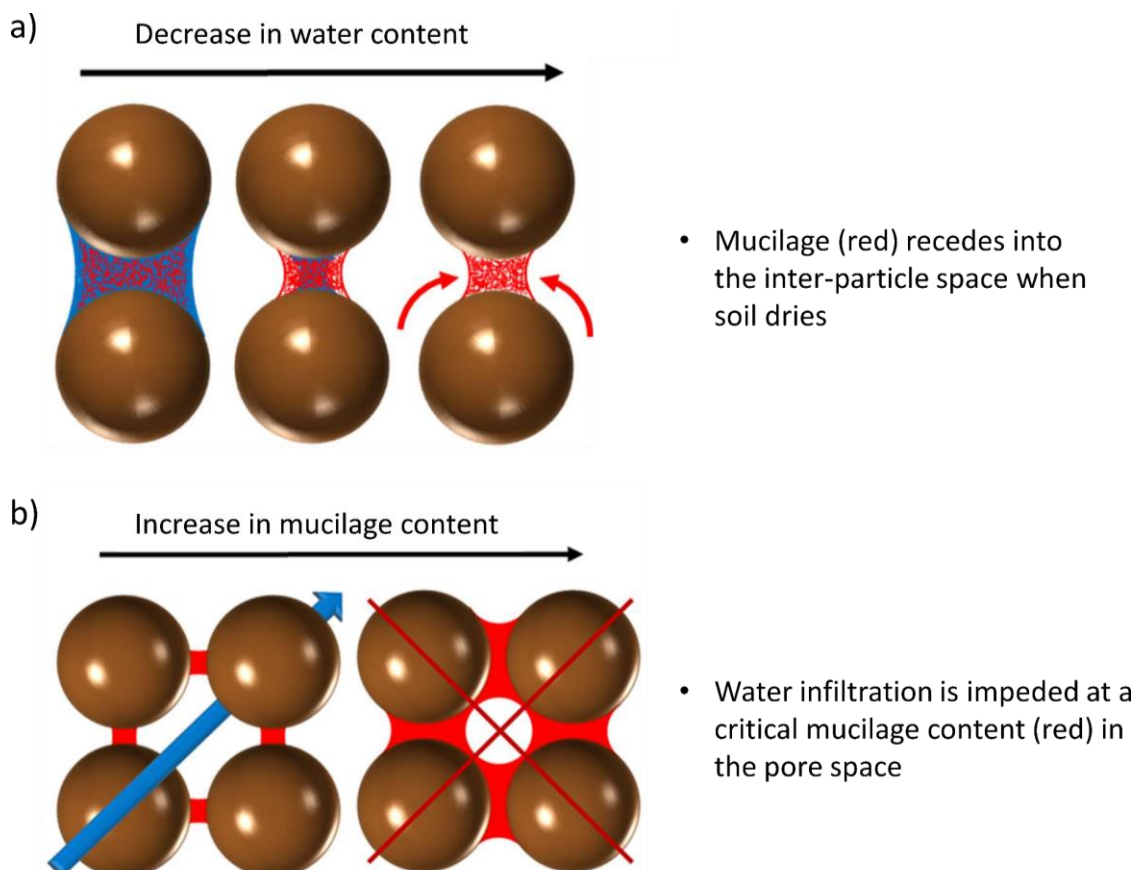
Fig. 3.1: (a) Mucilage distribution during drying is dominated by the displacement of liquid menisci toward the contact region between particles; as the water content decreases, mucilage viscosity increases and solid bridges form between particles (mucilage deposition on drying is shown in red). **(b)** At low mucilage content, the bridges are thin and can be bypassed by infiltrating water (left side), while at high mucilage content, bridges between particles are large and cover the inner pore cylinder, at which point the soil–mucilage mixture becomes water repellent.

The process of deposition is controlled by soil water content, pore size, and mucilage content. At low mucilage contents, the formation of bonds occurs only at a comparably low water content, when only fine pores are still water filled while large pores are already drained. At high mucilage contents, deposition and formation of solid mucilage structures occurs at higher water content, when the large pores have not yet been drained. In this case, a larger fraction of the pore space is occupied by mucilage. We expect that there is a critical mucilage content at which the fraction of pores occupied by mucilage is sufficient to impede the infiltration of water into the soil. At this critical point, the hydrophobicity of mucilage has the effect to induce soil water repellency on a macroscopic scale.

3.3. Material and Methods

Mucilage collection

As a root mucilage analog, we used mucilage extracted from chia seeds. The chemical composition of chia seed mucilage (primarily xylose, glucose, and uronic acids; Lin et al., 1994) and its physical properties are similar to those of mucilage exuded by lupin and maize roots as reported by Carminati and Vetterlein (2013). Furthermore, it can be easily extracted in large quantities. A layer of mucilage forms around chia seeds after the seeds are immersed in deionized water (Lin et al., 1994). To extract it, we mixed seeds at a gravimetric ratio of 1:10 with deionized water and stirred the mixture for 2 h. Then we filtered it through sieves of 0.5- and 0.2-mm mesh size by applying a suction of −800 hPa to separate seeds and gel.

Sample preparation

Different amounts of chia mucilage were mixed with particles of various grain sizes to achieve different mucilage contents (weight of dry mucilage per weight of dry soil). We used washed quartz sand from a sand pit located near Duingen (Germany) and sieved it to achieve the following range of particle sizes and mucilage contents: coarse-textured sand (0.5–0.63-mm diameter; mucilage content 0.22–2 mg g^{-1}), fine sand (0.125–0.2-mm diameter; 0.88–8.8 mg g^{-1}), and silt (36–63-µm diameter; 6.7–19.1 mg g^{-1}). We

also used glass beads (0.1–0.2-mm diameter; mucilage content 0.82–3.3 mg g^{-1}; SWARCO VESTGLAS GmbH). The range of contents of dry mucilage per weight of soil were selected according to preliminary tests performed according to the following methodology.

The wet weight of mucilage mixed with particles ranged from a minimum of one-third up to three times the weight of the particles to achieve the highest dry mucilage content in the finest particles (silt). Minimum weight was achieved by mixing mucilage with water and leaving it to fully swell in a closed container for 15 min. It was subsequently stirred for 3 min and mixed with particles of a given size. The weight of dry matter in fresh mucilage was derived by drying 200 g of wet mucilage at 60°C with ventilation for 96 h for each set of undisturbed and disturbed samples of a specific grain size. The ratio between the weight of dry and wet mucilage was 6 ± 0.5 mg g^{-1}.

For preparation of undisturbed samples, mucilage–soil mixtures were spread on glass slides and allowed to dry at 20°C for 48 h. In this way, the drying and deposition of mucilage in the pore space was mimicked. Note that in our model system the rhizosphere extended in a plane (on a glass slide) and drying occurred by evaporation rather than by root water uptake and drying of the surrounding bulk soil, which has a radial geometry. Samples were prepared in a way that their dry thickness was kept at 1.5 ± 0.1 mm so that drying was fast.

Parts of the same mixture were spread and let dry for 48 h at 20°C, then the mucilage–particle packings were gently crushed by hand to avoid breaking of particles and fixed to glass slides with double-sided tape according to the procedure described by Bachmann et al. (2000).

It is important to mention that undisturbed and repacked samples had different thicknesses. The undisturbed samples were multilayered porous media with a three-dimensional geometry, while the repacked samples were composed of a single layer of grains taped to a glass slide in a quasi-two-dimensional setup. The latter method is a well-established technique that allows the measurement of contact angles for a broad range of wettabilities, from hydrophobicity to subcritical water repellency (Bachmann et al., 2000). Comparison of the results obtained with these approaches is not straightforward but it provides important information, as discussed below.

Contact angle measurements

Contact angles were measured using the sessile drop method by placing 1-μL drops of deionized water with an automated syringe onto the sample surface. Contact angles were captured optically at the three-phase interface with a camera after the water drop was in contact with the sample surface for 300 ms (Drop Shape Analyzer DSA25S, Krüss GmbH). Water droplets of 2 μL were used for the coarse-textured sand samples (0.5–0.63-mm diameter). Concentrations with no apparent contact angle reading after 300 ms are discussed below. For each amount of mucilage and type of distribution, two slides were prepared and mean contact angles of 10 drops on each slide were captured.

It has to be mentioned that contact angle measurements on rough surfaces (like the multilayer packing of particles in the case of our undisturbed samples as well as the single layer of attached particles in the disturbed samples) do not allow clear identification of the exact origin of the contact line of the water–air interface on particle surfaces. The reported contact angle should be considered as an effective contact angle representative of a macroscopic wettability.

Transmission light microscopy imaging

Images of the undisturbed samples were captured with a digital camera (Olympus SC50) attached to a transmission light microscope (Olympus BX40). The images shown are a selection to illustrate the structure of dry mucilage bridges in fine sand and glass beads. Images of glass beads were captured using unstained samples. Undisturbed samples of fine sand were stained to enhance the contrast and visualize the full extent of the dry mucilage structures. After having been air dried for 48 h at 20°C, these samples were stained by immersion in an ink (Tinte 4001, Pelikan)–water solution mixed at a gravimetric ratio of 1:2. In this way we took advantage of the ability of mucilage to swell and absorb water, or in this case, an ink-water solution. Samples with a dry mucilage content of 2.8 mg g^{-1} were immersed for 5 min, then carefully rinsed with deionized water and dried for 48 h at 20°C. Samples with a dry mucilage content of 6.5 mg g^{-1} were immersed for 10 s and subsequently dried for 48 h at 20°C. Comparison of unstained and stained areas showed no visible deviation in dry mucilage structures (data not shown).

Quantification of structural extent of mucilage deposits

Radii of dry mucilage bridges in fine sand and glass beads were measured in situ by focusing through the upper two particle layers of undisturbed, unstained samples. The bridge radius was measured perpendicular to its longitudinal extension at mid-distance between pairs of connected particles. Bridges that exceeded the open pore space between neighboring particles were measured up to the contact line of the respective particles. We analyzed 10 random locations with a field of view of 0.75 by 0.56 mm in undisturbed samples with a mucilage content of 0.86 and 2.15 mg g^{-1} (glass beads, 0.1–0.2-mm diameter) and 2.8 and 6.5 mg g^{-1} (fine sand, 0.125–0.2-mm diameter).

3.4. Results

Contact angle measurements

The undisturbed samples showed a clear threshold-like behavior: below a critical mucilage content, the drop of water rapidly infiltrated within 300 ms (the highest mucilage content for which the drop infiltrated in <300 ms is indicated in Fig. 3.2a); above this critical mucilage content, infiltration into samples was impeded and a high contact angle was observed (Fig. 3.2a). The critical mucilage content increased with decreasing particle size.

The measurements on the disturbed samples showed a smoother behavior, with a gradual increase in contact angles with increasing mucilage content (Fig. 3.2b). The fact that the disturbed samples were made of a thin layer of soil particles arranged on a two-dimensional plane allowed measurements also of low contact angles (in the subcritical water repellency regime) (Bachmann et al., 2000).

To better understand the effect of soil texture on the curves shown in Fig. 3.2, we plotted the contact angles as a function of the weight of dry mucilage per solid surface area (Fig. 3.3). To calculate the specific surface area (area of the solid surface per volume) of quartz sand and glass beads, we assumed a spherical shape of all particles. Fig. 3.3 shows that approximately 0.01 mg cm^{-2} (interpolated) is needed to initially block water infiltration (contact angle ≥ 90°) in glass beads of size 0.1 to 0.2 mm in diameter. Within the other grain sizes, the initial infiltration was impeded in a narrow range of 0.019 mg cm^{-2} (0.5–0.63 mm) to 0.03 mg cm^{-2} (0.125–0.2 mm), and 0.027 mg cm^{-2} (36–63 µm). Previous sessile drop method measurements conducted on glass slides covered with

different amounts of mucilage per surface area followed a similar trend (Benard et al., 2016). The fact that sand particles are not perfect spheres might explain the greater amount of mucilage per surface area needed to impede the water drop infiltration compared with glass beads. As in Fig. 3.2b, the disturbed samples showed a gradual increase in contact angle for increasing mucilage amount per surface area. The slope of the curves is similar for all particle sizes. The slope is also similar to that of previous measurements of the contact angle of chia mucilage on glass slides (Benard et al., 2016).
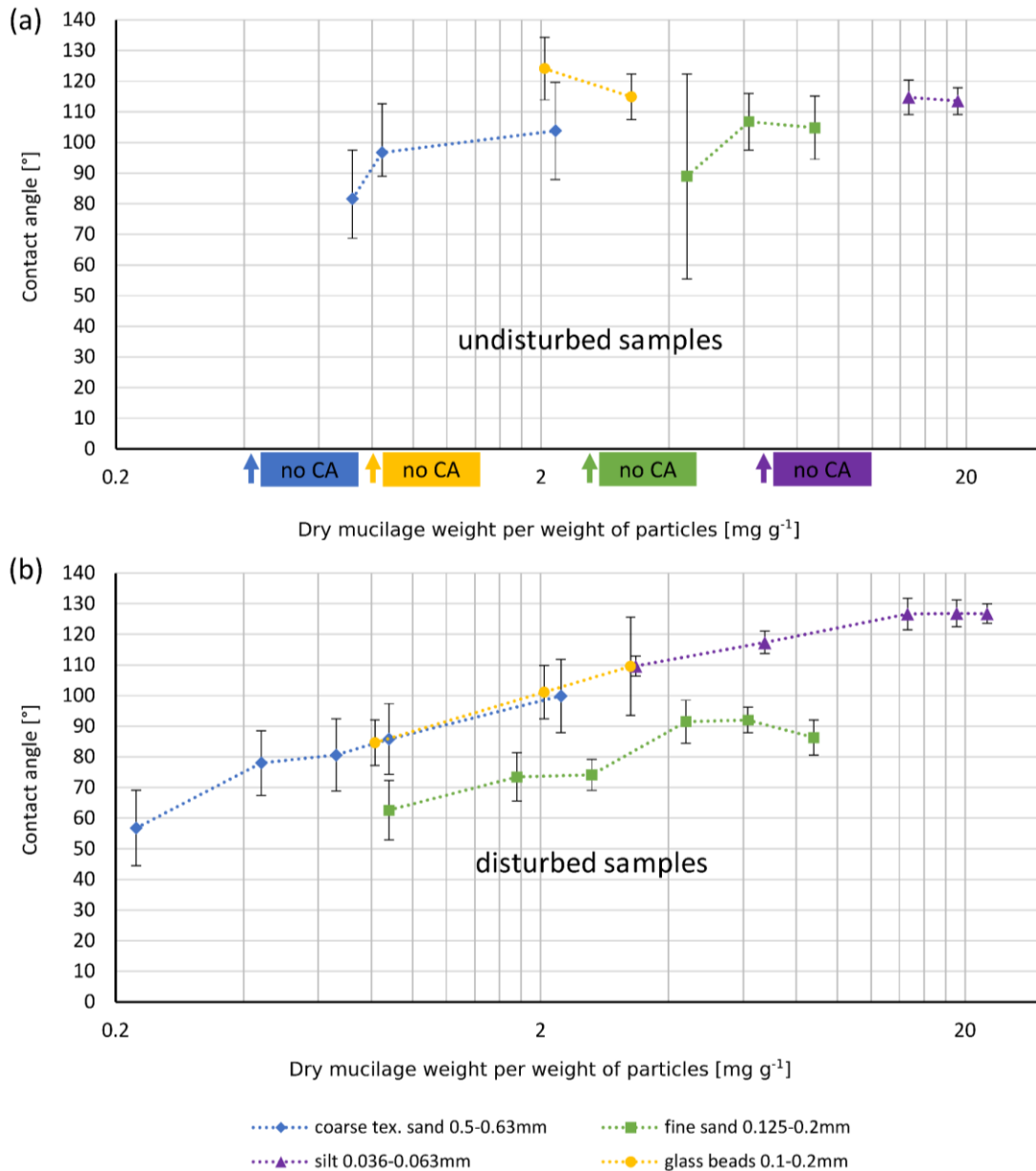
Fig. 3.2: Mean contact angle of **(a)** undisturbed and **(b)** disturbed dry mucilage–soil mixtures at various dry mucilage contents in sand and glass beads of different particle diameters. Contact angles of undisturbed samples followed a threshold-like behavior with a sudden occurrence of apparent contact angles, while contact angles of disturbed samples increased gradually with mucilage content. Different particle sizes are indicated by different colors. Standard deviations are indicated by gray error bars.
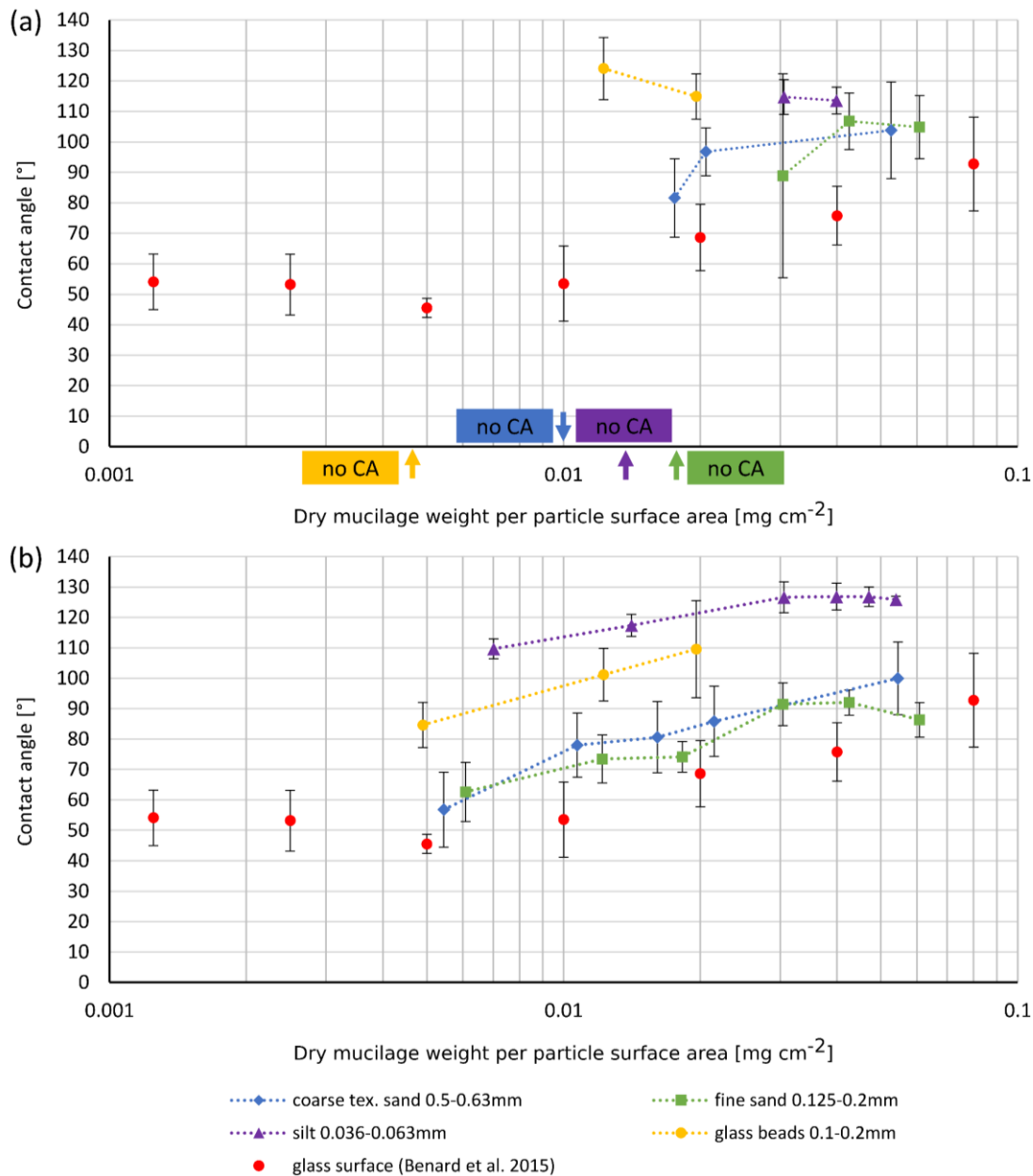
Fig. 3.3: Mean contact angles of **(a)** undisturbed and **(b)** disturbed dry mucilage–soil mixtures of various dry mucilage amounts normalized by the surface area of particles. The surface area was approximated assuming a spherical shape of particles. Different grain size distributions are indicated by color. Results of sessile drop method measurements conducted on glass slides covered with increasing amounts are indicated by red dots (Benard et al., 2016). Standard deviations are indicated by gray error bars.

Transmission light microscopy imaging

Light microscopy images of glass beads and fine sand with various mucilage contents support the conceptual model illustrated in Fig. 3.1. In undisturbed samples of fine sand, we observed that on drying, mucilage forms bridges connecting the soil particles. Images of fine sand (0.125–0.2 mm) mixed with varying amounts of mucilage are shown in Fig. 3.4. At low mucilage contents, 2.8 mg g^{-1}, thin filaments connected the sand particles

72

(Fig. 3.4a). Isolated spots of mucilage are also visible in cracks and pits on the grain surface. In samples with the same mucilage content, water drops placed on undisturbed samples infiltrated rapidly (<300 ms) (Fig. 3.2a). Disturbed samples showed a contact angle of about 72° (Fig. 3.2b). At a higher mucilage content (6.5 mg g^{-1}), the bridges between particles expanded and occupied a large fraction of the pore space (Fig. 3.4b). Covered spots on particle surfaces increased likewise. At this content (6.5 mg g^{-1}), the mean contact angle of the undisturbed samples was >90° (107° at 6.2 mg g^{-1}). Disturbed samples showed a mean contact angle of 91° for 6.2 mg g^{-1}.
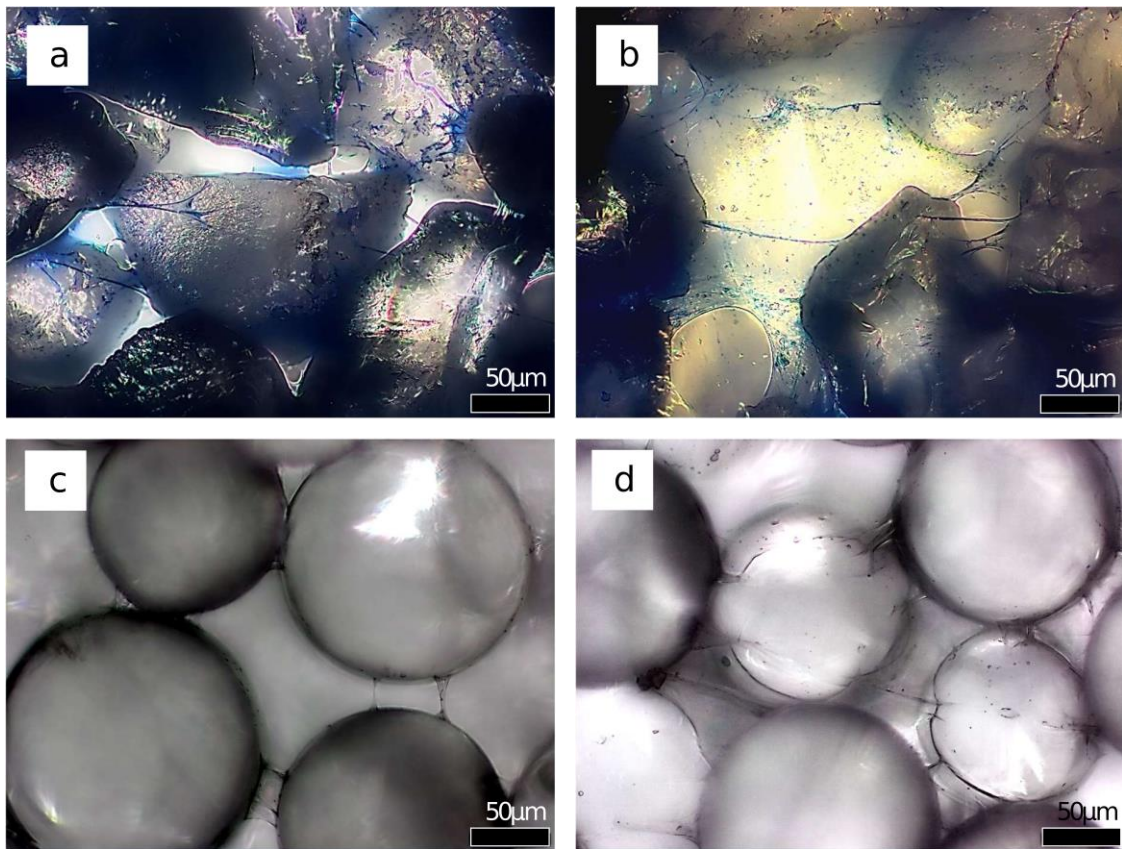
Fig. 3.4: Transmission light microscopy images of dry undisturbed samples of **(a,b)** fine sand (0.125–0.2-mm diameter) stained with an ink–water solution and **(c,d)** glass beads (0.1–0.2-mm diameter) with different mucilage contents (milligrams of dry mucilage per gram of particles): **(a)** at 2.8 mg g^{-1}, particles are connected by thin filaments of dry mucilage; **(b)** at 6.5 mg g^{-1}, bridges of mucilage cover the soil particles and extend through a large fraction of the pore space; **(c)** at 0.86 mg g^{-1}, beads are connected by thin filaments of dry mucilage; **(d)** at 2.15 mg g^{-1}, bridges of mucilage occupy a large fraction of the pore space.

Images of glass beads with a mucilage content of 0.86 mg g^{-1} (Fig. 3.4c) and 2.15 mg g^{-1} (Fig. 3.4d) followed a similar trend. For low mucilage contents (0.86 mg g^{-1}) thin bonds connect particles, leaving uncovered a large fraction of the beads' surface. The contact angle of undisturbed samples with the same mucilage content resulted in no

reading after 300 ms due to rapid water infiltration, while disturbed samples showed a mean contact angle of 85°. At a mucilage content of 2.15 mg g^{-1} the bonds between glass beads expanded into the open pore space. The mean initial contact angles of undisturbed and disturbed samples were 124 and 110°.

Quantification of the structural extent of mucilage deposits

The radius and number of mucilage bridges was measured in dry undisturbed samples for mucilage contents below and above the critical value (mucilage contents of 0.86 and 2.15 mg g^{-1} in glass beads and 2.8 and 6.5 mg g^{-1} in fine sand). The radius of the bridges increased with increasing mucilage content, while the number of bridges decreased with increasing mucilage content (Table 3.1). We used R 3.3.1 to test for statistical differences between treatments (low and high mucilage contents in particles of a specific size). Because the data were not normally distributed, a Kruskal–Wallis test was applied with a level of significance of $p < 0.05$. Based on the Kruskal–Wallis test, the differences in radii between treatments for glass beads and for fine sand were significant ($p < 0.05$).

Table 3.1: Mean dry mucilage bridge radii in glass beads and fine sand for mucilage contents in the mixture below and above the 300-ms infiltration threshold (in mg g^{-1}). Differences in the distribution of bridge radii between different mucilage contents within the same particle size were significant ($p < 0.05$). Mean bridge radii increased and number of observed discrete structures (n) decreased with increasing mucilage content.

	Dry mucilage bridge radius			
	Glass beads (0.1–0.2mm)		Fine sand (0.125–0.2mm)	
Parameter	0.86 mg g^{-1}	2.15 mg g^{-1}	2.8 mg g^{-1}	6.5 mg g^{-1}
Mean bridge radius, μm	30.09	79.59	20.9	80.42
Standard deviation	27.86	48.25	31.09	76.16
Standard error	1.90	3.90	2.28	6.02
N	215	153	186	160
p value	<0.05		<0.05	

3.5. Discussion

The water repellency of sand particles and glass beads mixed with wet mucilage, packed, and then let dry showed a threshold-like behavior. Below a critical mucilage content, water drops infiltrated within 300 ms into the undisturbed samples. Above the critical mucilage content, the undisturbed samples turned water repellent. Our hypothesis was that this threshold-like behavior was related to the microscopic distribution of mucilage in the pore space. We hypothesized that below the critical mucilage content, mucilage bridges are thin and are bypassed by infiltrating water, while above the critical mucilage

content, the mucilage bridges occupy a large fraction of the pore space, impeding the initial infiltration of water and making the samples water repellent. The microscopic images support this hypothesis.

The contact angle of the disturbed samples showed a different behavior. In the disturbed samples, the contact angle gradually increased with mucilage content. Surprisingly, the contact angle in the disturbed samples was not a function of the particle size. In fact, the relationship between contact angle and mucilage content (mass of dry mucilage per mass of dry soil) for the different quartz particles and glass beads fell on the same line, except for the fine sand, which had a slightly lower contact angle but the same slope (Fig. 3.2b). This is different than the undisturbed samples, for which the critical mucilage content increased with particle size (Fig. 3.2a). The fact that the amount of mucilage needed to induce water repellency increased with particle size is easily explainable. Coarse-textured media have a lower specific surface area (surface of the solid phase per volume), and less mucilage is needed to cover their surface. This was not the case in the disturbed samples. In the disturbed samples, mucilage structures were probably displaced from their original location and the contact angle of a single layer of particles was independent of the particle size. The fact that the contact angle of mucilage placed on glass slides plotted as a function of the mass of mucilage per solid surface has the same slope as in the disturbed samples (Fig. 3.3b) shows that the contact angle measurements in the disturbed samples provide an accurate estimation of the average contact angle caused by mucilage. However, such measurements are not representative of the water repellency in the undisturbed samples. The difference probably comes from the procedure of repacking the sand particles and glass beads in single layers placed on two-dimensional planes compared with the more realistic three-dimensional packing of the undisturbed samples.

Light microscopy images showed that mucilage was deposited in the contact region between grains. At low mucilage contents, mucilage formed thin filaments between particles. At higher mucilage contents, it formed extensive bridges that occupied a considerable fraction of the pore space. This was clearly visible in the packing of glass beads. In the packing of sand particles, which are not smooth and have a certain degree of surface roughness, mucilage was also deposited in small cavities on the particle surfaces. We expect this effect to be closely related to the receding water front, which becomes disconnected due to surface irregularities. The local deposition of mucilage in

isolated spots leads to a distribution of mucilage spread more throughout the pore space. On the contrary, smooth surfaces, like those of glass beads, cause a more preferential deposition of mucilage in the contact region between neighboring particles (Fig. 3.4) because the connectivity of the receding water front is more likely to be maintained during drying. This amplified preferential distribution on smooth surfaces explains the smaller amount of mucilage needed to impede the initial infiltration into samples of glass beads (2 mg g^{-1}) compared with fine sand (4.4 mg g^{-1}) (Fig. 3.2a). In a medium with the texture of the smooth glass beads, mucilage is concentrated in the bottlenecks between particles which results in an amplified effect of dry hydrophobic mucilage. The more scattered distribution of mucilage on rough particles and the increased mucilage content needed to induce water repellency provide further evidence of the importance of the continuity of the receding wetting front in the mechanism of mucilage distribution in soil.

The effect of a preferential mucilage distribution and the threshold-like occurrence of water repellency can be understood following percolation theory (Stauffer, 1985). Consider a network of pores either open or closed for water to flow. When a critical fraction of pores is blocked (at the percolation threshold), there is a 50% chance of open pores forming a connected cluster spanning from one side to the opposite side of the domain (Stauffer, 1985). Following this concept, let us simplify the packing of particles as a network in which mucilage is randomly distributed in the nodes. Infiltration is impeded when a sufficient fraction of nodes is blocked by the mucilage. Close to the percolation threshold, a slight change in mucilage content can cause the sample to switch from wettable to water repellent. The variability of the contact angles is therefore expected to increase close to the percolation threshold. This effect is visible in the large standard deviation of the contact angle for fine sand at a mucilage content of 4.4 mg g^{-1} (the measured contact angle ranged from <60° to >120°, Fig. 3.2a). For the other textures, a similar increase in variability is expected for amounts between the first achievable readings and the contents where no apparent contact angle was observed.

In the undisturbed samples, more mucilage was needed to induce the initial impedance of water infiltration in fine particles. This result confirms the studies of Kroener et al. (2015), where the concept of percolation in relation to water repellency was introduced. This observation seems to contradict our concept that water repellency occurs when a critical fraction of the pore volume is occupied by mucilage. In fact, we might expect a

similar pore volume in the fine and coarse textures we used. So, how can it be that more mucilage was needed to block the pore space of fine-textured soils? This apparent contradiction is explained by the geometry of the mucilage bridges. Microscopy images of broken mucilage bridges formed between glass beads of 1.7 to 2 mm in diameter revealed that these bridges were hollow structures (Fig. 3.5). Based on this observation, the amount of mucilage needed to block one pore scales with the surface of the bridge, which in turn scales with the surface of the particles. Because the specific surface of soils scales as the inverse of the particle diameter, 1/d, it becomes clear that the amount of mucilage needed to trigger water repellency increases in fine-textured soils.
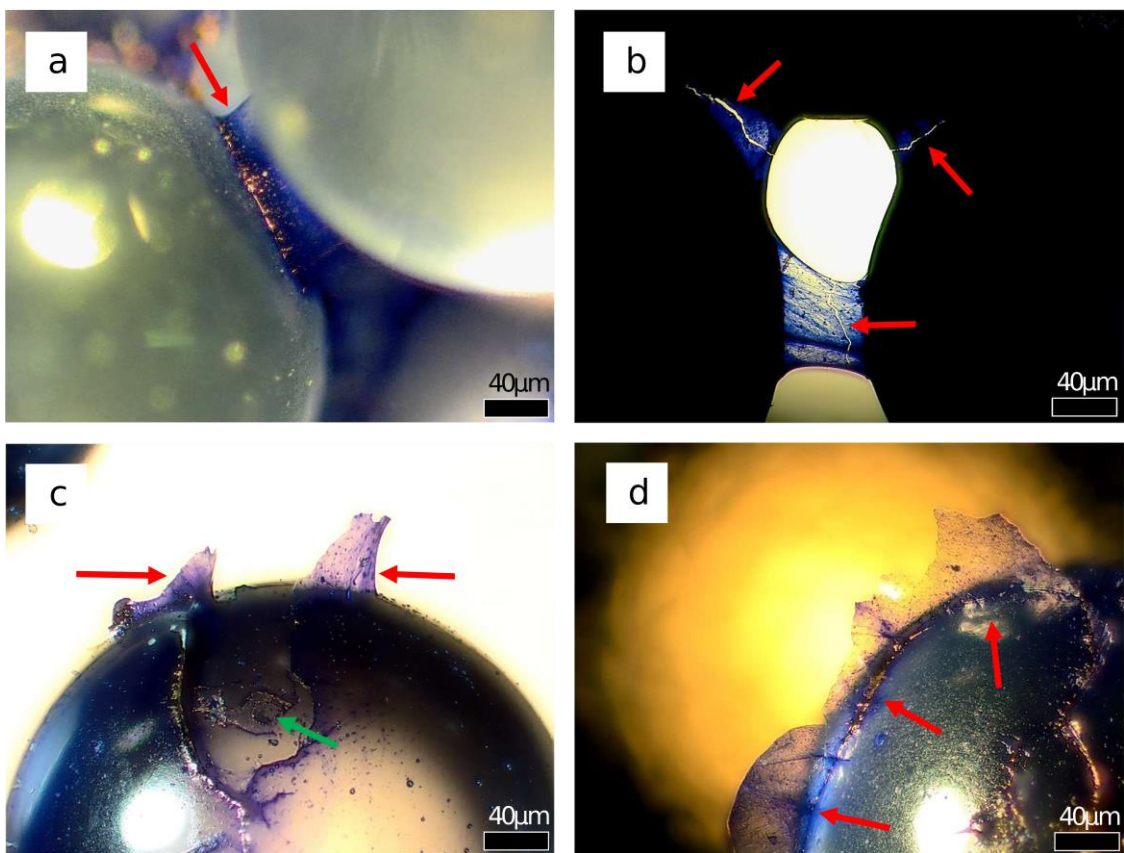
Fig. 3.5: Images of glass beads of 1.7- to 2-mm diameter with a dry mucilage content of 0.35 mg g^{-1} stained with a 33% ink–water solution: **(a)** intact mucilage bridge between glass beads (blue, red arrow); **(b)** broken mucilage bridges between glass beads (red arrows); and **(c,d)** remains of broken mucilage bridges attached to glass beads (red arrows), where **(c)** shows the spot of a former interparticle contact, indicated by green arrow surrounded by the basis (blue) of a former mucilage bridge. The images show that dry mucilage bridges are hollow structures.

This study is a first step toward a better understanding of pore-scale processes explaining the criticality of soil water repellency, as observed specifically in the rhizosphere (Carminati et al., 2010; Moradi et al., 2012) but also in a variety of soil types (e.g., Bachmann et al., 2007). Those observations were made in more natural environments,

which had a higher complexity than the simplified system we investigated. Our conceptual model is valid for mucilage with high viscosity and low surface tension (Carminati et al., 2017), such as mucilage from chia seeds and maize roots, and should not be generalized to other mucilages and dissolved organic matter. However, it is likely that such substances, like mucilage, are also heterogeneously distributed in the pore space, and the effect of such microscopic distribution on macroscopic properties, such as water repellency, remains to be studied. In conclusion, our study highlights the importance of the pore-scale distribution of mucilage for understanding the macroscopic wettability of the rhizosphere, and it calls for a similar approach in soil water repellency research.

3.6. Acknowledgements

3.7. References

Ahmed, M.A., E. Kroener, P. Benard, M. Zarebanadkouki, A. Kaestner, and A. Carminati. 2016. Drying of mucilage causes water repellency in the rhizosphere of maize: Measurements and modelling. Plant Soil 407:161–171. doi: 10.1007/s11104-015-2749-1

Albalasmeh, A.A., and T.A. Ghezzehei. 2014. Interplay between soil drying and root exudation in rhizosheath development. Plant Soil 374:739–751. doi: 10.1007/s11104-013-1910-y

Bachmann, J., M. Deurer, and G. Arye. 2007. Modeling water movement in heterogeneous water-repellent soil: 1. Development of a contact angle-dependent water-retention model. Vadose Zone J. 6:436–445. doi: 10.2136/vzj2006.0060

Bachmann, J., A. Ellies, and K.H. Hartge. 2000. Development and application of a new sessile drop contact angle method to assess soil water repellency. J. Hydrol. 231–232:66–75. doi: 10.1016/S0022-1694(00)00184-0

Benard, P., E. Kroener, P. Vontobel, A. Kaestner, and A. Carminati. 2016. Water percolation through the root–soil interface. Adv. Water Resour. 95:190–198. doi: 10.1016/j.advwatres.2015.09.014

Bengough, A.G. 2012. Water dynamics of the root zone: Rhizosphere biophysics and its control on soil hydrology. Vadose Zone J. 11(2). doi: 10.2136/vzj2011.0111

Brinker, C.J., and G.W. Scherer. 1990. Sol-gel science: The physics and chemistry of sol-gel processing. Academic Press, Boston.

Carminati, A. 2013. Rhizosphere wettability decreases with root age: A problem or a strategy to increase water uptake of young roots? Front. Plant Sci. 4:298. doi: 10.3389/fpls.2013.00298

Carminati, A., P. Benard, M.A. Ahmed, and M. Zarebanadkouki. 2017. Liquid bridges at the root–soil interface. Plant Soil (in press). doi: 10.1007/s11104-017-3227-8

Carminati, A., A.B. Moradi, D. Vetterlein, P. Vontobel, E. Lehmann, U. Weller, et al.. 2010. Dynamics of soil water content in the rhizosphere. Plant Soil 332:163–176. doi: 10.1007/s11104-010-0283-8

Carminati, A., and D. Vetterlein. 2013. Plasticity of rhizosphere hydraulic properties as a key for efficient utilization of scarce resources. Ann. Bot. 112:277–290. doi: 10.1093/aob/mcs262

Dakora, F.D., and D.A. Phillips. 2002. Root exudates as mediators of mineral acquisition in low-nutrient environments. Plant Soil 245:35–47. doi: 10.1023/A:1020809400075

Gregory, P.J. 2006. Roots, rhizosphere and soil: The route to a better understanding of soil science? Eur. J. Soil Sci. 57:2–12. doi: 10.1111/j.1365-2389.2005.00778.x

Hallett, P.D., D.C. Gordon, and A.G. Bengough. 2003. Plant influence on rhizosphere hydraulic properties: Direct measurements using a miniaturized infiltrometer. New Phytol. 157:597–603. doi: 10.1046/j.1469-8137.2003.00690.x

Hinsinger, P., A.G. Bengough, D. Vetterlein, and I.M. Young. 2009. Rhizosphere: Biophysics, biogeochemistry and ecological relevance. Plant Soil 321:117–152. doi: 10.1007/s11104-008-9885-9

Kroener, E., M.A. Ahmed, and A. Carminati. 2015. Roots at the percolation threshold. Phys. Rev. E 91(4):042706. doi: 10.1103/PhysRevE.91.042706

Lin, K.-Y., J.R. Daniel, and R.L. Whistler. 1994. Structure of chia seed polysaccharide exudate. Carbohydr. Polym. 23:13–18. doi: 10.1016/0144-8617(94)90085-X

Moradi, A.B., A. Carminati, A. Lamparter, S.K. Woche, J. Bachmann, D. Vetterlein, et al. 2012. Is the rhizosphere temporarily water repellent? Vadose Zone J. 11(3). doi: 10.2136/vzj2011.0120

Oades, J.M. 1978. Mucilages at the root surface. Eur. J. Soil Sci. 29:1–16. doi: 10.1111/j.1365-2389.1978.tb02025.x

Read, D.B., A.G. Bengough, P.J. Gregory, J.W. Crawford, D. Robinson, C.M. Scrimgeour, et al. 2003. Plant roots release phospholipid surfactants that modify the physical and chemical properties of soil. New Phytol. 157:315–326. doi: 10.1046/j.1469-8137.2003.00665.x

Read, D.B., P.J. Gregory, and A.E. Bell. 1999. Physical properties of axenic maize root mucilage. Plant Soil 211:87–91. doi: 10.1023/A:1004403812307

Roose, T., S.D. Keyes, K.R. Daly, A. Carminati, W. Otten, D. Vetterlein, and S. Peth. 2016. Challenges in imaging and predictive modeling of rhizosphere processes. Plant Soil 407:9–38. doi: 10.1007/s11104-016-2872-7

Sposito, G. 2013. Green water and global food security. Vadose Zone J. 12(4). doi: 10.2136/vzj2013.02.0041

Stauffer, D. 1985. Introduction to percolation theory. Taylor & Francis, London.

Watt, M., M.E. McCully, and C.E. Jeffree. 1993. Plant and bacterial mucilages of the maize rhizosphere: Comparison of their soil binding properties and histochemistry in a model system. Plant Soil 151:151–165. doi: 10.1007/BF00016280

York, L.M., A. Carminati, S.J. Mooney, K. Ritz, and M.J. Bennett. 2016. The holistic rhizosphere: Integrating zones, processes, and semantics in the soil influenced by roots. J. Exp. Bot. 67:3629–3643. doi: 10.1093/jxb/erw108

Young, I.M. 1995. Variation in moisture contents between bulk soil and the rhizosheath of wheat (*Triticum aestivum* L. cv. Wembley). New Phytol. 130:135–139. doi: 10.1111/j.1469-8137.1995.tb01823.x

Zarebanadkouki, M., M.A. Ahmed, and A. Carminati. 2016. Hydraulic conductivity of the root–soil interface of lupin in sandy soil after drying and rewetting. Plant Soil 398:267–280. doi: 10.1007/s11104-015-2668-1

Zickenrott, I.-M., S.K. Woche, J. Bachmann, M.A. Ahmed, and D. Vetterlein. 2016. An efficient method for the collection of root mucilage from different plant species: A case study on the effect of mucilage on soil water repellency. J. Plant Nutr. Soil Sci. 179:294–302. doi: 10.1002/jpln.201500511

4. IMPACT OF PORE-SCALE WETTABILITY ON RHIZOSPHERE REWETTING[†]

Pascal Benard[1,2*], Mohsen Zarebanadkouki[2], Andrea Carminati[2]

[1]   Division of Soil Hydrology, University of Göttingen, Göttingen, NI, Germany
[2]   Division of Soil Physics, University of Bayreuth, Bayreuth, BY, Germany

[*]   Corresponding Author

Abstract

Vast amounts of water flow through a thin layer of soil around the roots, the rhizosphere, where high microbial activity takes place – an important hydrological and biological hotspot. The rhizosphere was shown to turn water repellent upon drying, which has been interpreted as the effect of mucilage secreted by roots. The effects of such rhizosphere water dynamics on plant and microbial activity are unclear. Furthermore, our understanding of the biophysical mechanisms controlling the rhizosphere water repellency remains largely speculative. Our hypothesis is that the key to describe the emergence of water repellency lies within the microscopic distribution of wettability on the pore-scale. At a critical mucilage content, a sufficient fraction of pores is blocked and the rhizosphere turns water repellent. Here we tested whether a percolation approach is capable to predict the flow behavior near the critical mucilage content. The wettability of glass beads and sand mixed with chia seed mucilage was quantified by measuring the infiltration rate of water drops. Drop infiltration was simulated using a simple pore-network model in which mucilage was distributed heterogeneously throughout the pore space with a preference for small pores. The model approach proved capable to capture the percolation nature of the process, the sudden transition from wettable to water repellent and the high variability in infiltration rates near the percolation threshold. Our study highlights the importance of pore-scale distribution of mucilage in the emergent flow behavior across the rhizosphere.

4.1. Introduction

The rhizosphere is defined as the layer of soil particles actively modified by plant root growth and exudation (Gregory, 2006; Hinsinger et al., 2009). Regardless of its narrow extent ranging from millimeters to a few centimeters, this region is crossed by an immense amount of water. About 40% of all terrestrial precipitation flows across the root-soil interface when taken up by plants (Bengough, 2012; Sposito, 2013). In this context, the importance of the hydraulic properties of the rhizosphere, hosting a tremendous biodiversity (Philippot et al., 2013) ought to be acknowledged.

Alterations in rhizosphere physical and hydraulic properties induced by plant roots have been reported by an increasing number of studies (Young, 1995; Hallett et al., 2003; Carminati et al., 2010; Zarebanadkouki et al., 2016; Naveed et al., 2017). Several of these rhizosphere alterations were attributed to the presence of root exuded mucilage,

82

such as hysteretic fluctuations in water content during drying-wetting cycles in the rhizosphere of lupins (*Lupinus albus*) (Carminati et al., 2010). In this case, the authors related the observed increased water retention during drying and decreased wettability during rewetting to root exuded mucilage. Low rhizosphere wettability was also observed in maize (*Zea Mays*) (Ahmed et al., 2016).

Mucilage is a polymeric substance released from the root tip. It is mainly composed of polysaccharides and about 1% of lipids (Oades, 1978; Read et al., 2003). It can be classified as a hydrogel (Brinker and Scherer, 1990) and its polymer network is capable to increase the water retention when embedded in a soil matrix (Kroener et al., 2018). Recently, Kroener et al. (2018) hypothesized that mucilage polymers need to be anchored to soil particles to withstand shrinkage and subsequent collapse during soil drying. It has been shown that mucilage and other highly polymeric substances, like bacterial EPS (extracellular polymeric substances) and their analogues, form distinct structures within the soil pore space during drying (Roberson et al., 1993; Albalasmeh and Ghezzehei, 2014; Benard et al., 2018). At low content, mucilage forms thin threads between particles. When a critical mucilage content is reached, these threads extend throughout the pore space forming large 2D lamellar structures (Benard et al., 2018). The authors proposed that this critical mucilage content determines the onset of water repellency in the rhizosphere. A physical explanation for the formation of these structures in drying soil was provided by Carminati et al. (2017) and was related to the high viscosity of mucilage.

Dry root mucilage deposits reduce soil wettability depending on plant species and concentration (Zickenrott et al., 2016; Naveed et al., 2017) and they can potentially turn hydrophobic (Ahmed et al., 2016). Kroener et al. (2015) and Benard et al. (2016, 2018) made a first attempt to estimate the amount of mucilage needed to induce water repellency in the rhizosphere for varying soil textures. Using a percolation model, the authors were able to predict the mucilage content at which water could no longer penetrate into the soil. In the present paper, we aimed to further develop this model by including the temporal dynamics of water infiltration.

The water drop penetration time (WDPT) is typically used to characterize soil wettability. The method consists in placing water drops of known volume onto soil and capturing the time of their complete penetration into the pore space (Woudt, 1959; Dekker and Ritsema, 1996). We used this method to assess the water repellency of sand

particles and glass beads mixed with chia seed mucilage, which is used as a preliminary model of the rhizosphere. Our hypothesis that the water penetration time across the rhizosphere has a percolation nature which originates from the non-uniform distribution of mucilage (preferably deposited in small pores). This results in a heterogeneous distribution of wettability on the pore-scale, which in turns determines the on-set of water repellency. At a critical mucilage content (the percolation threshold), when a sufficient fraction of pores are non-wettable, the water penetration time increases and becomes highly variable. Above this threshold, the non-wettable pores block the water penetration, which becomes very slow, and macroscopic water repellency occurs. Surface roughness is expected to induce a more homogeneous distribution of mucilage and the percolation threshold is expected to occur at higher mucilage content. The effect of particle size on macroscopic wettability has been analyzed in a previous study (Benard et al., 2018), where it was shown that the finer are the soil particles, the higher is their specific surface and the critical mucilage content at which water repellency occurs.

Here, we focused on the temporal dynamics of water infiltration measured in sand and glass beads embedded with mucilage and simulated using a new percolation method. The model was designed as basic as possible to allow for an unbiased evaluation of its capabilities to capture the percolation nature of the process and assess the impact of pore-scale wettability on rhizosphere rewetting dynamics.

4.2. Material and Methods

Mucilage extraction & Sample preparation

A detailed description of mucilage extraction and sample preparation can be found in Benard et al. (2018). In summary, we mixed different amounts of mucilage with glass beads of 0.1-0.2 mm, and fine sand of 0.125 – 0.2 mm in diameter to achieve different dry mucilage contents (weight of dry mucilage per weight of particles). As an analog for root exuded mucilage, we used mucilage extracted from chia seeds (*Salvia hispanica* L.). Its physical properties are similar to mucilage exuded by maize roots in the sense that for increasing mucilage content the contact angle increases (Ahmed et al., 2016). The mixtures of mucilage and glass beads (and of mucilage and sand) were spread on glass slides and let dry at 20°C for 48 h. Upon drying the samples were not repacked to avoid artificial alterations of the microscopic mucilage distribution in the pore space.

Dry mucilage content of the samples ranged from 0.9 to 6 mg g^{-1} in glass beads, and 2.8 to 9.3 mg g^{-1} in sand. These ranges of mucilage content were selected according to preliminary tests. At higher contents the samples were repellent (contact angle above 90°), while at lower contents the samples were wettable. We focused on the interesting ranges of mucilage content when the samples switched between the two states. Sample thickness was approximately 1.5 ± 0.1 mm.

Wettability quantification

In a classical WDPT (water drop penetration time) test, drops of known volume are placed on a soil and the time for complete penetration is captured. The water drop penetration times are divided in discrete classes to characterize the wettability of different soils (Woudt, 1959; Dekker and Ritsema, 1996). In this study we focused on the infiltration dynamics in soil affected by dry mucilage deposits of reduced wettability. To capture the effect of mucilage on infiltration dynamics we placed 1 µL drops of deionized water on the dry samples and the infiltration process was recorded at intervals of about 200 ms (CCD camera; Drop Shape Analyzer DSA30, Krüss GmbH). The drop volume was estimated from the optically detected drop geometry and a manually set baseline. For each mucilage content two slides were prepared and the infiltration of at least 10 drops per slide was captured. Note that the decrease in volume could not always be easily captured from recorded image sequences. Due to that reason, the number of captured drop infiltrations per mucilage content ranged from 13 to 20 in glass beads and 19 to 31 in sand.

For high mucilage content, water did not completely infiltrate within the observation time of 5 minutes. Therefore, we calculated the WDPT from the slope of the infiltration rate over the square root of time. For consistency we followed this procedure for all measurements.

Measurements were conducted in a temperature-controlled room at about 25°C. Humidity was not measured in the process of wettability quantification. Evaporation loss was approximated for a relative humidity of 65%.

Model description

We developed a simple pore-network model based on the concept of percolation theory. In a percolation system, pores are randomly assigned open or closed. When a critical fraction of pores is blocked, the connectivity of the open pores is strongly reduced and

the system switches from conductive to non-conductive. Our idea is that such a concept can be used to predict and describe the transition of soils mixed with hydrophobic substances such as mucilage from wettable to water repellent. We assume that the pore-size distribution of our model system is random and during drying mucilage is preferentially deposited in the small pores. The contact angle in each pore depends on its specific surface and the amount of mucilage. If the contact angle is above 90° the pore is blocked.

The effect of the pore-scale distribution of wettability is illustrated in Fig. 1, in which pores are distributed on a 2D square lattice. When the fraction of hydrophobic pores reaches a critical value (at the percolation threshold), small variations in their number and distribution can cause a substantial change in macroscopic wettability, as in the central image of Fig. 4.1. For a low mucilage content in soil, most pores are wettable and so is the soil (left image). At the threshold mucilage content, there is a 50% chance for a connected cluster of wettable pores to span from the upper to the lower side of the system (central image). Macroscopic wettability is most critically affected by the pore-scale distribution of wettability at this point and preferential flow is likely to be observed. Above this threshold, the rhizosphere turns water repellent (right image).

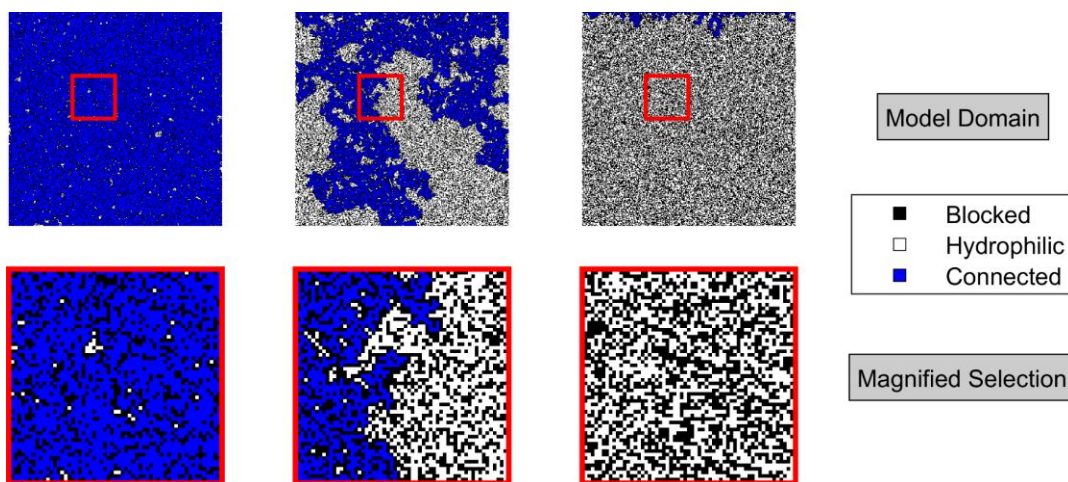**Fig. 4.1 top:** Results from a percolation model in a 2D square lattice of 300 x 300 sites. Probability of a pore to be hydrophobic, hence blocked from left to right: 0.3, 0.41, 0.5. **Bottom:** Magnification of indicated area (red rectangle) of 60 x 60 pores of above shown realizations. Hydrophobic pores are black. Hydrophilic pores are white. Open pores connected to the top of the system are blue.

The percolation model described hereafter was used to simulate the water drop infiltration experiments. The numerical model was written in MATLAB 2017b (The MathWorks, Inc.). Capillarity was considered to be the main driving force for infiltration of 1 µL of water. Pores can be filled only through saturated adjacent pores. In consecutive steps, the shortest time to fill a pore is calculated. The time is derived by approximation of water flow through a cylindrical pore, with the flow rate depending on the contact angle, pathway distance and pore radius. Saturation of each pore currently being filled is updated according to this interval. Simultaneously, the decrease in drop volume is corrected for loss by evaporation according to the approximation by Hu and Larson (2002). Final water drop penetration time is derived by summation of all consecutive infiltration and/or evaporation time steps needed to deplete a drop volume of 1 µL.

The soil pores are placed on a cubic lattice with a coordination number of 6, hence each pore is connected to its 6 adjacent neighbors. Pore volume is estimated from a random normal distribution of grain diameters between 0.1-0.2 (glass beads), respectively 0.125-0.2 mm (sand), assuming a porosity of 0.36, which is the porosity of a random close packing (RCP) of equally sized spheres (Torquato et al., 2000). The surface area of a pore derived for a cubic packing is corrected to fit the increase in surface area by 1.22 for a unit volume of an RCP of spheres. The surface area was doubled for simulations in sand, to account for roughness which induced an increase in the number of sites for preferential mucilage deposition (Benard et al., 2018). The mucilage content of each pore is derived from a random normal distribution of mucilage contents. Mucilage contents from high to low are assigned to pore volumes from small to large. In this way we mimicked the preferential deposition of mucilage in small pores.

Flow of water from a filled to an empty accessible (wettable) pore is calculated through a cylindrical capillary of length L, which is equal to the sum of the two grain radii of particles defining adjacent pores. The radius of the cylinder r is derived from the biggest circle that can be fit into the bottleneck of the smaller particle pack. The term bottleneck refers to the minimum radius of the six pathways towards the central pore in a cubic packing of spheres.

Flow from a filled into an empty pore through a cylindrical capillary is calculated employing the Hagen-Poiseuille equation (4.1):

$$Q = \frac{\pi r^4 \Delta p}{\eta 8 L} \tag{4.1}$$

where the volumetric flow rate Q [mm^3 ms^{-1}] depends on the radius of the connecting capillary r [mm], viscosity of water η [mN ms mm^{-2}], flow length L [mm], and the pressure gradient Δp [mN mm^{-2}]. The capillary pressure in a cylindrical tube is approximated employing the Young-Laplace equation (4.2):

$$P_c = \frac{2\,\gamma\,\cos(\alpha)}{r} \tag{4.2}$$

with surface tension γ [mN mm^{-1}], contact angle α [deg.], and pore radius r [mm]. Integrating (2) into (1) and given $Q = V/t$ one obtains the time t [ms] it takes to fill a pore of defined volume V [mm^3] through a cylindrical pipe (4.3):

$$t = \frac{\eta\,8}{\pi\,r^4}\frac{r}{2\,\gamma\,\cos(\alpha)}\frac{L_{tot}\,V}{1} \tag{4.3}$$

Note that L_{tot} is the length of the flow path from the placed drop of water through water filled pores to an empty accessible pore. The derived time to fill a pore and the current flux Q into a pore is updated for additional flow paths emerging in the process of water percolation through the system. In other words, when water finds an additional pathway to a partially unsaturated pore, this pore is filled quicker.

The contact angle α was calibrated using the measurements by Benard et al. (2016). In this study, the contact angle was measured for different concentrations of mucilage per surface area. Contact angles were derived after fitting the contact angle against the square root of dry mucilage concentration per surface area (Fig. 4.2).
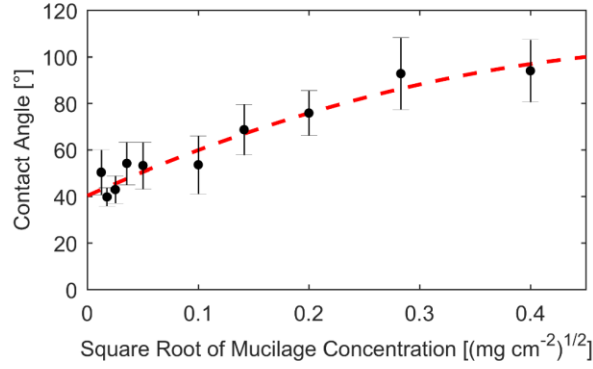
Fig. 4.2: Contact angle measured on glass slides covered with different concentrations of mucilage per surface area (dots). Standard deviation indicated by error bars. Fit of measured contact angles against square root of mucilage concentration per surface area (dashed line).

Since our measurements were based on optical measures of the decrease in drop volume, the decrease was corrected for loss by evaporation. In water repellent conditions when the contribution of infiltration diminishes, evaporation substantially contributes to the decrease in drop volume over time. The current evaporation rate $e(t)$ [µL s^{-1}] is approximated according to Hu and Larson (2002):

$$e(t) = -\pi RD(1 - H)c_v(0.27\alpha(t)^2 + 1.30) \qquad (4.4)$$

with contact-line radius R [mm], water vapor diffusivity D [mm^2 s^{-1}], relative humidity H [-], saturated water vapor concentration c_v [g mm^{-3}], and drop contact angle α [rad.] which changes over time. R [mm] was derived from the mean size of the 9 randomly generated grains in x- and y-direction below the imposed drop center. In this way a mean base radius of 0.68 mm for 0.1 to 0.2 mm particles (glass beads) and 0.73 mm for 0.125-0.2 mm particles (sand) was achieved.

For known initial drop volume (i.e. 1 µL), the contact angle α is derived integrating the height of the drop h [mm] in its center (4.5) into (4.6). The initial contact angle of a water drop on a sample is approximated in this first step based on the initial volume ($V(t=0)$, i.e. 1 µL) and base radius R. The drop volume is decreased by the sum of evaporated and infiltrated volume in each time step. As long as additional pores are being filled, α is adapted for a decrease in drop volume according to the shortest time step t needed to saturate an additional pore. Maximum time step for infiltration was fixed to 1000 ms to assure a constant update of evaporation and avoid overestimation of infiltration times, especially in the water repellent regime. When the infiltration of water was incomplete, due to a lack of accessible empty pores, the time step of constant

evaporation was fixed to 1000 ms. In this way the contact angle was adapted over time and evaporation was approximated stepwise with decrease in drop volume.

$$h(t) = R \tan[\frac{\alpha(t)}{2}] \qquad (4.5)$$

$$V(t) = \frac{\pi(h(t)) * (3R^2 + h(t)^2)}{6} \qquad (4.6)$$

$$V(t) = \frac{\pi(R \tan\left(\frac{\alpha(t)}{2}\right) * (3R^2 + (R \tan\left(\frac{\alpha(t)}{2}\right))^2)}{6} \qquad (4.7)$$

4.3. Results

Wettability Quantification

Measurements of decrease in drop volume over time were performed for a range of dry mucilage contents across the transition to water repellency. Individual infiltration slopes were obtained by fitting the decrease in drop volume as a function of square root of time. Results are presented as a summary of fitted slopes of infiltration curves at each mucilage content (Fig. 4.3).

The infiltration dynamics in glass beads showed a threshold-like decrease in wettability with increase in dry mucilage content. For 0.9 mg g^{-1} all drops penetrated within 300 ms corresponding to a slope of $\geq$0.058 µL ms$^{-1/2}$. At 2.2 mg g^{-1} a high variation was observed, with the infiltration slopes ranging from 0.015 to 0.004 µL ms$^{-1/2}$. Standard deviation decreased with increase in mucilage content. Mean infiltration slopes decreased to 0.0023, 0.0018 and 0.0018 µL ms$^{-1/2}$ for 3.5, 4.7, and 6 mg g^{-1} respectively (Fig. 4.3a).

For the lowest content of 2.8 mg g^{-1} in sand, all drops infiltrated within the detection limit of 300 ms (slope of $\geq$0.058 µL ms$^{-1/2}$). At 4.7 mg g^{-1} a high variability in infiltration slopes was observed. Slopes ranged from 0.018 to 0.038 µL ms$^{-1/2}$ with a mean of 0.003 µL ms$^{-1/2}$. With an increase to 6.5 mg g^{-1} variation in infiltration slope decreased to values between 0.011 and 0.002 µL ms$^{-1/2}$. The highest mucilage content of 9.3 mg g^{-1} resulted in a mean infiltration slope of 0.002 µL ms$^{-1/2}$ (Fig. 4.3b).
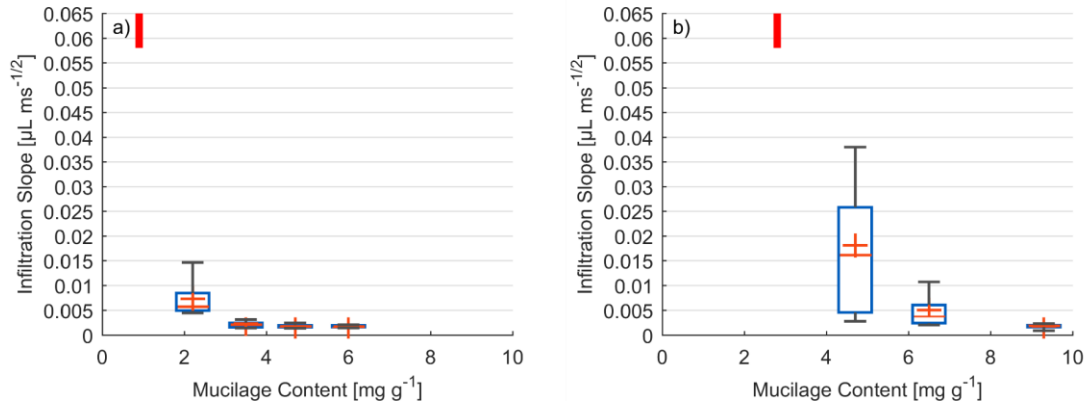
Fig. 4.3: Box and Whisker plots of infiltration slope derived from fit of volume against square root of time for water drops placed on glass bead **(a)** and sand **(b)** samples of different dry mucilage content; Lowest measured mucilage content (infiltration time below detection limit) indicated by red bar; Slope at 300 ms detection limit ≥ 0.058 µL ms$^{-1/2}$; Whiskers mark the upper and lower 25% (quartiles) of values excluding outliers exceeding 1.5 times the interquartile range (box); Median indicated by red line within the box separating second and third quartile. Mean indicated by red cross.

Water Drop Penetration Time (WDPT)

The derived water drop penetration time (WDPT) from measurements and simulations are shown alongside top views of exemplary cross sections of average, final water distributions from simulations (Fig. Fig. 4.4 and Fig. 4.5).

The square of the Pearson product moment correlation coefficient (r^2) of the mean water drop penetration time including the lowest mucilage content measured with an approximated WDPT of 150 ms the r^2 of the mean WDPT measured and simulated was 0.16. For glass beads it was 0.18 and for sand it was 0.55.

Fitted measurements and simulations of infiltration in glass beads showed increasing WDPT with increasing mucilage content (Fig. 4.4). The threshold mucilage content was identified between 2.5 and 2.8 mg g^{-1} from the simulations, marked by a maximum in variability in penetration time and followed by a drastic change in wettability. Likewise, a maximum in diversity of connected, water filled pore clusters (wetted front) was observed across the threshold. Mean WDPT from simulations above the repellent transition (> 3 mg g^{-1}) was about 19.7 min.

Fitted WDPT and simulations in sand showed a similar trend as in glass beads with a high variability and rapid change in wettability at 4.9 mg g^{-1} (Fig. 4.5). Derived mean WDPT from simulations above the repellent transition (> 5.5 mg g^{-1}) was about 19.1 min.

Fig. 4.4 top: Water drop penetration time (WDPT) derived from optically detected drop volume decrease (gray dots) and simulated WDPT (black dots) in glass beads (0.1-0.2 mm in diameter); Detection limit of 300 ms is indicated for the lowest measured mucilage content of 0.9 mg g⁻¹ by a red bar; **Bottom left to right:** Top view of average final water saturation of exemplary simulations of mucilage contents across the repellent transition.
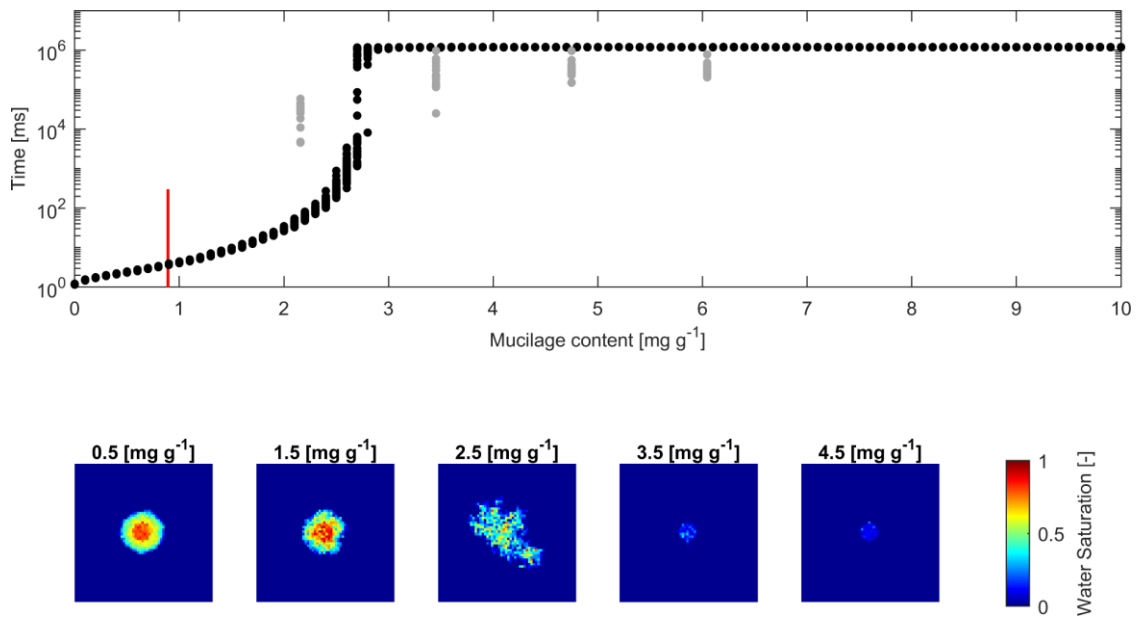

Fig. 4.5 top: Water drop penetration time (WDPT) fitted from optically detected drop volume decrease (gray dots) and simulated WDPT (black dots) in sand (0.125-0.2 mm in diameter); Detection limit of 300 ms is indicated for the lowest measured mucilage content of 2.8 mg g⁻¹ by a red bar; **Bottom left to right:** Top view of average final water saturation of exemplary simulations of mucilage contents across the repellent transition.
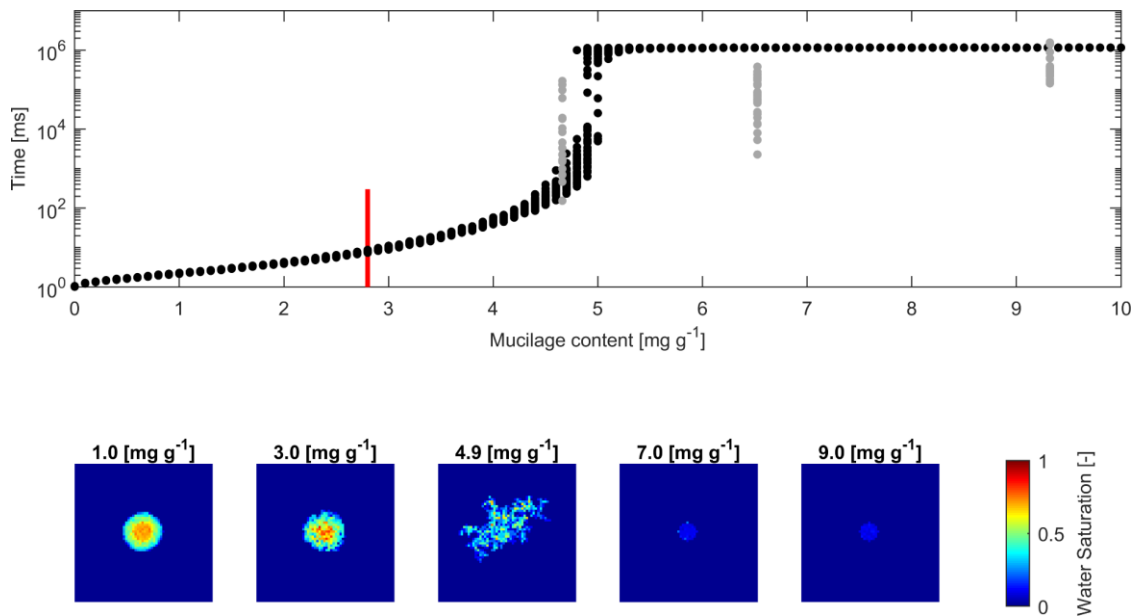
4.4. Discussion

The main hypothesis was that the occurrence of macroscopic water repellency and the critical nature of water infiltration in soils mixed with mucilage was related to the heterogeneous distribution of wettability on the pore-scale. We tested this hypothesis by monitoring the infiltration of water drops placed on particles of comparable size and different surface roughness mixed with varying mucilage content. Subsequently, a simple pore-network model was used to simulate the drop infiltration experiments.

The water drop penetration time in glass beads and sand mixed with mucilage showed the expected threshold-like behavior, with a sudden increase in water drop penetration time. Infiltration times increased from milliseconds to minutes for mucilage contents ranging from 1 to 6 mg g^{-1} in glass beads, respectively 3 to 9 mg g^{-1} in sand. The derived threshold for sand is in agreement with the results of Kroener et al. (2015), who observed it between 5 and 10 mg g^{-1}.

The highest variability in infiltration time was observed at the percolation threshold, confirming the percolation nature of the process. The threshold in penetration time was well predicted by the model in which mucilage was preferentially deposited in small pores inducing a heterogeneous spatial distribution of wettability. Measurements and simulations confirm the substantial impact of the heterogeneous pore-scale wettability on water flow through the rhizosphere. When the continuity of wettable pores was blocked, the onset of macroscopic soil water repellency was observed. Increased surface roughness in sand caused the expected shift to higher mucilage content needed to induce macroscopic water repellency.

The simulations showed a sharper transition in wettability than the measurements. This might be related to the assumption that mucilage is mainly deposited in small pores. This caused large pores to remain almost unaffected and highly conductive. An underestimation of infiltration time is therefore likely to occur below the repellent transition. Additionally, the difference might arise from the time dependent properties of mucilage not considered in the model. Wettability of substrates mixed with mucilage is expected to increase over time as a consequence of mucilage rehydration and decrease in contact angle, as reported in Moradi et al. (2012) and Zickenrott et al. (2016). Below the percolation threshold, water penetration is matter of milliseconds to seconds. Due to this reason, a decrease in contact angle upon rewetting does not impact water penetration. Nevertheless, pore clogging due to mucilage rehydration and swelling

might slow down the infiltration process at and above the wettability threshold. Above the repellent transition, mean infiltration time deviated by several minutes from measurements in glass beads and sand. Water adsorption by previously dry, hydrophobic mucilage deposits could be an explanation for the underestimated water penetration time.

The variability in infiltration times across the wettability threshold was bigger and the transition smoother in sand than in glass beads. This difference between sand and glass beads is possibly related to the increased surface roughness of sand particles. Rough surface leads to an increase in number of sites for preferential mucilage deposition (Benard et al., 2018), inducing a more uniform distribution of wettability and resulting in a smoother transition across the threshold. It also explains the higher mucilage content needed to achieve a similar magnitude of water repellency as observed in glass beads in terms of infiltration time.

This study shows that macroscopic water repellency in substrates mixed with mucilage emerges from the distribution of mucilage on the pore-scale and it has a percolation nature. Towards and above the percolation threshold, the fraction of non-wettable pores increases and eventually blocks the pathway for water infiltration and the porous medium turns water repellent. The fact that water repellency was observed repeatedly in the rhizosphere (Carminati et al., 2010; Moradi et al., 2012; Ahmed et al., 2016) indicates that mucilage content around the roots is close to or above the percolation threshold. If we assume that the size of connected pore clusters affected by high mucilage content (high enough to induce water repellency) increases across the percolation threshold[*], then the combination of water retention and preferential distribution has the potential to keep pores hydraulically connected at low matric potential, when otherwise this crucial link would be lost. Additionally, close to the percolation threshold, roots could effectively control the wettability, and therefore also the diffusion of oxygen, by slightly changing the exudation rate or the chemical composition of exudates.

In summary this study reveals that the wettability of soils embedded with mucilage emerges from pore-scale mechanisms and has a percolation nature – the connectivity of hydrophobic pores determines the switch from wettable to non-wettable soil. The mixture of sand (or glass beads) with chia mucilage has been used as analogue of the rhizosphere. Doing so, we implicitly assumed that 1) mucilage is the primary factor

controlling the rhizosphere wettability, 2) mucilage from chia seeds is a good analogue of root mucilage, and 3) the processes can be easily scaled for finer soil textures. All these assumptions are (over)simplifications of rhizosphere dynamics. First of all, mucilage from different plant species showed different degrees of water repellency (Zickenrott et al., 2016; Naveed et al., 2018). Secondly, in the rhizosphere root exudates are degraded by microorganisms, which can secret other polysaccharides altering the properties of the soil solution. Such complexities need to be studied and applied to varying soil textures, including structured soils. The importance of the current study is that it points to the pore-scale distribution of hydrophilic/hydrophobic region as the key factor determining the rhizosphere properties and it proposes the percolation theory as the key concept to link pore-scale to transport properties across the rhizosphere.

*This assumption implies that the coordination number of pores critically affected by mucilage is bigger than the one of hydraulically connected (hydrophilic) pores.

4.5. Author Contributions

P.B., M.Z. and A.C. conceived the experimental set-up. P.B. conducted the experiments and processed the data. P.B. and A.C. developed the conceptual model. P.B. developed the numerical code and wrote the manuscript in consultation with M.Z. and A.C..

4.6. Funding

4.7. Bibliography

Ahmed, M.A., E. Kroener, P. Benard, M. Zarebanadkouki, A. Kaestner, and A. Carminati. 2016. Drying of mucilage causes water repellency in the rhizosphere of maize: measurements and modelling. Plant Soil 407(1–2): 161–171. doi: 10.1007/s11104-015-2749-1

Albalasmeh, A.A., and T.A. Ghezzehei. 2014. Interplay between soil drying and root exudation in rhizosheath development. Plant Soil 374(1–2): 739–751. doi: 10.1007/s11104-013-1910-y

Benard, P., E. Kroener, P. Vontobel, A. Kaestner, and A. Carminati. 2016. Water percolation through the root-soil interface. Adv. Water Resour. 95: 190–198. doi: 10.1016/j.advwatres.2015.09.014

Benard, P., M. Zarebanadkouki, C. Hedwig, M. Holz, M.A. Ahmed, and A. Carminati. 2018. Pore-Scale Distribution of Mucilage Affecting Water Repellency in the Rhizosphere. Vadose Zone J. 17(1): 0. doi: 10.2136/vzj2017.01.0013

Bengough, A.G. 2012. Water Dynamics of the Root Zone: Rhizosphere Biophysics and Its Control on Soil Hydrology. Vadose Zone J. 11(2): 0. doi: 10.2136/vzj 2011.0111

Brinker, C.J., and G.W. Scherer. 1990. Sol-gel science: the physics and chemistry of sol-gel processing. Academic Press, Boston.

Carminati, A., P. Benard, M.A. Ahmed, and M. Zarebanadkouki. 2017. Liquid bridges at the root-soil interface. Plant Soil 417(1): 1–15. doi: 10.1007/s11104-017-3227-8

Carminati, A., A.B. Moradi, D. Vetterlein, P. Vontobel, E. Lehmann, U. Weller, H.-J. Vogel, and S.E. Oswald. 2010. Dynamics of soil water content in the rhizosphere. Plant Soil 332(1–2): 163–176. doi: 10.1007/s11104-010-0283-8

Dekker, L.W., and C.J. Ritsema. 1996. Variation in water content and wetting patterns in Dutch water repellent peaty clay and clayey peat soils. CATENA 28(1–2): 89–105. doi: 10.1016/S0341-8162(96)00047-1

Gregory, P.J. 2006. Roots, rhizosphere and soil: the route to a better understanding of soil science? Eur. J. Soil Sci. 57(1): 2–12. doi: 10.1111/j.1365-2389.2005 .00778.x

Hallett, P.D., D.C. Gordon, and A.G. Bengough. 2003. Plant influence on rhizosphere hydraulic properties: direct measurements using a miniaturized infiltrometer. New Phytol. 157(3): 597–603. doi: 10.1046/j.1469-8137.2003.00690.x

Hinsinger, P., A.G. Bengough, D. Vetterlein, and I.M. Young. 2009. Rhizosphere: biophysics, biogeochemistry and ecological relevance. Plant Soil 321(1–2): 117–152. doi: 10.1007/s11104-008-9885-9

Hu, H., and R.G. Larson. 2002. Evaporation of a Sessile Droplet on a Substrate. J. Phys. Chem. B 106(6): 1334–1344. doi: 10.1021/jp0118322

Kroener, E., M.A. Ahmed, and A. Carminati. 2015. Roots at the percolation threshold. Phys. Rev. E 91(4): 042706. doi: 10.1103/PhysRevE.91.042706

Kroener, E., M. Holz, M. Zarebanadkouki, M. Ahmed, and A. Carminati. 2018. Effects of Mucilage on Rhizosphere Hydraulic Functions Depend on Soil Particle Size. Vadose Zone J. 17(1): 0. doi: 10.2136/vzj2017.03.0056

Moradi, A.B., A. Carminati, A. Lamparter, S.K. Woche, J. Bachmann, D. Vetterlein, H.-J. Vogel, and S.E. Oswald. 2012. Is the Rhizosphere Temporarily Water Repellent? Vadose Zone J. 11(3): 0. doi: 10.2136/vzj2011.0120

Naveed, M., L.K. Brown, A.C. Raffan, T.S. George, A.G. Bengough, T. Roose, I. Sinclair, N. Koebernick, L. Cooper, C.A. Hackett, and P.D. Hallett. 2017. Plant exudates may stabilize or weaken soil depending on species, origin and time: Effect of plant exudates on rhizosphere formation. Eur. J. Soil Sci. (68): 806–816. doi: 10.1111/ejss.12487

Naveed, M., L.K. Brown, A.C. Raffan, T.S. George, A.G. Bengough, T. Roose, I. Sinclair, N. Koebernick, L. Cooper, and P.D. Hallett. 2018. Rhizosphere-Scale Quantification of Hydraulic and Mechanical Properties of Soil Impacted by Root and Seed Exudates. Vadose Zone J. 17(1): 0. doi: 10.2136/vzj2017.04.0083

Oades, J.M. 1978. Mucilages at the root surface. Eur. J. Soil Sci. 29(1): 1–16. doi: 10.1111/j.1365-2389.1978.tb02025.x

Philippot, L., J.M. Raaijmakers, P. Lemanceau, and W.H. van der Putten. 2013. Going back to the roots: the microbial ecology of the rhizosphere. Nat. Rev. Microbiol. 11(11): 789–799. doi: 10.1038/nrmicro3109

Read, D.B., A.G. Bengough, P.J. Gregory, J.W. Crawford, D. Robinson, C.M. Scrimgeour, I.M. Young, K. Zhang, and X. Zhang. 2003. Plant roots release phospholipid surfactants that modify the physical and chemical properties of soil. New Phytol. 157(2): 315–326. doi: 10.1046/j.1469-8137.2003.00665.x

Roberson, E.B., C. Chenu, and M.K. Firestone. 1993. Microstructural changes in bacterial exopolysaccharides during desiccation. Soil Biol. Biochem. 25(9): 1299–1301. doi: 10.1016/0038-0717(93)90230-9

Sposito, G. 2013. Green Water and Global Food Security. Vadose Zone J. 12(4): 0. doi: 10.2136/vzj2013.02.0041

Torquato, S., T.M. Truskett, and P.G. Debenedetti. 2000. Is random close packing of spheres well defined? Phys. Rev. Lett. 84(10): 2064. doi: 10.1103/PhysRevLett.84.2064

van't Woudt, B.D.. 1959. Particle coatings affecting the wettability of soils. J. Geophys. Res. 64(2): 263–267. doi: 10.1029/JZ064i002p00263

Young, I.M. 1995. Variation in moisture contents between bulk soil and the rhizosheath of wheat (Triticum aestivum L. cv. Wembley). New Phytol. 130(1): 135–139. doi: 10.1111/j.1469-8137.1995.tb01823.x

Zarebanadkouki, M., M.A. Ahmed, and A. Carminati. 2016. Hydraulic conductivity of the root-soil interface of lupin in sandy soil after drying and rewetting. Plant Soil 398(1–2): 267–280. doi: 10.1007/s11104-015-2668-1

Zickenrott, I.-M., S.K. Woche, J. Bachmann, M.A. Ahmed, and D. Vetterlein. 2016. An efficient method for the collection of root mucilage from different plant species-A case study on the effect of mucilage on soil water repellency. J. Plant Nutr. Soil Sci. 179(2): 294–302. doi: 10.1002/jpln.201500511

A   DRYING OF MUCILAGE CAUSES WATER REPELLENCY IN THE RHIZOSPHERE OF MAIZE: MEASUREMENT AND MODELLING

Ahmed M.A., Kroener E., Benard P., Zarebanadkouki M., Kaestner A., Carminati A.

Abstract

Background and Aims Although maize roots have been extensively studied, there is limited information on the effect of root exudates on the hydraulic properties of maize rhizosphere. Recent experiments suggested that the mucilaginous fraction of root exudates may cause water repellency of the rhizosphere. Our objectives were: 1) to investigate whether maize rhizosphere turns hydrophobic after drying and subsequent rewetting; 2) to test whether maize mucilage is hydrophobic; and 3) to find a quantitative relation between rhizosphere rewetting, particle size, soil matric potential and mucilage concentration.

Methods Maize plants were grown in aluminium containers filled with a sandy soil. When the plants were 3-weeks-old, the soil was let dry and then it was irrigated. The soil water content during irrigation was imaged using neutron radiography. In a parallel experiment, ten maize plants were grown in sandy soil for 5 weeks. Mucilage was collected from young brace roots growing above the soil. Mucilage was placed on glass slides and let dry. The contact angle was measured with the sessile drop method for varying mucilage concentration. Additionally, capillary rise experiments were performed in soils of varying particle size mixed with maize mucilage. We then used a pore-network model in which mucilage was randomly distributed in a cubic lattice. The general idea was that rewetting of a pore is impeded when the concentration of mucilage on the pore surface (g cm^{-2}) is higher than a given threshold value. The threshold value depended on soil matric potential, pore radius and contract angle. Then, we randomly distributed mucilage in the pore network and we calculated the percolation of water across a cubic lattice for varying soil particle size, mucilage concentration and matric potential.

Results Our results showed that: 1) the rhizosphere of maize stayed temporarily dry after irrigation; 2) mucilage became water repellent after drying. Mucilage contact angle increased with mucilage surface concentration (gram of dry mucilage per surface area); 3) Water could easily cross the rhizosphere when the mucilage concentration was below a given threshold. In contrast, above a critical mucilage concentration water could not flow through the rhizosphere. The critical mucilage concentration decreased with increasing particle size and decreasing matric potential.

Conclusions These results show the importance of mucilage exudation for the water fluxes across the root-soil interface. Our percolation model predicts at what mucilage concentration the rhizosphere turns hydrophobic depending on soil texture and matric potential. Further studies are needed to extend these results to varying soil conditions and to upscale them to the entire root system.

B   LIQUID BRIDGES AT THE ROOT-SOIL INTERFACE

Carminati A., Benard P., Ahmed M.A., Zarebanadkouki M.

Abstract

Background The role of the root-soil interface on soil-plant water relations is unclear. Despite many experimental studies proved that the soil close to the root surface, the rhizosphere, has different properties compared to the adjacent bulk soil, the mechanisms underlying such differences are poorly understood and the implications for plant-water relations remain largely speculative.

Scope The objective of this review is to identify the key elements affecting water dynamics in the rhizosphere. Special attention is dedicated to the role of mucilage exuded by roots in shaping the hydraulic properties of the rhizosphere. We identified three key properties: 1) mucilage absorbs water decreasing its water potential; 2) mucilage decreases the surface tension of the soil solution; 3) mucilage increases the viscosity of the soil solution. These three properties determine the retention and spatial

configuration of the liquid phase in porous media. The increase in viscosity and the decrease in surface tension (quantified by the Ohnesorge number)

allow the persistence of long liquid filaments even at very negative water potentials. At high mucilage concentrations these filaments form a network that creates an additional matric potential and maintains the continuity of the liquid phase during drying.

Conclusion The biophysical interactions between mucilage and the pore space determine the physical properties of the rhizosphere. Mucilage forms a network that provides mechanical stability to soils upon drying and that maintains the continuity of the liquid phase across the soil-root interface. Such biophysical properties are functional to create an interconnected matrix that maintains the roots in contact with the soil, which is of particular importance when the soil is drying and the transpiration rate is high.

C   PHYSICS AND HYDRAULICS OF THE RHIZOSPHERE NETWORK

Benard P., Zarebanadkouki M., and Carminati A.

Abstract

Take home message Mucilage secreted by roots and EPS produced by microorganisms alter the physical properties of the soil solution and impact the water dynamics in the rhizosphere. The high viscosity of mucilage and EPS is responsible for the formation of thin filaments and interconnected thin lamellae that span throughout the soil matrix maintaining the continuity of the liquid phase across the pore space even during severe drying. The impact of these mechanisms on plant and microorganisms needs to be explored.

D   SPATIAL DISTRIBUTION OF MUCILAGE IN THE RHIZOSPHERE MEASURED WITH INFRARED SPECTROSCOPY

Holz M., Leue M., Ahmed M.A., Benard P., Gerke H.H., and Carminati A.

Abstract

Mucilage is receiving increasing attention because of its putative effects on plant growth, but so far no method is available to measure its spatial distribution in the rhizosphere. We tested whether the C-H signal related to mucilage fatty acids is detectable by infrared spectroscopy and if this method can be used to determine the spatial distribution of mucilage in the rhizosphere. Maize plants were grown in rhizoboxes filled with soil free of organic matter. Infrared measurements were carried out along transects perpendicular as well as axially to the root channels. The perpendicular gradients of the C-H proportions showed a decrease of C-H with increasing distance: 0.8mm apart from the root center the C-H signals achieved a level near zero. The measured concentrations of mucilage were comparable with results obtained in previous studies, which encourages the use of infrared spectroscopy to quantitatively image mucilage in the rhizosphere.

E   RHIZOSPHERE HYDROPHOBICITY LIMITS ROOT WATER UPTAKE AFTER DRYING AND SUBSEQUENT REWETTING

Zarebanadkouki M., Ahmed M., Hedwig C., Benard P., Kostka S.J., Kaestner A., Carminati A.

Abstract

Background and Aims Recent experiments showed that rhizosphere of several plant species turns temporarily hydrophobic after severe drying and subsequent rewetting. Whether or not such hydrophobicity limits root water uptake is not known.

Methods A set of experiments was performed to test whether rhizosphere water repellency negatively affects root water uptake. To this end, a commercial surfactant was used as a rewetting agent to facilitate the wettability of the rhizosphere of lupins (Lupinus albus) in a sandy soil. Lupin plants were grown in rhizoboxes and were subjected to a severe drying cycle. Then half of the plants were irrigated with water and half with the surfactant solution. Time-series neutron radiography technique was used to monitor water redistribution in the rhizosphere during irrigation. In a second experimental set-up, lupins were grown in a sandy soil partitioned in five vertical compartments separated by a 1-cm layer of coarse sand (acting as a capillary barrier). Water and surfactant were injected in different compartments and the rehydration of the root tissues beyond the irrigated compartments was monitored with neutron radiography for 2–3 h. Root rehydration rates were used to estimate the water fluxes across the root-soil interface.

Results The rhizosphere of lupin roots in sandy soil irrigated with water remained partly dry for at least 2–3 h, while it was rapidly rewetted when irrigated with surfactant. Water flow into the roots irrigated with surfactant solution was 6.5 times faster than into the roots irrigated with water.

Conclusions These results prove that water repellency of the rhizosphere of lupins in sandy soils limited the water fluxes into the roots and root rehydration during the first

two to three hours after irrigation. This might not always be negative, because it can limit water losses from roots to dry soil and therefore avoid severe root dehydration.

F   SURFACE TENSION, RHEOLOGY AND HYDROPHOBICITY OF RHIZODEPOSITS AND SEED MUCILAGE INFLUENCE SOIL WATER RETENTION AND HYSTERESIS

Naveed M., Ahmed M.A., Benard P., Brown L.K., George T.S., Bengough A.G., Roose T., Koebernick N., Hallett P.D.

Abstract

Aims Rhizodeposits collected from hydroponic solutions with roots of maize and barley, and seed mucilage washed from chia, were added to soil to measure their impact on water retention and hysteresis in a sandy loam soil at a range of concentrations. We test the hypothesis that the effect of plant exudates and mucilages on hydraulic properties of soils depends on their physicochemical characteristics and origin.

Methods Surface tension and viscosity of the exudate solutions were measured using the Du Noüy ring method and a cone-plate rheometer, respectively. The contact angle of water on exudate treated soil was measured with the sessile drop method. Water retention and hysteresis were measured by equilibrating soil samples, treated with exudates and mucilages at 0.46 and 4.6 mg g^{-1} concentration, on dialysis tubing filled with polyethylene glycol (PEG) solution of known osmotic potential. Results Surface tension decreased and viscosity increased with increasing concentration of the exudates and mucilage in solutions. Change in surface tension and viscosity was greatest for chia seed exudate and least for barley root exudate. Contact angle increased with increasing maize root and chia seed exudate concentration in soil, but not barley root. Chia seed mucilage and maize root rhizodeposits enhanced soil water retention and increased hysteresis index, whereas barley root rhizodeposits decreased soil water retention and the hysteresis effect. The impact of exudates and mucilages on soil water retention almost ceased when approaching wilting point at −1500 kPa matric potential.

Conclusions Barley rhizodeposits behaved as surfactants, drying the rhizosphere at smaller suctions. Chia seed mucilage and maize root rhizodeposits behaved as hydrogels that hold more water in the rhizosphere, but with slower rewetting and greater hysteresis.

(Eidesstattliche) Versicherungen und Erklärungen

(§ 8 Satz 2 Nr. 3 PromO Fakultät)

Hiermit versichere ich eidesstattlich, dass ich die Arbeit selbstständig verfasst und keine anderen als die von mir angegebenen Quellen und Hilfsmittel benutzt habe (vgl. Art. 64 Abs. 1 Satz 6 BayHSchG).

(§ 8 Satz 2 Nr. 3 PromO Fakultät)

Hiermit erkläre ich, dass ich die Dissertation nicht bereits zur Erlangung eines akademischen Grades eingereicht habe und dass ich nicht bereits diese oder eine gleichartige Doktorprüfung endgültig nicht bestanden habe.

(§ 8 Satz 2 Nr. 4 PromO Fakultät)

Hiermit erkläre ich, dass ich Hilfe von gewerblichen Promotionsberatern bzw. – vermittlern oder ähnlichen Dienstleistern weder bisher in Anspruch genommen habe noch künftig in Anspruch nehmen werde.

(§ 8 Satz 2 Nr. 7 PromO Fakultät)

Hiermit erkläre ich mein Einverständnis, dass die elektronische Fassung der Dissertation unter Wahrung meiner Urheberrechte und des Datenschutzes einer gesonderten Überprüfung unterzogen werden kann.

(§ 8 Satz 2 Nr. 8 PromO Fakultät)

Hiermit erkläre ich mein Einverständnis, dass bei Verdacht wissenschaftlichen Fehlverhaltens Ermittlungen durch universitätsinterne Organe der wissenschaftlichen Selbstkontrolle stattfinden können.

……………………………………………………………………………………….

Ort, Datum, Unterschrift